

# The effect of different moisture contents and forms of low-rank coal on CO<sub>2</sub> adsorption capacity

セオドラ ノエリ タンバリア

<https://hdl.handle.net/2324/6787588>

---

出版情報 : Kyushu University, 2022, 博士 (工学), 課程博士  
バージョン :  
権利関係 :

**The effect of different moisture contents and forms of low-  
rank coal on CO<sub>2</sub> adsorption capacity**

**Doctoral Dissertation**

**Theodora Noely Tambaria**

**Department of Earth Resources Engineering**

**Kyushu University**

**Fukuoka**

**2023**



**九州大学**  
KYUSHU UNIVERSITY

**THE EFFECT OF DIFFERENT MOISTURE  
CONTENTS AND FORMS OF LOW-RANK COAL  
ON CO<sub>2</sub> ADSORPTION CAPACITY**

**A doctoral dissertation  
Submitted in Partial Fulfillment  
of the Requirements for the Degree  
Doctor of Philosophy**

**by  
Theodora Noely Tambaria**

**Supervised by  
Professor Yuichi Sugai**

**DEPARTMENT OF EARTH RESOURCES ENGINEERING  
KYUSHU UNIVERSITY**

## **Abstract**

Growing interest in coal seam sequestration has prompted researchers to measure the amount of CO<sub>2</sub> adsorption in coal as a potential long-term solution to global warming. Low-rank coal is capable of adsorbing CO<sub>2</sub>, but most of the time it contains high moisture levels, which can make it difficult to adsorb CO<sub>2</sub>. The crushing and drying of low rank coal was conducted in the laboratory in order to enhance its CO<sub>2</sub> adsorption capacity. The purpose of this study was to evaluate CO<sub>2</sub> adsorption capacities and the effect of CO<sub>2</sub> adsorption on low rank coal under different coal conditions. CO<sub>2</sub> adsorption experiments were conducted at 318.15 K and 0.5 MPa to 3 MPa using a volumetric adsorption apparatus. Low temperature nitrogen adsorption (LTNA) and scanning electron microscopy (SEM) were used to investigate the effect of CO<sub>2</sub> adsorption in this study.

Coal samples of low rank were collected from three coalfields located in the South Sumatra Basin, namely West Banko (WB), East Banko (EB), and North Muara Tiga Besar (NMTB). All coal samples have similar fixed carbon and volatile matter, but the WB area has a lower moisture content. Comparing CO<sub>2</sub> adsorption in samples from other countries, samples with lower moisture content showed higher CO<sub>2</sub> adsorption capacity, proving moisture is an important factor in CO<sub>2</sub> adsorption. Experimental studies showed CO<sub>2</sub> adsorption capacity was greatest in the WB area with the lowest moisture content, followed by the EB area with a lower moisture content than the NMTB area. Under raw conditions, CO<sub>2</sub> adsorption capacity varies at higher pressures (2-3 MPa). Under raw conditions, CO<sub>2</sub> adsorption on both powdered coal and block coal from the WB area varies 1.1 times at low pressures (0.5-2 MPa), and 1.4 times at high pressures (2-3 MPa). Despite no significant differences in CO<sub>2</sub> adsorption on coal blocks under raw conditions, CO<sub>2</sub> adsorption at 3 MPa indicated that samples from the WB area exhibited the highest of CO<sub>2</sub> adsorption. According to a comparison at 3 MPa,

crushed coal can improve CO<sub>2</sub> adsorption capacity by 1.2 times. In dry conditions at 3 MPa, CO<sub>2</sub> adsorbed on powder increases by 1.9 to 2.2 times. Coal blocks adsorbed significantly less CO<sub>2</sub> under dry conditions than coal powder, which increased by only 1.7 to 1.8 times. Using the fitted curves and correlation coefficients between experimental data and Langmuir, Freundlich, and Temkin isotherms, Langmuir and Freundlich fit the data the most closely, indicating that CO<sub>2</sub> can be adsorbed in a monolayer or multilayer. When the adsorption of CO<sub>2</sub> on coal samples from three different areas of the South Sumatra Basin is compared, it has been found that the coal samples from WB have a greater potential for CO<sub>2</sub> storage due to their lower moisture content than those from EB or NMTB.

Adsorption of CO<sub>2</sub> has been studied on coal from five coal seams in West Banko, South Sumatra. Due to their lower moisture content and higher fixed carbon, seam B1 and seam C resulted in higher CO<sub>2</sub> adsorption than other coal seams. CO<sub>2</sub> adsorption at 3 MPa was increased by 1.6 to 1.8 times by drying blocks, while CO<sub>2</sub> adsorption was increased by 1.9 to 2.1 times by drying powder. The SSE and ARE statistical evaluations were used to validate Langmuir and Freundlich are the most accurate adsorption models, as they show CO<sub>2</sub> adsorption in both monolayers and multilayers. KH values were determined for powder dry coal > block dry coal > powder raw coal > block raw coal based on the results of the experiment. The KH value of dry coal is higher than that of raw coal because the drying process increases the availability of micropores that are capable of adsorbing CO<sub>2</sub>. In addition to increasing micropore availability, the drying process also increases surface potential and Gibbs free energy. CO<sub>2</sub> adsorption on coal is feasible and spontaneous under all conditions. The drying process facilitated and enhanced the adsorption of CO<sub>2</sub> into low rank coal. In spite of the similarity of coal samples under all conditions, moisture is not the only factor affecting CO<sub>2</sub> adsorption in this chapter. There is more moisture in seam B1 than in seam C, but there is more fixed carbon in seam B1 than in seam C, resulting in a similar

capacity for adsorption of CO<sub>2</sub>. As a result of the coal properties of seams B1 and C, they are better suited to storing CO<sub>2</sub>.

There are different effects that are caused by CO<sub>2</sub> adsorption under different conditions. Huminite exhibits a strong correlation with CO<sub>2</sub> adsorption, especially when conditions are dry. The adsorption of CO<sub>2</sub> by liptinite is weak in all conditions. There is a negative correlation between inertinite and CO<sub>2</sub> adsorption on coal and drying did not affect this correlation. LTNA and SEM were used to analyze the change in pore structure characteristics associated with CO<sub>2</sub> adsorption under varying conditions. The swelling caused by CO<sub>2</sub> adsorption resulted in the reduction of micropores. The presence of micropores can still be seen in dry coal after CO<sub>2</sub> adsorption due to the shrinkage of coal during the drying process. By SEM analysis, mineral dissolution on coal pores due to acidic environments from CO<sub>2</sub> adsorption can be analyzed. Mineral dissolution results in a rise in mesopores. For safe CO<sub>2</sub> storage in low-rank coal, CO<sub>2</sub> injection into dry coal has a lower chance of swelling than CO<sub>2</sub> injection into raw coal, However, the drying process results in shrinkage, which plays a crucial role in considering dry coal's potential.

The results of this study could help understand how significant CO<sub>2</sub> adsorption occurs at low-rank with different sample preparations and the impact of CO<sub>2</sub> adsorption. Furthermore, the results of the study may provide insight for future research.

## **Acknowledgements**

I sincerely thank my supervisor, Professor Yuichi Sugai, for his priceless guidance and support while finishing this dissertation.

I would also like to thank my co-supervisors, Dr. Ronald Nguele, and Dr. Esaki Takehiro. I am grateful for their continuous guidance, valuable advice, and untiring support over the past three years.

I also thank Associate Professor Takashi Sasaoka, Professor Hirokazu Okawa and Associate Professor Ferian Anggara, as thesis examiners, for the corrections and comments to improve this thesis.

My gratitude also goes to PT Bukit Asam and the Unconventional Geo-Resources Research Group, Faculty of Engineering, Universitas Gadjah Mada, for providing the coal samples and so helpfully sending the coal samples in complex covid conditions.

I sincerely appreciate and acknowledge the JICA KIZUNA program for supporting my study at Kyushu university through scholarship. My acknowledgment also goes to Universitas Gadjah Mada for recommending me to get the scholarship.

Special acknowledgment also goes to my former and present colleagues in the RSPE laboratory for their assistance and friendship.

I thank my family for their support, love, prayer, and guidance.

## Table of Contents

Abstract .....	iii
Acknowledgements .....	vi
Table of Contents .....	vii
List of Figures .....	xi
List of Tables.....	xiv
Acronyms .....	xv
CHAPTER I .....	1
1. Introduction .....	1
1.1 General Introduction.....	1
1.2 Hypotheses and objectives .....	3
1.3 Outlines .....	3
CHAPTER II.....	5
2. Literature review .....	5
2.1 History of CO <sub>2</sub> adsorption on coal .....	5
2.2 Parameters affecting adsorption capacity .....	6
2.2.1 Effects of Sample Condition .....	6
2.2.2 Moisture Effects .....	7
2.2.3 Maceral Effects .....	8
2.2.4 Coal Pore Effects.....	9
2.2.5 Temperature and Pressure Effects.....	10
2.3 Adsorption measurement methods .....	11
2.4 Adsorption Isotherms .....	11



2.4.1	Langmuir isotherm model .....	12
2.4.2	Freundlich isotherm model .....	12
2.4.3	Temkin isotherm model .....	12
2.5	Gibbs free energy and surface potential .....	13
2.6	Adsorption effects .....	13
CHAPTER III .....		15
3.	CO <sub>2</sub> Adsorption on Low-Rank Coal from Different Area .....	15
3.1	Introduction .....	15
3.2	Experimental preparation .....	18
3.2.1	Coal characteristic measurements .....	18
3.2.2	Adsorption measurements .....	19
3.2.3	Experimental setups .....	21
3.3	Results and Discussion .....	22
3.3.1	Coal characteristic .....	22
3.3.2	CO <sub>2</sub> adsorption measurement .....	23
3.3.3	Comparing low-rank coal with other countries in CO <sub>2</sub> adsorption .....	25
3.3.4	Isotherm analysis .....	28
3.3.5	Langmuir parameter on CO <sub>2</sub> adsorption on coal .....	29
3.3.6	Effect of different on CO <sub>2</sub> adsorption capacity on coal .....	31
3.3.7	Effect of coal characteristics on CO <sub>2</sub> adsorption capacity of coal .....	32
3.4	Summary and Conclusions .....	33
CHAPTER IV .....		34

4.	CO <sub>2</sub> adsorption on different coal seams: A thermodynamics study surface potential and Gibbs free energy .....	34
4.1	Introduction .....	34
4.2	Theory models .....	35
4.2.1	Adsorption isotherm model and statistical evaluations.....	35
4.2.2	Henry law .....	36
4.2.3	Gibbs free energy change and surface potential .....	36
4.3	Experimental section .....	36
4.3.1	Experimental process .....	36
4.3.2	Experimental samples .....	37
4.4	Results and discussion.....	37
4.4.1	Coal assay .....	37
4.4.2	CO <sub>2</sub> adsorption on coal .....	38
4.4.3	Simulation of isothermal adsorption of CO <sub>2</sub> on coals.....	39
4.4.4	Statistical evaluation and model parameters for Langmuir, Freundlich and Temkin.....	41
4.4.5	Henry coefficient of CO <sub>2</sub> on coals .....	42
4.4.6	Surface potentials of CO <sub>2</sub> on coals.....	43
4.4.7	Gibbs free energy changes of CO <sub>2</sub> on coals .....	44
4.5	Conclusion.....	46
	CHAPTER V.....	47
5.	The Effect of CO <sub>2</sub> Adsorption.....	47
5.1	Introduction .....	47

5.2	Experimental work .....	48
5.2.1	Organic petrography.....	48
5.2.2	Low pressure nitrogen adsorption (LTNA) isotherm and pore shape...	49
5.2.3	Scanning Electron Microscopy (SEM) .....	50
5.3	Results and discussion.....	51
5.3.1	Coal assay .....	51
5.3.2	LTNA analysis .....	56
5.3.3	SEM analysis.....	60
5.4	Conclusions .....	61
CHAPTER VI .....		63
6.	Conclusions and Outlook .....	63
References .....		66

## List of Figures

Figure 1. The ECBM extraction process based on gas injection. Adapted from (Godec et al., 2014; Harpalani and Schraufnagel, 1990; Mukherjee and Misra, 2018; Qi et al., 2017; Vishal et al., 2018) .....	6
Figure 2 CO <sub>2</sub> injection scenarios for ECBM modified from (Van Bergen et al., 2011) .....	8
Figure 3 Pore-distributions in different coal ranks as determined using an NMR method. Modified from (Qin et al., 2020).....	10
Figure 4 General sketch of CO <sub>2</sub> adsorption on coal with various conditions .....	17
Figure 5 The location of the research area in South Sumatra Basin, Indonesia.....	18
Figure 6 The lithotype of coal samples from (a) WB, (b) EB, and (c) NMTB.....	18
Figure 7 Flowchart of experimental process in this study .....	20
Figure 8 Volumetric method for (a) coal powder and (b) coal block .....	21
Figure 9 (a) The result of proximate analysis and (b) the differences coal samples with samples contained the lowest value of moisture, fixed carbon and volatile matter ....	23
Figure 10 CO <sub>2</sub> adsorption on the difference between coal form and moisture: (a) powder samples under raw conditions, (b) powder samples under dry condition, (c) block samples under raw conditions, and (d) block samples under dry conditions....	24
Figure 11 Comparison of different CO <sub>2</sub> adsorption experiment and isotherm fitting curve from WB coal samples with various conditions: (a) powder samples under raw condition, (b) powder samples under dry condition, (c) block samples under raw condition, and (d) block samples under dry condition.....	28
Figure 12 Langmuir parameters for CO <sub>2</sub> adsorption of all measured samples: (a) Langmuir volume capacity and (b) Langmuir pressure. ....	30
Figure 13 The difference in Langmuir volume capacity on EB and NMTB from WB coal sample.....	31
Figure 14 The discrepancy in Langmuir volume due to various coal conditions .....	32

Figure 15 Sample location map of study area: South Sumatra, Indonesia.....	37
Figure 16 CO <sub>2</sub> adsorption on (a) block samples and (b) powder samples .....	38
Figure 17 The Langmuir, Freundlich, and Temkin isotherm model fits CO <sub>2</sub> adsorption on B coal seam in raw or dry conditions for (1) powder and (2) block. ....	40
Figure 18 Value of SSE of isotherm models from (a) powder samples under raw condition, (b) powder samples under dry condition, (c) block samples under raw condition, and (d) block samples under dry condition .....	41
Figure 19 Value of ARE of isotherm models from (a) powder samples under raw condition, (b) powder samples under dry condition, (c) block samples under raw condition, and (d) block samples under dry condition .....	42
Figure 20 Henry's coefficients of CO <sub>2</sub> on all coal samples .....	43
Figure 21. The surface potentials of CO <sub>2</sub> under four different conditions are presented here: (a) powder-raw, (b) powder-raw, (c) block-raw, and (d) block-dry .....	44
Figure 22 The Gibbs free energy of CO <sub>2</sub> under four different conditions are presented here: (a) powder-raw, (b) powder-raw, (c) block-raw, and (d) block-dry .....	45
Figure 23 Reflected light microscope .....	48
Figure 24 Hysteresis loops and their corresponding pore shapes .....	49
Figure 25. Types of pores .....	49
Figure 26 The SEM apparatus.....	50
Figure 27 Huminite and mineral on coal sample on image under white light .....	52
Figure 28 The result of differences coal samples with samples contained the lowest value of huminite, liptinite and inertinite from (a)different area and (b) different coal seams. ....	52
Figure 29 The relationship between CO <sub>2</sub> adsorption and huminite content in (a) powder coal in raw condition, (b) powder coal in dry condition, (c) block coal in raw condition, and (d) block coal in dry condition .....	53
Figure 30 The relationship between CO <sub>2</sub> adsorption and liptinite content in (a) powder coal in raw condition, (b) powder coal in dry condition, (c) block coal in raw condition, and (d) block coal in dry condition .....	54

Figure 31 The relationship between CO <sub>2</sub> adsorption and inertinite content in (a) powder coal in raw condition, (b) powder coal in dry condition, (c) block coal in raw condition, and (d) block coal in dry condition .....	55
Figure 32 LTNA isotherms of coal samples before and after CO <sub>2</sub> injection in different conditions .....	57
Figure 33 Micropore size distribution of coal samples before and after CO <sub>2</sub> injection under different conditions. ....	58
Figure 34 Mesopore size distribution of coal after CO <sub>2</sub> injection under different conditions. ....	59
Figure 35 SEM images of different coal samples in raw condition .....	60
Figure 36 SEM image of different condition, (a) raw condition, (b) raw condition after CO <sub>2</sub> adsorption and (c) dry condition after CO <sub>2</sub> adsorption .....	61

## List of Tables

Table 1 Coal sample from all coal fields in different coal forms.....	19
Table 2 Results of proximate analysis of coal samples from different area .....	22
Table 3 Summary of the CO <sub>2</sub> adsorption on low rank under various conditions.....	27
Table 4 CO <sub>2</sub> adsorption isotherm model from different area.....	29
Table 5 Results of proximate analysis of all coal seam from WB area .....	38
Table 6 CO <sub>2</sub> adsorption isotherm model of all coal seam from WB area.....	39
Table 7 The experimental data results of lithotypes, petrographic and reflectance (Ro%) .....	51

## Acronyms

$A_{cs}$	: adsorbate cross sectional area (0.162 nm <sup>2</sup> for N <sub>2</sub> )
$A_T$	: the equilibrium binding constant
$b_T$	: Temkin isotherm constant
$C$	: constant related to the net heat of adsorption
$G_a$	: Langmuir isotherm model adsorbed-gas storage capacity
$K_f$	: constant of Freundlich isotherm model
$M$	: molecular weight of the adsorbate (N <sub>2</sub> is $28.0134 \times 10^{-3}$ g/mol)
$m$	: mass of coal (g)
$n$	: heterogeneity factor
$N_{av}$	: Avogadro's number ( $6.023 \times 10^{23}$ /mol)
$n^{ex}$	: Gibbs excess adsorption (mmol g <sup>-1</sup> )
$P$	: pressure (MPa)
$P_c$	: critical pressure (CO <sub>2</sub> is 7.39 MPa)
$P_L$	: Langmuir pressure (MPa)
$P_r$	: reduced pressure
$P_{rci}$	: initial pressure at reference cells (MPa)
$P_{rcf}$	: final pressure at reference cells (MPa)
$P_{sci}$	: initial pressure at sample cells (MPa)
$P_{scf}$	: final pressure at sample cells (MPa)
$P/P_0$	: relative pressure
$Q_e$	: Freundlich isotherm model adsorbed-gas storage capacity
$R$	: molar gas constant (8.314 J mol <sup>-1</sup> K <sup>-1</sup> )
$R_0$	: huminite reflectance (%)
$r_m$	: pore radius (nm)
$T$	: temperature (K)
$T_c$	: critical temperature (CO <sub>2</sub> is 304.2 K)



- $T_r$  : reduced temperature
- $V_a$  : volume of gas adsorbed ( $\text{cm}^3 \text{g}^{-1}$ )
- $V_L$  : Langmuir volume ( $\text{cm}^3 \text{g}^{-1}$ )
- $V_m$  : volume of adsorbate as a monolayer ( $\text{cm}^3/\text{g}$ )
- $VM_{daf}$  : volatile matter (dry ash-free basis) (%)
- $V_{rc}$  : reference cell ( $\text{cm}^3$ )
- $V_{void}$  : void volume ( $\text{cm}^3$ )
- $\omega$  : acentric factor ( $\text{CO}_2$  is 0.224)
- $Z$  : compressibility factor
- $Z_{rcf}$  : reference cell final compressibility factor
- $Z_{rci}$  : reference cell initial compressibility factor
- $Z_{scf}$  : sample cell final compressibility factor
- $Z_{sci}$  : sample cell initial compressibility factor
- $\gamma$  : surface tension of the adsorbate ( $\text{J}/\text{m}^2$ )

# **CHAPTER I**

## **1. Introduction**

### **1.1 General Introduction**

Policies and regulations encourage cleaner energy sources, resulting in a decline in long-term coal consumption estimates (Miller, 2017). Most policymakers have a consensus that global temperatures should not rise by more than 2 degrees Celsius by 2050, and more than 80% of the world's coal reserves cannot be exploited (McGlade and Ekins, 2015; Meinshausen et al., 2009). Developing energy-efficient and low-carbon technologies is essential to addressing climate change and meeting the growing demand for affordable energy. Despite reducing greenhouse gas emissions associated with coal consumption, this energy source can still be efficiently utilized by capturing CO<sub>2</sub> that otherwise would be released into the atmosphere and injecting it into deep geological formations.

Low-rank coals are one of the most abundant fossil fuel sources worldwide (Dong, 2011). Low-rank coal is usually used for electricity generation, hot water production, low-grade steam, or other applications (Schobert, 2017). Low-rank coal emits more CO<sub>2</sub> than other fuels, such as natural gas, due to its low rank, usually high moisture, and low heating value (Agraniotis et al., 2017). Furthermore, low-rank coal energy-producing facilities, like power plants, will consume more coal but generate less power (Lee et al., 2017). In the near future, there will be fewer opportunities to mine coal, and an abundance of unmined coal will be a significant concern, especially for low-rank coal. Manufacturing coal absorbent for carbon capture and storage represents one solution for low-rank utilities. The injection of CO<sub>2</sub> into low-rank coal may serve as a carbon storage system and enhance coal bed methane recovery (Ranathunga et al., 2017). The proven CBM resources in China are primarily concentrated in low-rank coals, which account for more than 40% of the total proven CBM resources (Yu and Wang, 2020). The presence of a large number of micropores is capable of adsorbing

large amounts of methane (Yang et al., 2021). Low-rank coal contains more micropores, so it has a greater probability of diffusing CH<sub>4</sub> (Laxminarayana and Crosdale, 1999; J. Zhao et al., 2018). This potential value makes CO<sub>2</sub> an attractive prospect for enhanced coal bed methane.

In order to gain a better understanding of CO<sub>2</sub> storage in low-rank coal, it is necessary to gain a basic understanding of the process. Adsorption is the mechanism by which carbon dioxide is stored in coal seams since bonds are formed between the molecules of an adsorbate and an adsorbent. The adsorption of CO<sub>2</sub> on low-rank coal is complex in some studies. Low-rank coal generally absorbs the least amount of CO<sub>2</sub> compared to other coal ranks (Goodman et al., 2004). The cause of this phenomenon can be attributed to the fact that low-rank coal is more affected by moisture than high-rank coal (Day et al., 2008). For laboratory-scale CO<sub>2</sub> adsorption, CO<sub>2</sub> is typically adsorbed in a dry and powdery form to minimize the effects of moisture and maximize the available surface area. Nevertheless, this situation differs from natural conditions in which underground coal is always saturated with water and deposits in a massive form. A challenging gap in the adsorption capacity measurement of low-rank coal exists since the samples for the experiment have yet to be prepared under natural conditions.

The purpose of this study is to utilize a volumetric approach to measure the adsorption capacity of low-rank coal in various sample preparations. In this study, low-rank coal samples are taken from different areas and coal seams of Indonesian coal field. The adsorption capacity of these samples was determined at 318.15 K and pressures up to 3 MPa in steps of 0.5 MPa. Further analysis should be conducted to confirm the relationship between adsorption capacity, the available space for molecules to adhere, and the effect of CO<sub>2</sub> adsorption on low-rank coal.

## **1.2 Hypotheses and objectives**

This study evaluated CO<sub>2</sub> adsorption capacities on low rank coal under different coal conditions and its effect on CO<sub>2</sub> adsorption. Low-rank coal known has the potential to serve as an effective and economical source of carbon sequestration. Many researchers have studied the adsorption capacity of coal-containing moisture and massive coal samples to find similar results to those measured in the field. Research on a different method of data preparation and comparison of data from a coal basin with different areas and seams remains to be done. Thanks to PT Bukit Asam and the Unconventional Geo-Resources Research Group at Universitas Gadjah Mada provided low-rank coal from various areas and seams. Furthermore, preparing different conditions of coal samples and measuring adsorption capacity with a volumetric apparatus were conducted at Kyushu University. The purpose of this research is to address the following questions:

- a. What are the effects of different coal preparations on the CO<sub>2</sub> adsorption capacity of low-rank coal?
- b. How does CO<sub>2</sub> adsorption capacity affect different areas and coal seams?
- c. What is the effect of CO<sub>2</sub> adsorption in low-rank coal under different conditions?

The adsorption capacity of low-rank coal was measured in order to resolve this issue and address several discrepancies. Moreover, different characterization tests are conducted to determine the influence of CO<sub>2</sub> adsorption on low-rank coal.

## **1.3 Outlines**

Chapter 2 presents an overview of CO<sub>2</sub> adsorption in coal and reviews studies conducted to assess the effect of various influencing parameters. It also provides a brief overview of the methods used for measuring adsorption factors. In addition, recent studies on the adsorption of CO<sub>2</sub> in low-rank coal are discussed to demonstrate the need for this research.

In Chapter 3, an experiment was conducted to examine the adsorption capacity of CO<sub>2</sub> in coal seams from different areas. In order to determine the results, coal samples were divided into four categories: block-raw, block-dry, powder-raw, and powder-dry. Experimental results of volumetric adsorption at pressures ranging from 0.5 MPa to 3 MPa were observed. The CO<sub>2</sub> adsorption capacity of different areas is analyzed based on various conditions and the adsorption isotherm.

It was discussed in Chapter 4 how much CO<sub>2</sub> could be absorbed in potential coal seams from a potential area. CO<sub>2</sub> adsorption capacity from different coal conditions was analyzed following adsorption affinity and different adsorption isotherm models. It is presented and discussed that a thermodynamic analysis of CO<sub>2</sub> adsorption surface potential and Gibbs free energy change has been conducted.

The purpose of Chapter 5 is to examine the effect of CO<sub>2</sub> adsorption under different coal conditions. This chapter discusses organic petrography and surface analyzer apparatus specifications. In addition, a scanning electron microscope analysis was presented to enhance the results.

In Chapter 6, a summary of the research is provided, and recommendations are made for possible future research.

## **CHAPTER II**

### **2. Literature review**

#### **2.1 History of CO<sub>2</sub> adsorption on coal**

The extraction of coal bed methane (CBM) from coal seams has been undertaken for many years with great success (Alexis et al., 2015). Evidence shows that gas injection can provide maximum recovery of up to 90% of methane (Zarrouk and Moore, 2009). The extraction process comprises gas injection into the CBM reservoir, followed by the selective adsorption of the gas on the coal surfaces and in the coal pores, methane desorption from the coal matrix, and methane flow along fractures in the bed based on Darcy's Law (Godec et al., 2014; Harpalani and Schraufnagel, 1990; Mukherjee and Misra, 2018; Qi et al., 2017; Vishal et al., 2018) (Figure 1). Adsorption and gas injection rates in the coal bed play a crucial role in helping determine the extent to which methane is recovered from the coal (Hol et al., 2011; Kim et al., 2011; Mukherjee and Misra, 2018; Pan and Connell, 2007). Accurate predictions of gas adsorption must also consider the possibility of sequestration of the injected gas (Godec et al., 2014). CO<sub>2</sub> is an acidic gas (Zhou et al., 2019a) that has been widely used for methane recovery from ECBMs due to its high extraction efficiency (Shimada et al., 2005). There is a high adsorption affinity between coal and CO<sub>2</sub>, which results in the gas being adsorbed rapidly and seeping into micropores of the coal (Beamish and Crosdale, 1998; Busch et al., 2007, 2004; Cui et al., 2004; Karacan and Mitchell, 2003; Yamazaki et al., 2006; Zheng et al., 2013). Additionally, the CO<sub>2</sub> molecule is small in diameter and can replace the methane that was originally present in the micropores (Bhowmik and Dutta, 2013; Oudinot et al., 2017; Shimada et al., 2005). The storage capacity of CO<sub>2</sub> may be affected by temperature and pressure, both of which may result in a change in the coal structure and permeability (Battistutta et al., 2010; Charrière et al., 2010; Fang et al., 2019; Li et al., 2018; Merkel et al., 2015; Wang et al., 2020; J. Zhao et al., 2018).

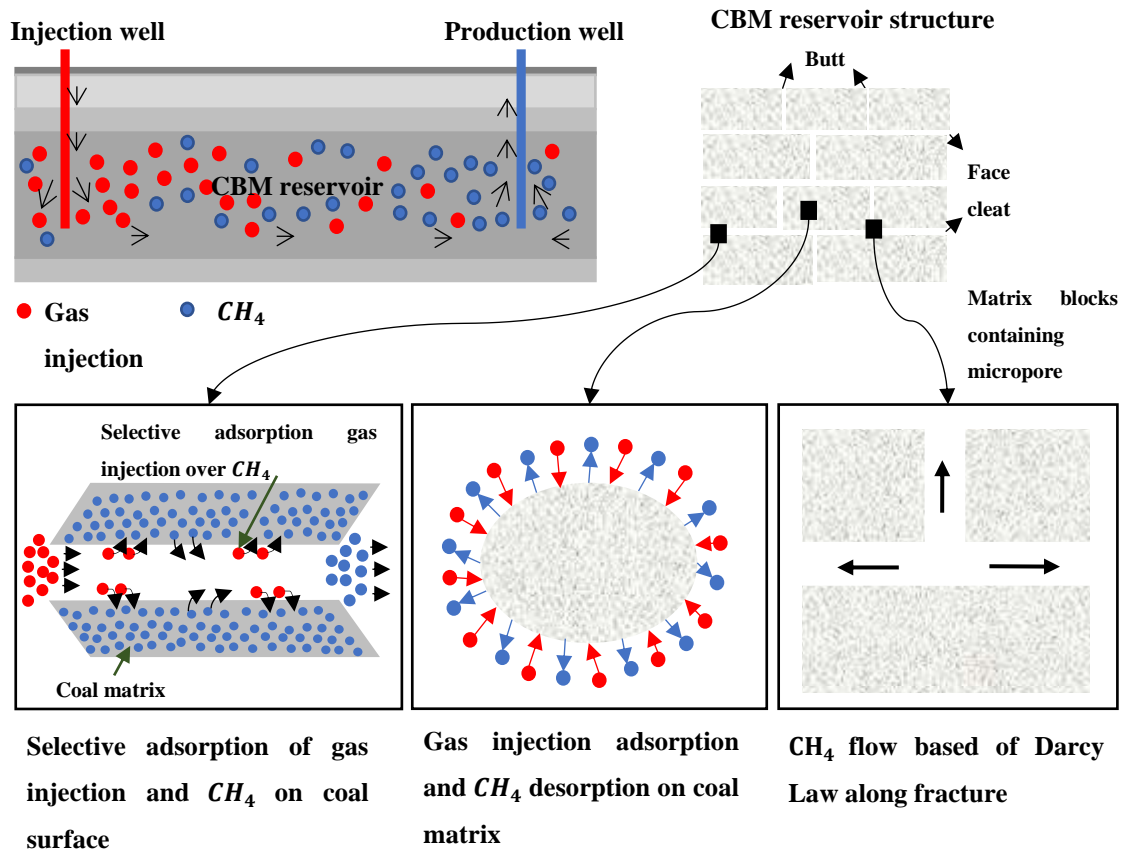


Figure 1. The ECBM extraction process based on gas injection. Adapted from (Godec et al., 2014; Harpalani and Schraufnagel, 1990; Mukherjee and Misra, 2018; Qi et al., 2017; Vishal et al., 2018)

## 2.2 Parameters affecting adsorption capacity

The adsorption of a gas on coal is influenced by several factors, including the coal's specific characteristics, temperature, and pressure. In the study, it was determined that the specific attributes of coal are influenced by a number of factors, including coal condition, moisture content, maceral content, and pore distribution.

### 2.2.1 Effects of Sample Condition

Many reports suggest that particle size is one of the most significant factors affecting coal gas adsorption tests. It has been found that block samples of coal adsorb gases at a slower rate than crushed coal samples (Olajossy, 2017). Typically, crushed coal for

adsorption studies is in the range of 100-60 mesh (A. Busch et al., 2003; Mastalerz et al., 2004), whereas coal block samples are typically 2 cm (Kim et al., 2019). In comparison to coal blocks, crushed coal exhibits greater diffusivity and requires less measurement time to reach equilibrium (Battistutta et al., 2010; Ozdemir et al., 2004; Pone et al., 2009). Although crushed coal is an effective adsorbent, it has several harmful effects. As an example, this material will have damaged pores with opened pores. Thus, the sample surface area will be increased in such a way as to increase the adsorption capacity (Olajosy, 2017) artificially. The crushed coal is relatively challenging to observe shrinkage or swelling because of adsorption, compared with trials using coal block (Skoczylas et al., 2019).

### 2.2.2 Moisture Effects

Moisture is an influential factor in adsorption because water molecules are highly polar (Švábová et al., 2012), altering the gas adsorption kinetics, mechanisms, and capacities (Battistutta et al., 2010). For the purpose of predicting optimal carbon storage and production of ECBM, there are two possible scenarios. In the first scenario, CO<sub>2</sub> will be injected along with CBM production, while in the second scenario, CO<sub>2</sub> will be injected after CBM production (Figure 2) (Van Bergen et al., 2011). The first scenario was based on coal in its natural state, while the second scenario made optimal use of dewatering and degassing methane to make coal drier. Thus, it becomes interesting to investigate the adsorption of coal both raw and dry. An ECBM extraction trial using moist and dry coals found that the adsorption efficiency of the coal was significantly better under drier conditions when compared to moist coals (Hao et al., 2018). Gas adsorption occurs when moisture-occupied adsorption sites become available for gas adsorption (Chen et al., 2018; Laxminarayana and Crosdale, 1999). Previously, it was mentioned that dry coal possesses the highest adsorption capacity for coal gas; however, because coal in the field contains natural moisture, this can result in a significant correction factor that has to be taken into consideration (Busch et al., 2004; Cai et al., 2013).



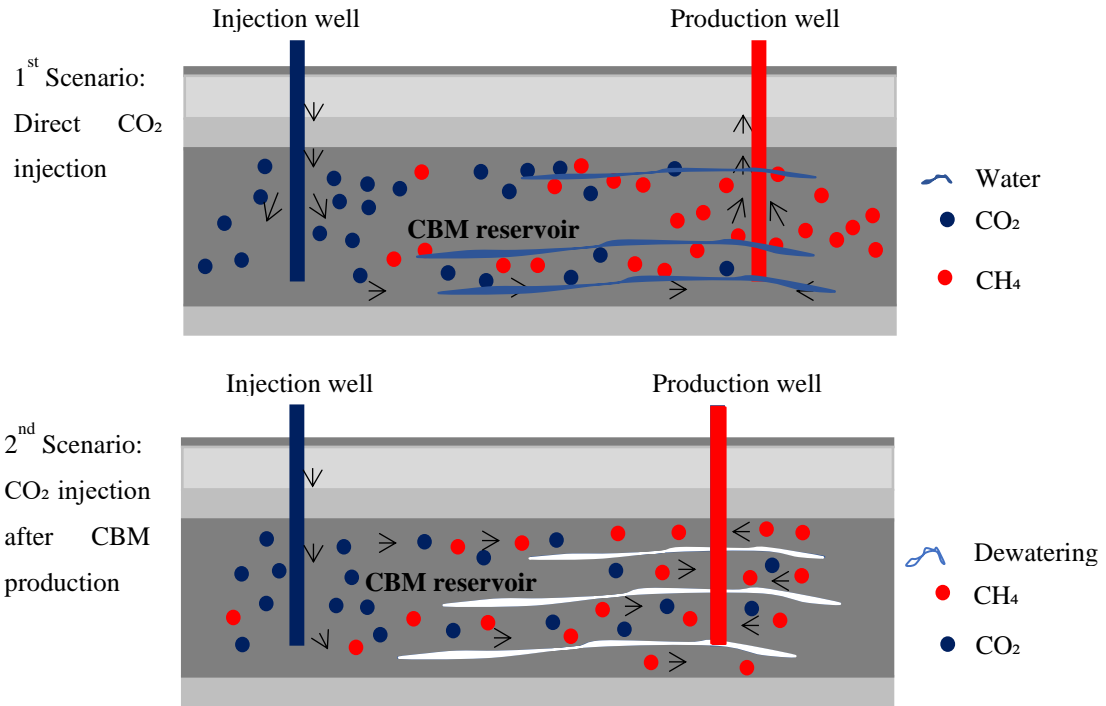


Figure 2 CO<sub>2</sub> injection scenarios for ECBM modified from (Van Bergen et al., 2011)

### 2.2.3 Maceral Effects

In coal, organic matter is referred to as the maceral component, and it is this material that plays a significant role in the adsorption of gases (A. Busch et al., 2003). The feasibility of ECBM recovery is generally determined by evaluating the huminite content of the coal (Godec et al., 2014). As well as its intrinsic properties, huminite also affects the pore structure of coals (Bustin and Clarkson, 1998), and in particular the coal micropores and the pore distribution in coals (Shen et al., 2019). Several studies have shown that there is an association between a high huminite content and a substantial void volume (Rodrigues and Lemos De Sousa, 2002), a larger specific surface area (SSA) (Skoczylas et al., 2019) as well as an increase in adsorption capacity (Kumar et al., 2019). Due to the presence of huminite, coal reacts more effectively to CO<sub>2</sub> injections and swells more readily (Karacan and Mitchell, 2003; Larsen, 2004).

Liptinite is the second type of maceral that affects coal mesopores (Shen et al., 2019). It has been found that liptinite can allow the adsorption of CO<sub>2</sub> to occur due to its ability to promote surface diffusion and act as a medium for gas transportation while adsorbing CO<sub>2</sub> (Karacan and Mitchell, 2003). Huminite and liptinite differ from inertinite because they have more macropores than micropores (Unsworth et al., 1989). Inertinite reduces the apparent surface area of coal due to the presence of macropores (Shen et al., 2019), allowing equilibrium to be reached faster (Keshavarz et al., 2017), as well as causing significant swelling upon CO<sub>2</sub> injection (Larsen, 2004).

#### 2.2.4 Coal Pore Effects

Figure 3 presents the nuclear magnetic resonance (NMR) analysis of pore size distribution curves for coal of various ranks (Qin et al., 2020). In low-rank coal, there are irregularly shaped and poorly connected primary epigenetic pores. Specifically, the pore structure of coal, including pore size distribution, pore volume, specific surface area, pore shape, pore connectivity, and porosity, is essential to fluid migration. Even though the dehydration of lignite to low-rank coal reduces the moisture content and oxygen-to-carbon ratios (Levine, 1993), low-rank coal exhibits a high degree of porosity and low pore compressibility (Oudinot et al., 2017).

A number of studies have shown that the injection of CO<sub>2</sub> will likely cause coal to swell as a result of the CO<sub>2</sub> being injected (Busch and Gensterblum, 2011). Carbon dioxide dissolves in the coal structure and changes the coal pore structure (Battistutta et al., 2010). Moreover, the experiment at low-rank illustrates the complexity of CO<sub>2</sub> injection, especially considering that different types of coal display varying swelling characteristics as a result of CO<sub>2</sub> injection (Anggara et al., 2014). It is crucial that research is conducted into the sorption and transport characteristics of CO<sub>2</sub> in low-rank coal in order to ensure that CO<sub>2</sub> is safely stored.

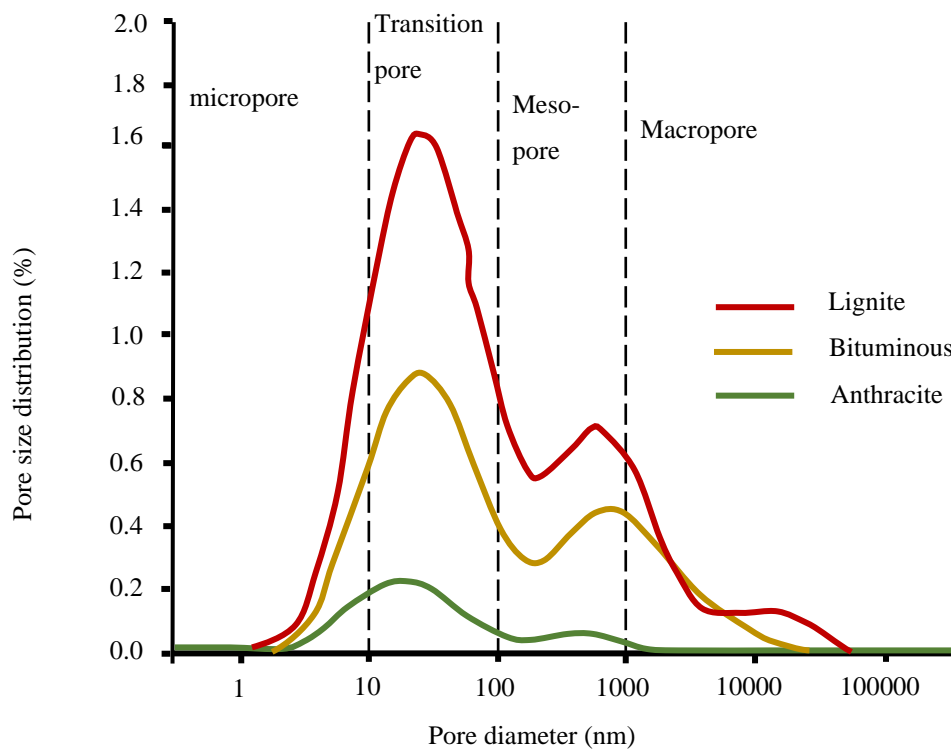


Figure 3 Pore-distributions in different coal ranks as determined using an NMR method. Modified from (Qin et al., 2020)

### 2.2.5 Temperature and Pressure Effects

Experimental adsorption methods are not only influenced by the coal sample's conditions, but also by pressure and temperature settings. CO<sub>2</sub> injected into coal under high pressure was a commonly used arrangement as it improved the efficiency of CH<sub>4</sub> recovery and CO<sub>2</sub> storage (A. Busch et al., 2003; Zhu et al., 2019). A higher pressure results in a higher density of adsorbate, greater surface coverage, and stronger interactions between the adsorbate molecules and the coal surface (Zheng et al., 2019). However, injecting CO<sub>2</sub> under high pressure led to problems such as reduced coal permeability (Wang et al., 2016) and the possibility of over-caprock integrity and leakage (Masum et al., 2022).

The temperature is also a critical factor in adsorption, as an increase in temperature will decrease the kinetic energy of the gas molecules, decreasing the amount of adsorption

that can occur (Zhou et al., 2019a). As the temperature increases, the gas adsorption capacity of the coal matrix decreases, the residual force on the coal matrix surface is reduced, and the bonds between gas molecules and the coal matrix are broken (Abunowara et al., 2020). Therefore, it is detrimental to increase the temperature because it will result in gas desorption rather than adsorption (Hao et al., 2021). In addition, CO<sub>2</sub> injections over 4 MPa at 323 K have a marginal effect on the cumulative desorption of CH<sub>4</sub> gas (Wen et al., 2022).

### 2.3 Adsorption measurement methods

A volumetric approach is commonly used to calculate the CO<sub>2</sub> adsorption in coal (Romanov et al., 2006). Adsorption is assessed using volumetric methods employing variations in the pressure of the adsorbate gas in the sample (Day et al., 2005; Siemons and Busch, 2007; Sudibandriyo et al., 2003; White et al., 2005). A related equation is presented in (Sudibandriyo et al., 2003)

$$\Delta n^{ex} = \left( \frac{1}{RTm} \right) \left( V_{rc} \left( \frac{P_{rci}}{Z_{rci}} - \frac{P_{rcf}}{Z_{rcf}} \right) - V_{void} \left( \frac{P_{scf}}{Z_{scf}} - \frac{P_{sci}}{Z_{sci}} \right) \right)$$

The value of Z is calculated using the equation (Abunowara et al., 2020)

$$Z = 1 + \left( 0.083 - \frac{0.422}{T_r^{1.6}} \right) \frac{P_r}{T_r} + \omega \left( 0.139 - \frac{0.172}{T_r^{4.2}} \right) \frac{P_r}{T_r}$$

$$P_r = \frac{P}{P_c}$$

$$T_r = \frac{T}{T_c}$$

### 2.4 Adsorption Isotherms

Isotherms of adsorption provide information about physical adsorption at equilibrium pressure. The Langmuir, Freundlich, and Temkin methods are commonly used to analyze coal adsorption isotherms. The three methods described above assess different types of adsorptions and generate different types of curves.

#### 2.4.1 Langmuir isotherm model

Based on dynamic equilibrium, the Langmuir method is used in conjunction with type I isotherms (Clarkson et al., 1997). According to this method, results are similar to those observed in experiments (Kumar et al., 2019) since the Langmuir pressure is generally reduced with an increase in moisture concentration (Guo et al., 2015). Langmuir's model has the disadvantage of involving only monolayer adsorption on solid surfaces (Adams, 2014; Montoya et al., 2014). The adsorption used in this method of calculation is (Langmuir, 1918)

$$V = \frac{V_L P}{P_L + P}$$

#### 2.4.2 Freundlich isotherm model

The Freundlich model refers to the heterogeneity of coal surfaces due to the presence of distinct adsorption energies in the formation of multilayers (Mahmoud et al., 2019).  $Q_e$  calculated with detailed as follows (Guarín Romero et al., 2018).

$$Q_e = K_f P C O_2^{\frac{1}{n}}$$

#### 2.4.3 Temkin isotherm model

An adsorption isotherm model is applied to evaluate the adsorption potential of CO<sub>2</sub> on the surface of coal using the Temkin model. Temkin's equation for the isotherm model can be expressed as follows (Mabuza et al., 2022).

$$q_e = \frac{RT}{b_T} \ln(A_T P_e)$$

The linear form of this expression is:

$$q_e = B_T \ln A_T + B_T \ln P_e$$

Where,

$$B_T = \frac{RT}{b_T}$$

## 2.5 Gibbs free energy and surface potential

Adsorption on coal surfaces can be understood based on thermodynamic parameters, such as change in Gibbs free energy ( $\Delta G$ ) and surface potential ( $\Omega$ ) (Du et al., 2021a). The energy released from the adsorbate attaching to the adsorbent surface, otherwise known as the surface potential ( $\Omega$ ) can be determined as (Hao et al., 2021).

$$\Omega = -RT \int_0^P \frac{V}{P} dP$$

The Gibbs free energy ( $\Delta G$ ) is an indicator of the reaction spontaneity and is calculated as (Hao et al., 2021).

$$\Delta G = \frac{\Omega}{V}$$

## 2.6 Adsorption effects

Low-rank coal's maceral content and pore size have a distinct correlation. Coal deposition significantly affects maceral content, whereas coalification has a more significant impact on pore size. Several internal and external factors affect the process of coal porous formation and evolution. The internal factors include coal quality as well as maceral composition. External factors include metamorphism and surface water, which can cause moisture to accumulate within the coal. External factors that affect the pore architecture of coal pore surfaces include their size, surface area, and internal pore structure (Mangi et al., 2020).

Various additional measurement devices may be employed to assess the change in volume within an instant (Romanov et al., 2006). A pressure-based methodology can demonstrate early fracturing and indicate higher gas release levels than non-pressured methods (Pirzada et al., 2018). The increase in adsorption pressure promotes the expansion of the coal matrix, resulting in a reduction in cleat apertures and the closure of pre-existing fractures (Pone et al., 2009). As a preventative measure, this study

analyzes the effect of CO<sub>2</sub> adsorption on coal pores and surfaces under different coal conditions to prevent an error.

Adsorption of nitrogen at low temperatures was used to evaluate the effect of adsorption on coal pores. Micromeritics Instrument Corporation manufactured the surface analyzer and pore-size distribution determiner used for determining the pore parameters of coal samples by nitrogen adsorption at low temperatures. Samples were pulverized into 0.5 mm and then vacuum dried for 6 hours in an oven at 80 Celsius. Following the drying of the coal sample, pressurized nitrogen injection was performed at 77 K. Porous volume and specific surface area was measured using the Brunauer, Emmet, and Teller (BET) method. BET equation to calculates adsorption as follows (Clarkson et al., 1997):

$$\frac{1}{V\left(\frac{P_0}{P} - 1\right)} = \frac{1}{V_m C} + \frac{C - 1}{V_m C} \left(\frac{P}{P_0}\right)$$

The total surface area ( $S_t$ , m<sup>2</sup>/g) can be derived from (Anovitz and Cole, 2015).

$$S_t = \frac{V_m N_{AV} A_{cs}}{M}$$

In contrast, porosity size distribution (PSD) was measured using the Barret, Joyner, and Halenda method (BJH). PSD curves can be analyzed qualitatively to determine dominant pore size, range of pore size, and PSD peak (Nie et al., 2015). The BJH calculation is expressed by (Li et al., 2019):

$$r_m = \frac{2\gamma V_m}{RT \ln(P/P_0)}$$

Coal surface adsorption was investigated using a scanning electron microscope (SEM). This technique is usually used to determine the porous structure of coal samples as well as the degree of pore-fracture (Li et al., 2012; Wan et al., 2015). As part of this study, SEM was employed to analyze pore connectivity as well as cracks with a width of 1-2 μm (Ma et al., 2017). Even though SEM can determine pore size, it has some limitations. Considering that SEM cannot identify uneven surfaces, the sample should be polished before SEM analysis (Harpalani and Schraufnagel, 1990).

## **CHAPTER III**

### **3. CO<sub>2</sub> Adsorption on Low-Rank Coal from Different Area**

#### **3.1 Introduction**

Carbon dioxide storage is one of the alternatives available for reducing carbon dioxide emissions to the atmosphere. In terms of its ability to store CO<sub>2</sub> over a long duration, geological storage is one of the most effective methods. Geological storage has been shown to contain large volumes of CO<sub>2</sub> while providing benefits such as reduced negative impacts and improved oil recovery (AlRassas et al., 2021; Khanal and Shahriar, 2022; Safaei-Farouji et al., 2022; Vo Thanh et al., 2019). Coal seams facilitate the geological sequestration of CO<sub>2</sub> since the carbon dioxide bonds with the coal, resulting in the CO<sub>2</sub> becoming physically trapped (Wahid et al., 2018). The primary mechanism for storing CO<sub>2</sub> in coal seams is adsorption, which accounts for approximately 95-98% of the total storage (De Silva et al., 2012). Moreover, CO<sub>2</sub> causes CH<sub>4</sub> to escape from the coal seam, thus leading to enhanced coal bed methane (ECBM) that is expected to reduce the costs associated with sequestration (Anggara et al., 2016, 2014; Day et al., 2010).

The adsorption capacity of low rank coal can be higher than that of high rank coals (Kolak and Burruss, 2004; Sripada et al., 2018). However, low rank coal has the greatest capacity for water adsorption compared to higher rank coals (Liu et al., 2018). Identifying the possibility of increasing CO<sub>2</sub> storage in coal seams has become an exciting topic due to changes in moisture content (Abunowara et al., 2020; Gao et al., 2019; Hao et al., 2018). It has been established in many studies that there is a difference in storage capacity of CO<sub>2</sub> between dry and wet coal due to moisture content (Chen et al., 2018; Pan et al., 2010; Švábová et al., 2012).

Traditionally, coal powder samples have been used to study the effects of moisture on the adsorption of CO<sub>2</sub> (Abunowara et al., 2020; Gensterblum et al., 2013). Especially in low-rank coals, the powdering process has affected the porous structure (Mangi et



al., 2022). For adsorption experiments using coal powder samples, additional analysis is required due to physical changes causing variations in the amount of gas adsorbed (Anggara et al., 2010). However, a significant disadvantage of using coal powder is that it needs to properly represent the underground storage conditions that occur when coal is compacted. In order to resolve this problem, one possible method is to compare gas adsorption on coal powder and compact coal samples (Kim et al., 2019).

Understanding CO<sub>2</sub> adsorption on coal is challenging not only due to coal conditions but also due to the way it occurs. The adsorption isotherm model describes CO<sub>2</sub> adsorption on coal. Adsorption isotherm models such as Langmuir, Freundlich, and Temkin are widely used to analyze adsorption capacity (Mabuza et al., 2022). There have been only a few publications that report isotherm parameters based on a various of coal sample conditions.

South Sumatra coal has varying moisture contents (Sosrowidjojo, 2013) and is primarily low-rank coal (Amijaya and Littke, 2005). In Indonesia, the South Sumatra coal basin is one of the largest and most significant coal mining areas (Amijaya and Littke, 2005; Belkin et al., 2009). There is the potential for CBM resources from this area to amount to up to 40% of the total potential for coal reserves in Indonesia (Wahid et al., 2018). Researchers in the South Sumatra Basin has evolved from studying CBM to investigating ECBM recovery. Coal samples from the South Sumatra Basin were taken and are being studied for their potential for CO<sub>2</sub> geological storage as well as ECBM recovery (Anggara, 2017; Anggara et al., 2010). It has also been studied whether ECBM can be recovered from the South Sumatra CBM field using numerical simulations (Wahid et al., 2018). Further, South Sumatra coal exhibits heterogeneous coal characteristics, which may influence the adsorption of CO<sub>2</sub> into coal (Afikah et al., 2018). In most of these studies, the adsorption characteristics of coal samples from non-specific regions have been examined. According to the study, there is a significant value in increasing the accuracy of CO<sub>2</sub> adsorption predictions in South Sumatra.

This study aims to comprehensively assess coal characteristics and sample preparation procedures for evaluating CO<sub>2</sub> adsorption capacity, along with an analysis of isotherm

parameters. The progress in identifying the CO<sub>2</sub> adsorption capacity of coal is shown in Figure 4. Three samples were taken from the thickest coal seam in the South Sumatra basin (seam B) from three separate locations (Figure 5). Then, samples were prepared from powdered coal and blocks of coal in dry and raw coal conditions. The study used samples under various conditions with CO<sub>2</sub> adsorption at the maximum pressure of 3 MPa and 318.15 K to examine the possibility of CO<sub>2</sub> storage. CO<sub>2</sub> adsorption in coal in various forms and under different conditions has been studied using the volumetric method. This isotherm parameter was obtained using the Langmuir, Freundlich, and Temkin isotherm models.

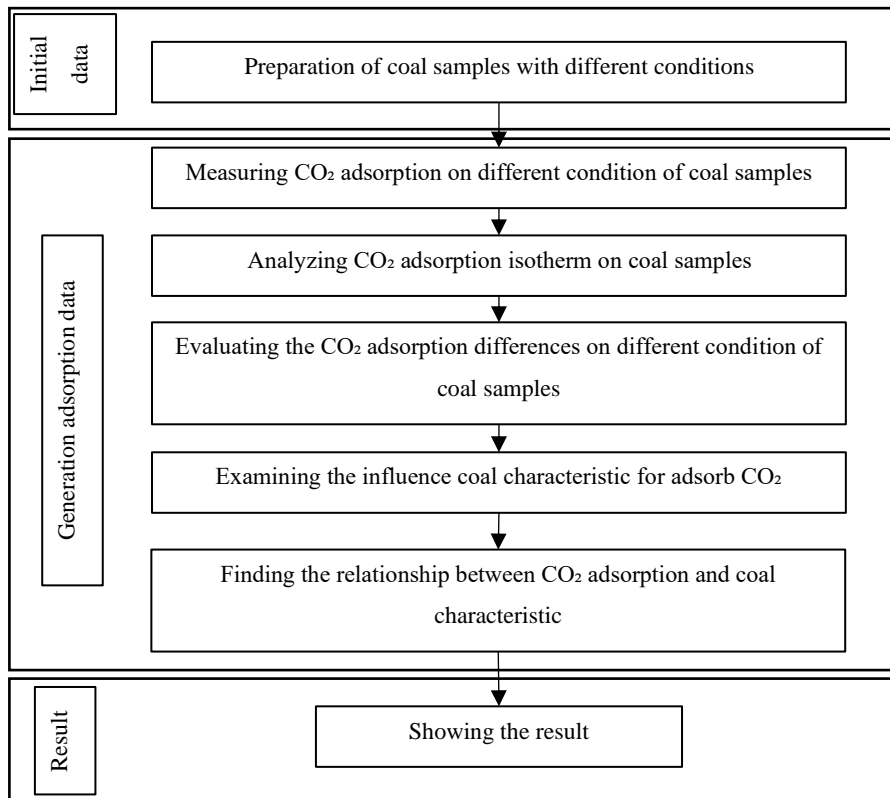


Figure 4 General sketch of CO<sub>2</sub> adsorption on coal with various conditions

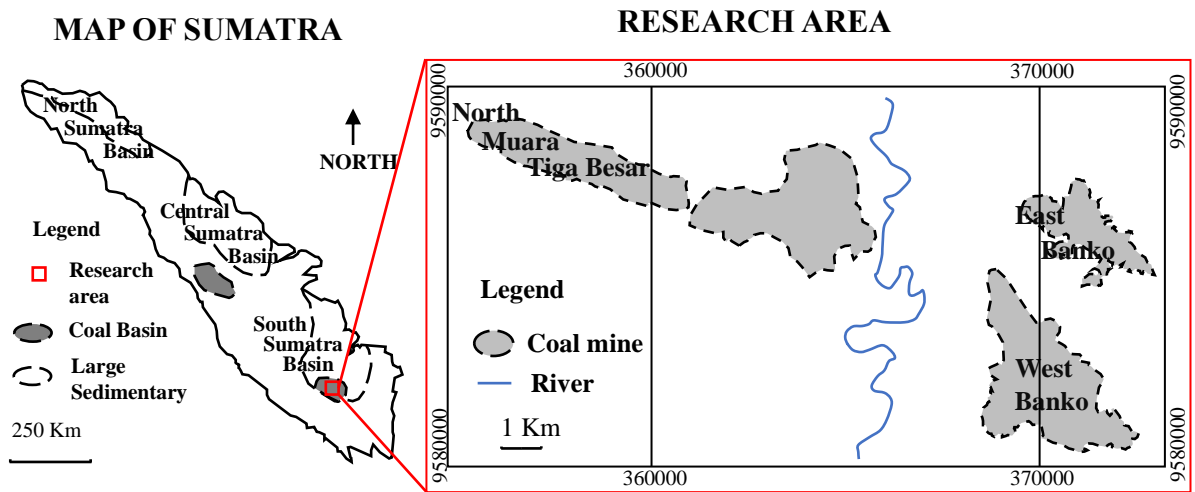


Figure 5 The location of the research area in South Sumatra Basin, Indonesia

### 3.2 Experimental preparation

#### 3.2.1 Coal characteristic measurements

Several samples from the South Sumatra Basin, Indonesia, have been collected and selected coal seams from three areas, namely West Banko (WB), East Banko (EB), and North Muara Tiga Besar (NMTB). Coal samples collected from WB and EB were banded-dull, while coal samples collected from NMTB were dull (Figure 6). The moisture content of coal powder has been determined based on ASTM D3173-73 guidelines by weighing an approximately 1 g of coal at room temperature, then heating it to 105 °C and reweighing the sample after it has cooled down.


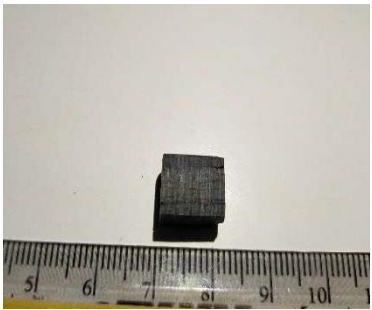






Figure 6 The lithotype of coal samples from (a) WB, (b) EB, and (c) NMTB

### 3.2.2 Adsorption measurements

The coal samples used for the adsorption analysis were obtained by crushing into particles of 0.25 mm (60 mesh), and by creating coal blocks out of irregular-shaped coal and smoothing them with sandpaper to make them uniform in size (Table 1).

Table 1 Coal sample from all coal fields in different coal forms

Sample ID	Coal powder	Coal block
WB		
EB		
NMTB		

The EB coal block sample was found to be more brittle and had more cleats than the other coal block samples. Adsorption experiments were conducted using coal blocks

and 5 grams of coal powder from all coalfields. To remove moisture from coal samples, samples were dried in a vacuum oven for 2-5 hours at 105 degrees Celsius until their weights remained constant. To avoid oxidation or moisture contamination after the coal samples had been dried, they were transferred abruptly to the sample cell. The flowchart below illustrates the steps of the experimental process for identifying CO<sub>2</sub> adsorption on coal (Figure 7).

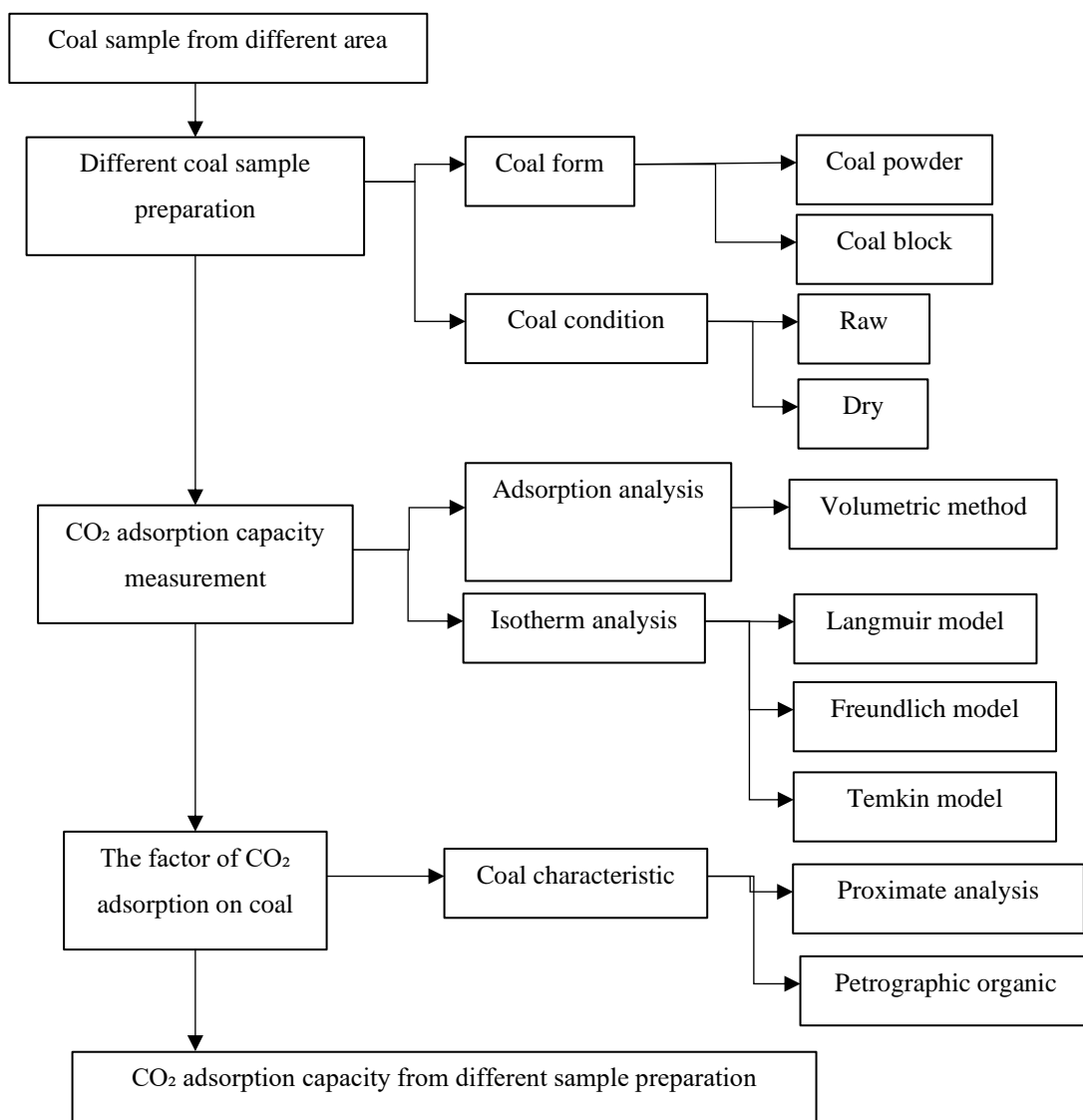


Figure 7 Flowchart of experimental process in this study

### 3.2.3 Experimental setups

CO<sub>2</sub> adsorption on coal was determined by the volumetric method in this study. This study examined coal powder and coal blocks using different equipment. Since conventional equipment only allows a small volume to be analyzed, CO<sub>2</sub> adsorption on coal powder is commonly studied using conventional equipment. Newly manufactured equipment for analyzing CO<sub>2</sub> adsorption on coal blocks in large quantities. It is designed with a curved bottom to allow CO<sub>2</sub> to be absorbed on all sides of the coal block adsorption equipment. For coal powder, the  $V_{rc}$  was 40 cm<sup>3</sup> and  $V_{sc}$  was 75 cm<sup>3</sup> (Figure 8a). The  $V_{rc}$  and  $V_{sc}$  were the same for the coal block, 201 cm<sup>3</sup> (Figure 8.b). The entire setup was maintained at a constant temperature (318.15 K). The  $V_{void}$  was calculated by subtracting sample volume from empty sample cell volume (Andreas Busch et al., 2003).

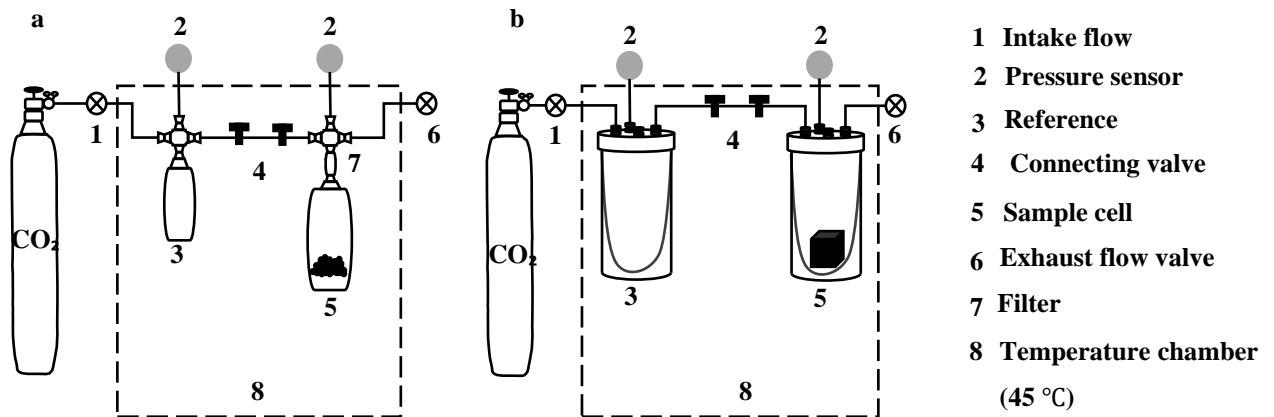


Figure 8 Volumetric method for (a) coal powder and (b) coal block

The sample volume was determined by dividing the mass of coal by the density of coal. In this experiment, adsorption analysis was performed under six pressure steps (0.5, 1.0, 1.5, 2.0, 2.5, and 3.0 MPa) at a temperature of 318.15 K. The CO<sub>2</sub> was then introduced into the reference cell and allowed to equilibrate until there was no change in pressure for 30 minutes. The reference cell was opened as a final step, and the system was allowed to equilibrate for 24 hours without any pressure changes.

### 3.3 Results and Discussion

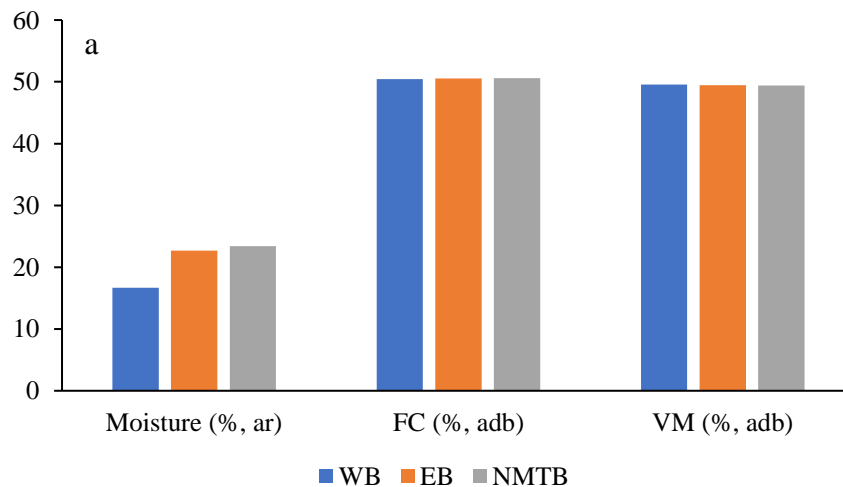
#### 3.3.1 Coal characteristic

In this study, low rank coal samples ranged in moisture content from 16.67% to 23.40% but showed similar fixed carbon content. In Table 2, details of the proximate analysis are presented.

Table 2 Results of proximate analysis of coal samples from different area

Parameter	Sample		
	WB	EB	NMTB
Moisture (% , ar)	16.67	22.68	23.40
ash (% , adb)	2.12	1.09	1.76
VM (% , adb)	49.58	49.46	49.39
FC (% , adb)	50.42	50.54	50.61

Samples from three different areas varied in moisture content, but the fixed carbon and volatile matter values were comparable (Figure 9a). Moisture has a greater degree of change than fixed carbon and volatile matter compared to the lowest values of moisture content, fixed carbon, and volatile matter (Figure 9b). The moisture content of coal from West Banko (WB) was lower (16%, a.r.) than coal from East Banko (EB) (22%, a.r.) and North Muara Tiga Besar (NMTB) (23%, a.r.).



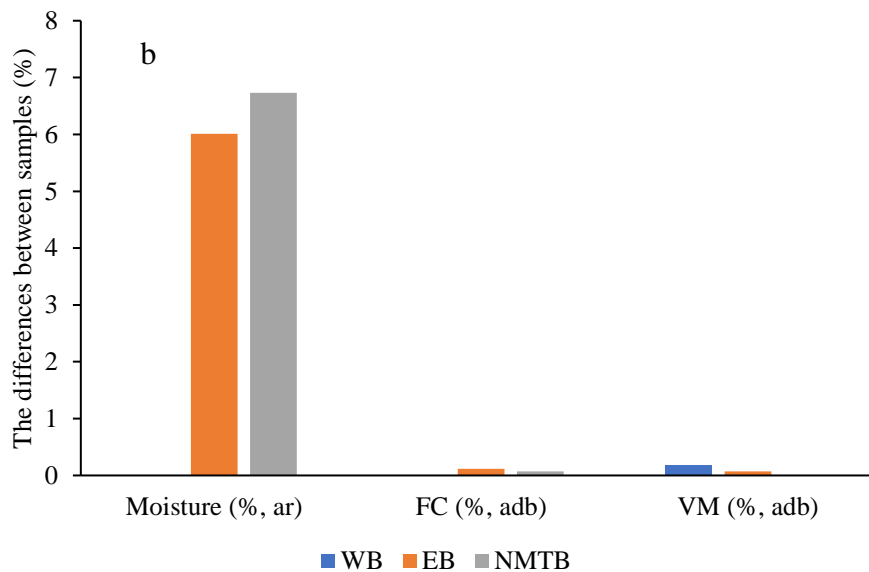


Figure 9 (a) The result of proximate analysis and (b) the differences coal samples with samples contained the lowest value of moisture, fixed carbon and volatile matter

### 3.3.2 CO<sub>2</sub> adsorption measurement

The adsorption of CO<sub>2</sub> over coal forms and moisture content of coal has been studied. The equilibrium time varies depending on the parameters that are being used. Raw coal blocks took the longest time to reach equilibrium, while dry coal powder took the shortest time to reach equilibrium. It is estimated that it takes about 12 hours for raw coal powder adsorption to achieve equilibrium at every pressure step, whereas dry coal powder adsorption takes about 6-10 hours.

Observations have shown that raw coal blocks require 24-30 hours to reach equilibrium at every pressure step, while dry coal blocks require 14-16 hours at every pressure step, according to experimental data. In this study, the amount of gas that has been experimentally determined as adsorbed on coal is called excess adsorption. After adjusting the parameters for coal form and moisture content, it was observed that the adsorption of CO<sub>2</sub> followed a consistent pattern as a result of adjusting the parameters (Figure 10).



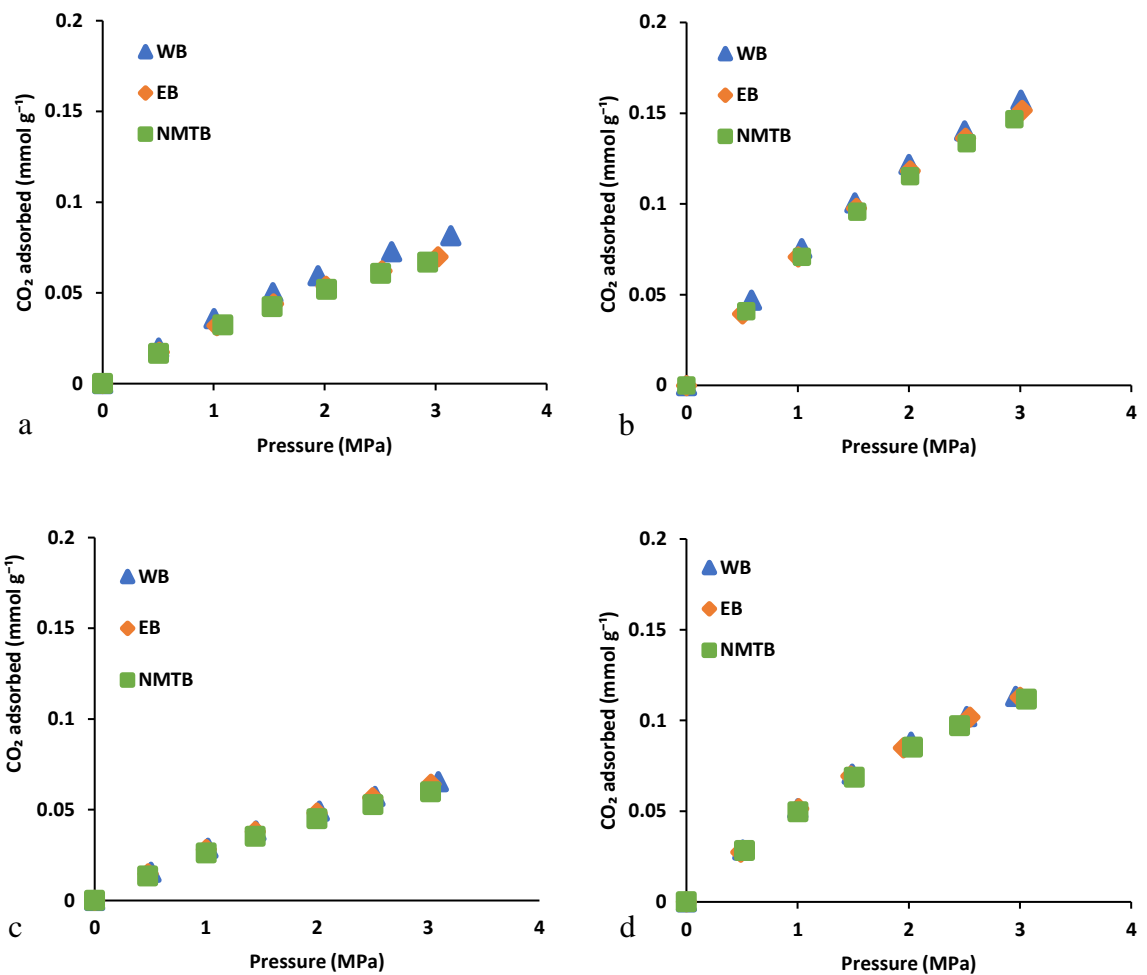


Figure 10 CO<sub>2</sub> adsorption on the difference between coal form and moisture: (a) powder samples under raw conditions, (b) powder samples under dry condition, (c) block samples under raw conditions, and (d) block samples under dry conditions.

In comparison to coal samples that are powdered and dry, there is a significant difference in the amount of CO<sub>2</sub> adsorption that occurs between coal samples that are block coal and coal samples that are raw coal. Based on the results of the study, it can be concluded that the amount of CO<sub>2</sub> adsorption to coal was greater regardless of the method used for preparing the coal as well as the difference in air pressure under all circumstances.

It was found that under raw conditions of 0.5 to 2 MPa, CO<sub>2</sub> adsorption on coal powder was similar in all areas of the experiment. During increased pressure conditions, particularly between 2 and 3 MPa, the region of the WB that had the lowest moisture content exhibited the greatest CO<sub>2</sub> adsorption capacity, followed by the region of the EB that had a lower moisture content than the region of the NMTB when pressure conditions increased.

It is noteworthy that the results obtained from block coal under raw conditions were similar to those obtained from powder coal under raw conditions. Although there was an increase in pressure, it was not as significant as that observed in powder coal. As a comparison, CO<sub>2</sub> adsorption on powder and block coal from the WB area is 1.1 times greater at lower pressures (0.5-2 MPa), and 1.4 times greater at higher pressures (2-3 MPa). There were no significant differences between coal blocks adsorbing CO<sub>2</sub> under raw conditions, which made it difficult to determine whether they were different. In spite of this, CO<sub>2</sub> adsorption measurements at 3 MPa indicate that samples from the WB area have the highest CO<sub>2</sub> adsorption values. The capacity of crushed coal to adsorb CO<sub>2</sub>, depending on the pressure at which it is crushed, can be increased by 1.2 times at 3 MPa.

There was no significant difference in the drying process between coal powder and coal blocks even though the pressure was increased. When CO<sub>2</sub> is adsorbed on powder under dry conditions at 3 MPa, it increases the capacity of the adsorption of CO<sub>2</sub> by 1.9 to 2.2 times. The dry concentration of CO<sub>2</sub> absorbed by coal blocks was much lower than that absorbed by coal powder, which increased only by 1.7 to 1.8 times.

### 3.3.3 Comparing low-rank coal with other countries in CO<sub>2</sub> adsorption

Besides evaluating the adsorption capacity of the coal in the studied area, similar coal ranks from different coal fields in different countries were also evaluated (Table 3). The results of this analysis were compared against those of another sample, which showed a comparable trend. In comparison with other sources of low rank coal that

have been investigated, it can be said that South Sumatra coal has similar characteristics to low rank coal that comes from Malaysia.

As a result of comparing the results at 3 MPa, Malaysian low rank coal has a higher CO<sub>2</sub> adsorption capacity as compared to South Sumatra low rank coal. In these cases, it can be attributed to the lower moisture content of low rank coal from Malaysia (11-13%) (Abunowara et al., 2016) in comparison to coal samples from South Sumatra (16-23%). Considering that drying coal will enhance its ability to adsorb CO<sub>2</sub>, there may be a possibility of increasing the CO<sub>2</sub> adsorption capacity of the study's results through the reduction or elimination of moisture content.

Table 3 Summary of the CO<sub>2</sub> adsorption on low rank under various conditions

<b>Coal sample</b>	<b>Coal form</b>	<b>Experimental temperature</b>	<b>Experimental pressure</b>	<b>Wet CO<sub>2</sub> adsorption capacity (mmol g<sup>-1</sup>)</b>	<b>Dry CO<sub>2</sub> adsorption capacity (mmol g<sup>-1</sup>)</b>	<b>Ref</b>
<b>Bituminous Czech Republic coal samples</b>	Coal powder (2 mm)	318 K and 328 K	0.1-0.8 MPa	0.98	1.2	(Weniger et al., 2012)
<b>High to low volatile bituminous Czech Republic coal samples</b>	Coal powder (0.2 mm)	318K	20 MPa	0.75	1.29	(Švábová et al., 2012)
<b>Subbituminous US coal samples</b>	Coal powder (150-500 μm)	328 K	12 MPa	0.68	0.95	(Romanov et al., 2013)
<b>Subbituminous Malaysian coal samples</b>	Coal powder (2.5-5 cm)	348 K	6 MPa	0.2	0.7	(Abunowara et al., 2020)
<b>Subbituminous China coal samples</b>	Coal core	323.15 K	16 MPa		0.3	(Zhang et al., 2018)
<b>High volatile bituminous Indonesian coal samples</b>	Coal powder (0.25 mm)	318.15 K	3 MPa	0.082	0.17	This study
	Coal block (1x1 cm)	318.15 K	3 MPa	0.065	0.12	

### 3.3.4 Isotherm analysis

Based on experimental data, the least-squares method was used to estimate the Langmuir, Freundlich, and Temkin isotherm models in Excel using the Excel solver function. This was done in order to draw a curve fitting each of these models based on the experimental data (Figure 11).

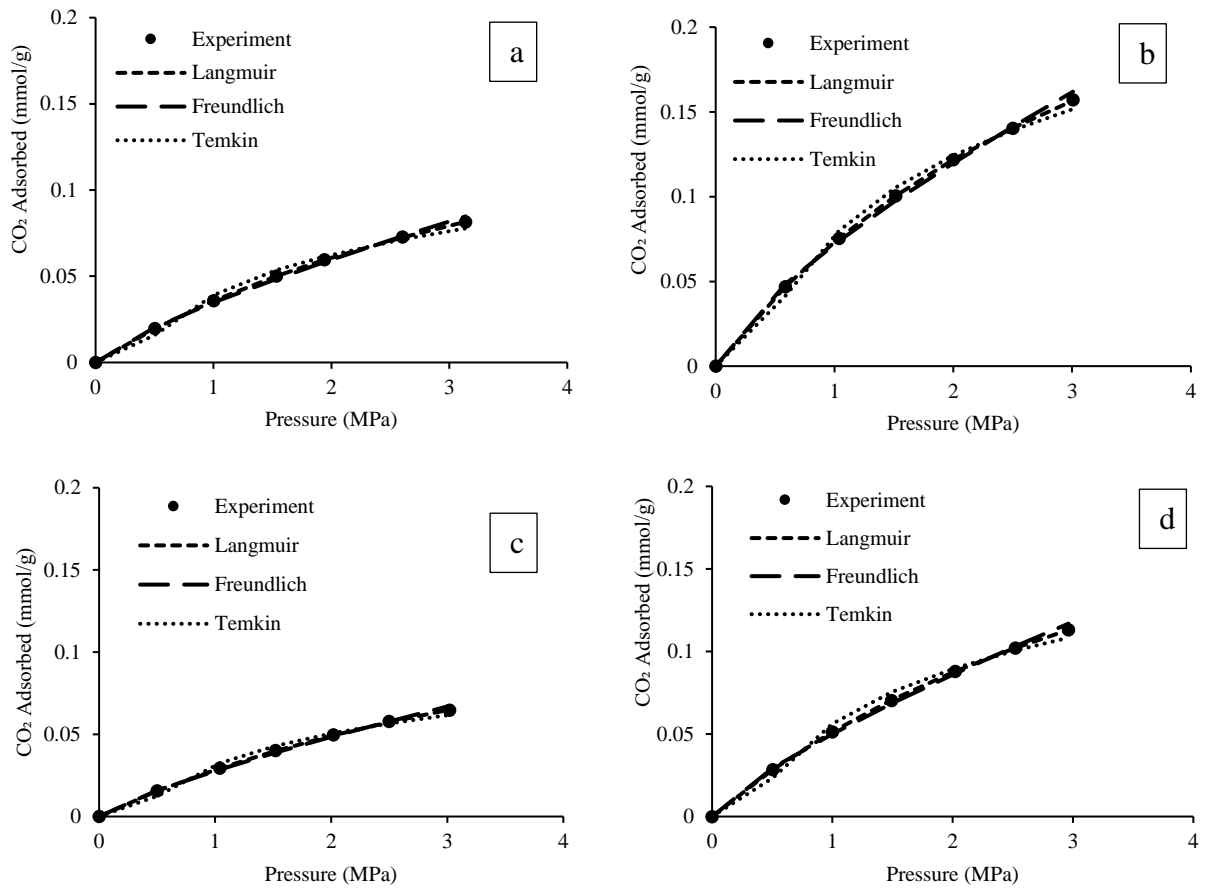


Figure 11 Comparison of different CO<sub>2</sub> adsorption experiment and isotherm fitting curve from WB coal samples with various conditions: (a) powder samples under raw condition, (b) powder samples under dry condition, (c) block samples under raw condition, and (d) block samples under dry condition

There is a correlation between the experimental data and the model data ( $R^2$ ), which indicates that both a Langmuir isotherm model and a Freundlich isotherm model can

be fitted (Table 4), indicating that monolayer and multilayer adsorption of CO<sub>2</sub> has been observed. In the Temkin isotherm model, there is a poor correlation between the experimental data and the model predictions. It is apparent that the Temkin equations are inadequate for describing complex adsorption systems, such as isotherms in the liquid phase. Due to the uncertainty associated with the Temkin equation, it was not possible to accurately assess the potential for coal surfaces to adsorb CO<sub>2</sub>.

Table 4 CO<sub>2</sub> adsorption isotherm model from different area

Area	Coal condition	Isotherm model									
		Langmuir			Freundlich			Temkin			
		VL	PL	R <sup>2</sup>	n	K	R <sup>2</sup>	BT	KT	R <sup>2</sup>	
WB	powder	Raw	0.19	4.08	0.9996	0.75	0.04	0.9990	0.03	3.18	0.9789
		Dry	0.36	3.91	0.9997	0.74	0.07	0.9993	0.07	3.16	0.9867
	block	Raw	0.18	5.27	0.9982	0.80	0.03	0.9984	0.03	3.07	0.9762
		Dry	0.29	4.66	0.9960	0.78	0.05	0.9988	0.05	3.22	0.9796
EB	powder	Raw	0.18	4.77	0.9939	0.78	0.03	0.9987	0.03	3.19	0.9794
		Dry	0.35	4.02	0.9983	0.76	0.07	0.9990	0.06	3.37	0.9841
	block	Raw	0.18	5.27	0.9982	0.80	0.03	0.9983	0.03	3.19	0.9746
		Dry	0.29	4.67	0.9994	0.78	0.05	0.9985	0.05	3.25	0.9784
NMTB	powder	Raw	0.18	4.94	0.9993	0.79	0.03	0.9985	0.03	3.21	0.9778
		Dry	0.35	4.06	0.9993	0.75	0.07	0.9992	0.06	3.27	0.9845
	block	Raw	0.17	5.39	0.9857	0.81	0.03	0.9982	0.03	3.16	0.9742
		Dry	0.28	4.72	0.9998	0.78	0.05	0.9985	0.05	3.15	0.9796

### 3.3.5 Langmuir parameter on CO<sub>2</sub> adsorption on coal

According to Langmuir volume capacity, the results are similar under all conditions, however, there is a discernible difference between the two conditions. The Langmuir volume capacity of the WB coal sample was found to be the highest, while the Langmuir volume capacity of the NTMB coal sample was found to be the lowest (Figure 12).

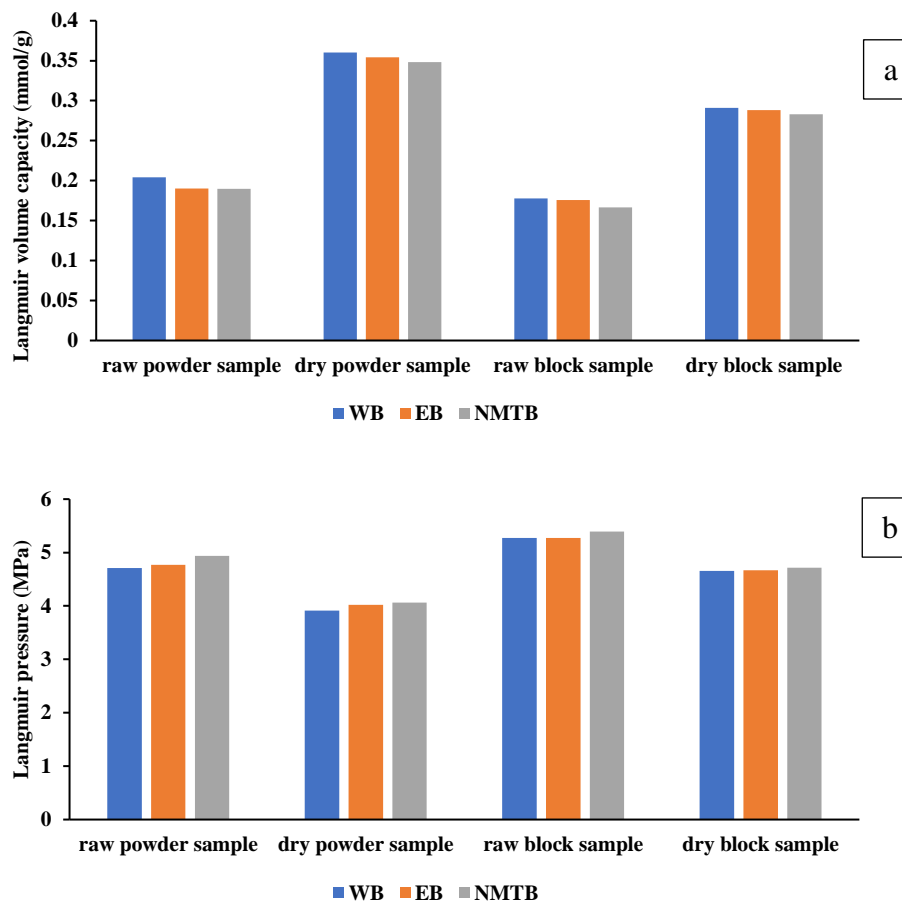


Figure 12 Langmuir parameters for CO<sub>2</sub> adsorption of all measured samples: (a) Langmuir volume capacity and (b) Langmuir pressure.

WB coal sample was compared with other samples on raw and dry conditions and showed that moisture content had a significant effect (Figure 13). Powder coal is more easily differentiated when dry than when raw. The EB coal sample in block form has cleats that allows gas to be more readily absorbed into the sample. Langmuir pressure increased as water content and coal compactness increased. Studies have shown that  $P_L$  and  $V_L$  are reciprocal in coal, especially in low-rank coal (Gensterblum et al., 2013).  $P_L$  in the raw and block condition was higher than in the dry and powder condition. Therefore, CO<sub>2</sub> is absorbed more rapidly in dry and powder conditions than in raw and block conditions.

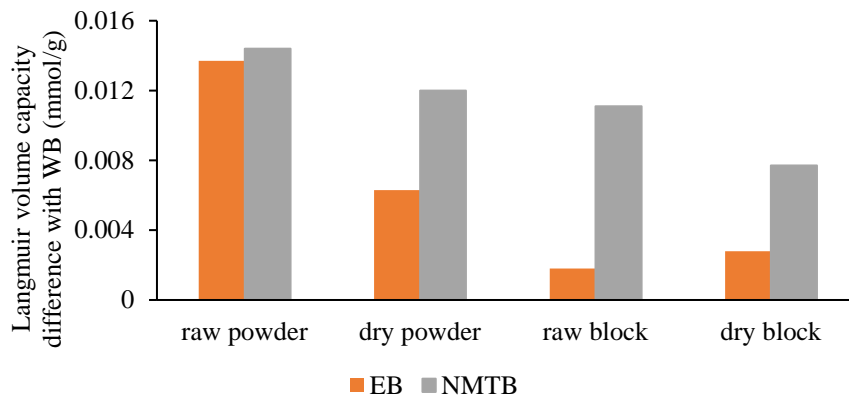


Figure 13 The difference in Langmuir volume capacity on EB and NMTB from WB coal sample

### 3.3.6 Effect of different on CO<sub>2</sub> adsorption capacity on coal

As discussed previously, coal adsorbs more CO<sub>2</sub> when crushed and dried. The drying process increases CO<sub>2</sub> adsorption by 1.7 to 2.2 times meanwhile crushing process increasing CO<sub>2</sub> adsorption by 1.2 times. The discrepancy in Langmuir volumes shows that drying results in higher differences than crushers (Figure 14). Previous research has demonstrated that crushing coal results in an open porosity network (Olajossy, 2017), thus increasing the surface area and producing more adsorption sites for gas, so coal powder has a greater capacity for gas adsorption. However, coal blocks and coal powder have similar adsorption capacities when they are raw. Similarities indicate that despite surface area changes, pore size distribution remains unchanged (Qi et al., 2017), indicating that the changes are not significant. Furthermore, injecting CO<sub>2</sub> into raw coal caused CO<sub>2</sub> molecules to diffuse through or dissolve in the capillary water to access the interior of the coal matrix, resulting in the desorption of some water molecules from coal micropores and mesopores (Sun et al., 2016). Sun (2016) conducted experiments on low-rank coal at varying temperatures and pressures, resulting in the desorption of water from coal surfaces at higher pressures and lower temperatures. Based on the study's temperature and pressure, it was determined that this study had the lowest chance of water desorbing since it was conducted at a lower pressure and higher temperature.



The drying process had a significant effect on the CO<sub>2</sub> adsorption capacity on low-rank coal. Water is a significant component of low-rank coal as the lack of water in the pores causes significant changes to the coal's properties (Olajossy, 2017; Yu et al., 2013). When water content is reduced, water film is lost on the surface of the pore wall as well as in the pore space (Y. Zhao et al., 2018) which increases the surface area of the micropores, thereby enhancing the CO<sub>2</sub> adsorption capability (Yu et al., 2013). The drying process increased the possibility of CO<sub>2</sub> bonding with active sites in coal (Abunowara et al., 2020).

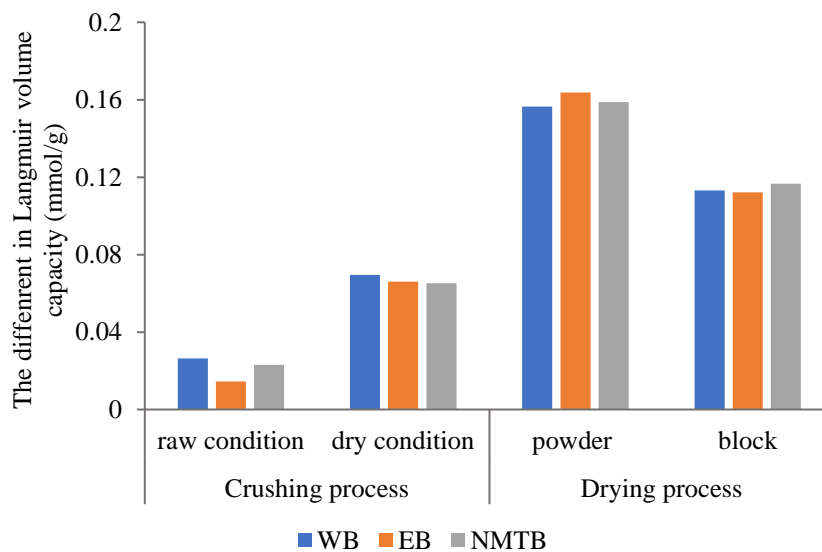


Figure 14 The discrepancy in Langmuir volume due to various coal conditions

### 3.3.7 Effect of coal characteristics on CO<sub>2</sub> adsorption capacity of coal

A correlation analysis has been used in this study (Dutta et al., 2011) to investigate the significant effect of coal characteristics on CO<sub>2</sub> adsorption. In the raw condition, the moisture effect is more significant than the fixed carbon and volatile matter effects (Figure 9). The elimination of moisture content by the drying process resulted in fixed carbon and volatile matter affects more on CO<sub>2</sub> adsorption capacity (Figure 13). CO<sub>2</sub> adsorption capacity increases with the increase in fixed carbon (Dutta et al., 2011), which was also the case for the WB coal sample with the highest fixed carbon resulting

in the highest CO<sub>2</sub> adsorption capacity. CO<sub>2</sub> adsorption capacity increased as volatile matter decreased (Ramasamy et al., 2014). There was a similarity in CO<sub>2</sub> adsorption capacity between EB and NTMB in dry conditions due to EB and NTMB containing lower volatile matter than WB.

### **3.4 Summary and Conclusions**

Following are different coal preparation methods to measure CO<sub>2</sub> adsorption in different areas of the South Sumatra Basin, Indonesia, leading to different CO<sub>2</sub> adsorption capacity.

- In the study of coal samples under different conditions, monolayer and multilayer CO<sub>2</sub> adsorption was observed.
- It was found that the CO<sub>2</sub> adsorption capacity in all four conditions was similar. However, there were a few slight variations where crushed coal could increase CO<sub>2</sub> adsorption capacity by 1.2 times. The fact that powdered coal exhibits a higher capacity for CO<sub>2</sub> adsorption than block coal in raw conditions can be directly attributed to the coal's changing pore structure.
- The CO<sub>2</sub> adsorption capacity of samples from other countries was higher in samples with lower moisture content, indicating moisture is a significant factor in CO<sub>2</sub> adsorption.
- The drying process allowed more accessible sites and increased the capacity for CO<sub>2</sub> adsorption by 1.7 to 2.2 times. Drying increases the ability of fixed carbon and volatile matter to adsorb CO<sub>2</sub>, even if the drying process does not depict a realistic situation.
- WB coal samples are more promising for CO<sub>2</sub> storage because they contain less moisture than coal samples from EB and NMTB.

This study used an experimental technique to compare adsorption capacity where preparations such as drying, and crushing cannot accurately replicate in-situ conditions. Furthermore, it is impossible to dry low-rank coal in natural conditions.

## **CHAPTER IV**

### **4. CO<sub>2</sub> adsorption on different coal seams: A thermodynamics study surface potential and Gibbs free energy**

#### **4.1 Introduction**

CO<sub>2</sub> sequestration in coal is largely determined by the kinetics of adsorption. Different coal seams have different surface areas (Karayiğit et al., 2018) and pore parameters (Wu et al., 2014). The differences would lead to a variety of gas adsorption capabilities. In order to increase the effectiveness of CO<sub>2</sub> adsorption from different coal seams, the accuracy of the process must be considered. Gas adsorption isotherm models are involved to predict adsorption performance and to understand adsorption mechanisms and to design adsorption systems, as well as predictive modelling (Chen, 2015). Regression analysis has therefore been one of the most commonly used tools for identifying the best fit for adsorption models because it quantifies the distribution of adsorbates, analyzes the adsorption system, and verifies the consistency of theoretical assumptions (Ayawei et al., 2017). Simulating adsorption data at constant temperature typically involves Langmuir, Freundlich, and Temkin models. The mathematical relationship between the experimental adsorption isotherm and the model produced by the modelling analysis provides the basis for the operational design and practical application of adsorption systems (Foo and Hameed, 2010). A thermodynamic viewpoint on the adsorption of CO<sub>2</sub> on coal can provide useful information to identify the intrinsic mechanisms of adsorption of CO<sub>2</sub> and to verify its displacement ability. There are several possible explanations, including the adsorption affinity and thermodynamic factors such as Gibbs free energy change and surface potential. The thermodynamics of CO<sub>2</sub> in low-rank coal should therefore be studied in order to gain a comprehensive understanding of this process.

In this study, CO<sub>2</sub> adsorption on low rank coal was determined by using the volumetric method and fitted with the Langmuir, Freundlich, and Temkin model. The statical

evaluation was added in order to understand the closeness of the closest fit adsorption isotherm model to the experimental data. The Henry coefficients, surface potential, and Gibbs free energy change of CO<sub>2</sub> were analyzed based on the adsorption data. This study could provide some theoretical support for CO<sub>2</sub> geological storage in low-rank coal formations.

## 4.2 Theory models

### 4.2.1 Adsorption isotherm model and statistical evaluations

The adsorption of CO<sub>2</sub> was modeled using three well-known empirical adsorption isotherm models. The three isotherm models are the Langmuir, Freundlich, and Temkin models. Calculating the isotherm is as easy as converting the equation to a linear form and utilizing regression to determine the isotherm. An isotherm model is used to describe the adsorption process (Kumar Singh and Anil Kumar, 2018). The statistical analysis of linear regression is one of the best tools for defining the best-fitting relationship, including the quantitative distribution of adsorbates, the mathematical analyses of adsorption systems, and the verification of isotherm models. The statistical goodness-of-fit assessment was performed by using sum square error (SSE) and average relative error (ARE) methods of data analysis. SSE is most commonly used for liquid-phase concentrations, and in these concentration ranges the magnitude and square of the error tend to increase, indicating a better fit for the isotherm (Mane et al., 2007). An analysis of the SSE was performed by (Piccin et al., 2011),

$$SSE = \sum_{i=1}^n (q_{model} - q_{experimental\ data})_i^2$$

The ARE model indicates a tendency to underestimate the experimental data or to overestimate the experimental data in order to minimize the fractional error distribution across the entire concentration range that is being studied (Kapoor and Yang, 1989). This ARE method has been applied by (Piccin et al., 2011),

$$ARE = \frac{100}{n} \sum_{i=1}^n \left| \frac{q_{model} - q_{experimental\ data}}{q_{experimental\ data}} \right|$$

#### 4.2.2 Henry law

Henry's Law applies to adsorption systems at low pressures, where adsorption quantity is proportional to pressure (Tang et al., 2015). Surface molecules on porous media surfaces can be measured through adsorption in Henry's region (X. Zhou et al., 2012). Accordingly, Henry's coefficient ( $K_H$ ) is a measure of the affinity of adsorbate molecules to surfaces of porous media. Adsorption affinity increases with the increase in Henry coefficient (Montoya et al., 2014).  $K_H$  can be calculated at low pressure by fitting the linear region of  $\ln(P/q)$  versus adsorption amount ( $q$ ) (Deng et al., 2012).

$$\ln(P/q) = A_0 + A_1q$$

#### 4.2.3 Gibbs free energy change and surface potential

The thermodynamics of adsorption is useful for understanding the mechanism of spontaneous adsorption (Song et al., 2017). Specifically, the thermodynamic analysis of this work focuses on the change in surface potential and Gibbs free energy. Surface potential serves as an indicator of the amount of isothermal work required to achieve adsorption equilibrium. The Gibbs free energy plays an important role in evaluating adsorption spontaneity.

### 4.3 Experimental section

#### 4.3.1 Experimental process

To determine the adsorption of  $CO_2$ , a volumetric adsorption apparatus was constructed. The experiment pressure was up to 3 MPa at 318.15 K. An explanation of the apparatus used in the experiment is provided in chapter 3. Various isotherm models such as Langmuir, Freundlich, and Temkin were used to fit the  $CO_2$  adsorption isotherm. In order to determine which model has the least error, the adsorption isotherm model was evaluated by a statistical evaluation. For a better understanding of how  $CO_2$  adsorbs on coal, Henry coefficient surface potential and Gibbs free energy are also considered.

### 4.3.2 Experimental samples

Samples were taken from all coal seams in the most potential area, West Banko, South Sumatra Basin, Indonesia (Figure 15). In this study, the size of used coal particle for adsorption experiment ranges from 0.25 mm (60 mesh) particles and coal block (1x1 cm) from different conditions.

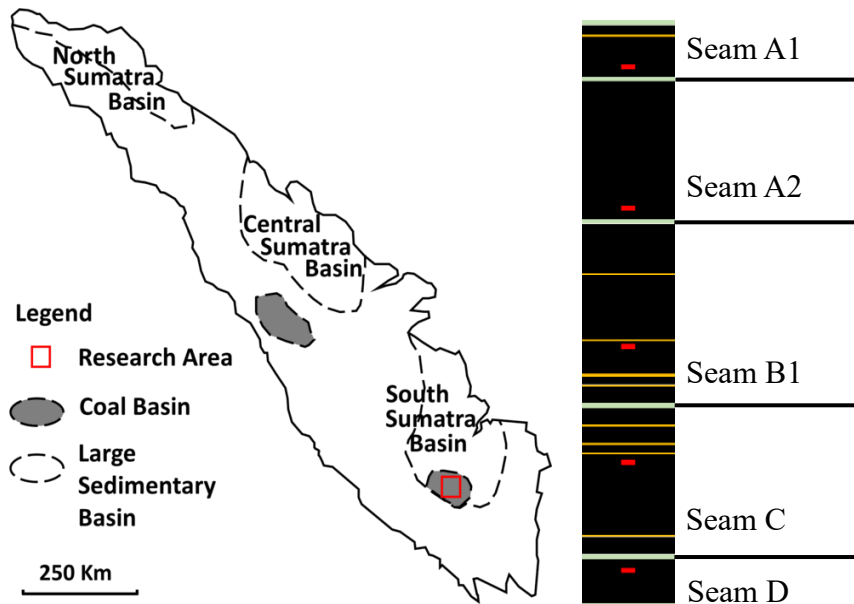


Figure 15 Sample location map of study area: South Sumatra, Indonesia

## 4.4 Results and discussion

### 4.4.1 Coal assay

Table 5 shows the experimental results of proximate analysis samples that were collected from all seams in WB, which thickness ranged from 2.5 m to 10.5 m. On the air received basis, the moisture content of coal samples was relatively high and ranged from 15.39% to 20.11%. The volatile matter (VM) was variable, range from 49.21% to 55.08%, whereas ash content of most coal samples was variable and within the range 1.96 of 2.98. The fixed carbon content was similar, varying from 44.92% to 50.79%. As a result of coal deposition, the coal sample had a low ash yield and no significant marine influences have been detected in this research area (Amijaya and Littke, 2005).

Table 5 Results of proximate analysis of all coal seam from WB area

Coal seam	Thickness(m)	Moisture (% , a.r)	ash (% , adb)	VM (% , adb)	FC (% , adb)
A1	2.5	17.12	1.96	49.80	50.20
A2	8.6	15.39	2.90	55.08	44.92
B1	10.5	16.48	2.53	49.21	50.79
C	8.5	15.18	2.98	50.29	49.71
D	3.6	20.11	1.97	51.66	48.34

#### 4.4.2 CO<sub>2</sub> adsorption on coal

The CO<sub>2</sub> adsorption measurements from different coal forms and different conditions were similar to those in chapter 3. It takes the longest time for raw coal to reach equilibrium, whereas it takes the shortest time for dry coal to reach equilibrium. On raw condition, seam B1 and seam C resulted higher CO<sub>2</sub> adsorption than other coal seams, this condition due to lower moisture and higher fixed carbon than other coal seams. In comparison to CO<sub>2</sub> adsorption at 3 MPa, the drying effect on blocks increased CO<sub>2</sub> adsorption by 1.6 to 1.8 times (Figure 16.a), whereas it was found that the drying effect on powder increased the amount of CO<sub>2</sub> adsorption by 1.9 to 2.1 times (Figure 16.b).

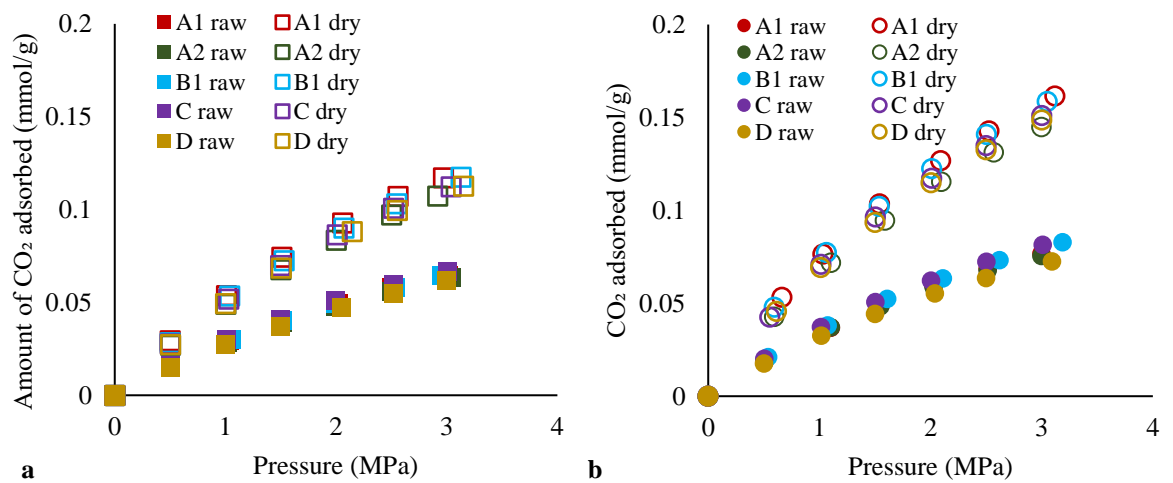


Figure 16 CO<sub>2</sub> adsorption on (a) block samples and (b) powder samples

#### 4.4.3 Simulation of isothermal adsorption of CO<sub>2</sub> on coals

Isothermal adsorption was simulated on coal samples and the results are shown in Figure 17, along with the isothermal parameters obtained for CO<sub>2</sub> in Table 6. In general, the experimental data agree well with the adsorption isotherm model results, and the nonlinear regression coefficients are greater than 0.97.

Table 6 CO<sub>2</sub> adsorption isotherm model of all coal seam from WB area

Coal seam	Coal condition	Isotherm model									
		Langmuir			Freundlich			Temkin			
		VL	PL	R <sup>2</sup>	n	K	R <sup>2</sup>	BT	KT	R <sup>2</sup>	
A1	powder	Raw	0.21	4.68	0.8328	0.80	0.03	0.9990	0.03	3.17	0.9808
		Dry	0.36	3.81	0.9994	0.72	0.07	0.9996	0.07	3.01	0.9914
	block	Raw	0.18	5.27	0.9997	0.80	0.03	0.9983	0.03	3.13	0.9816
		Dry	0.30	4.65	0.9995	0.78	0.05	0.9989	0.05	3.24	0.9797
A2	powder	Raw	0.19	4.69	0.9989	0.78	0.03	0.9987	0.03	3.23	0.9806
		Dry	0.35	4.29	0.9997	0.75	0.07	0.9992	0.06	3.05	0.9855
	block	Raw	0.18	5.31	0.9759	0.80	0.03	0.9984	0.03	3.12	0.9793
		Dry	0.28	4.73	0.9991	0.79	0.05	0.9988	0.05	3.23	0.9767
B1	powder	Raw	0.20	4.68	0.9974	0.77	0.04	0.9988	0.03	3.08	0.9812
		Dry	0.36	3.86	0.9999	0.77	0.04	0.8361	0.07	3.15	0.9869
	block	Raw	0.18	5.27	0.9942	0.80	0.03	0.9987	0.03	3.14	0.9796
		Dry	0.29	4.66	0.9986	0.78	0.05	0.9985	0.05	3.21	0.9778
C	powder	Raw	0.21	4.65	0.9994	0.78	0.04	0.9986	0.03	3.22	0.9799
		Dry	0.36	4.07	0.9995	0.75	0.07	0.9992	0.06	3.39	0.9879
	block	Raw	0.18	5.26	0.9999	0.80	0.03	0.9985	0.03	3.13	0.9805
		Dry	0.29	4.67	1.0000	0.72	0.05	0.9261	0.05	3.23	0.9797
D	powder	Raw	0.18	4.75	0.9996	0.78	0.03	0.9985	0.03	3.19	0.9792
		Dry	0.35	4.13	0.9995	0.74	0.07	0.9994	0.07	3.04	0.9874
	block	Raw	0.17	5.32	0.9996	0.80	0.03	0.9983	0.03	3.11	0.9806
		Dry	0.28	4.69	0.9993	0.78	0.05	0.9983	0.05	3.18	0.9757



To analyze the adsorption data, it is appropriate to employ the Langmuir and Freundlich model. The Langmuir and Freundlich calculated data are significantly correlated with the experimental data. CO<sub>2</sub> experimental data fit well with an isotherm regression with a minimal average relative. All coal samples can be described by the Langmuir and Freundlich isotherm model. This correlation suggests that the Langmuir equation can be used to estimate the maximum sorption capacity corresponding to complete monolayer coverage on coal surfaces.

In some research, it has been found that the Freundlich isotherm regression does not fit well with the experimental data when the pressure is high (Mabuza et al., 2022). Since the study was conducted at a low pressure, the Freundlich isotherm fits the experimental data. For CO<sub>2</sub> adsorption at low pressure, both monolayer and multilayer coverage is demonstrated in this study.

In this study, it has been shown that the Temkin adsorption isotherm model does not adequately explain the experimental data obtained from the studies. It is suggested that the Temkin equation is compatible with multilayer adsorption (Kalam et al., 2021) but it is not suitable for liquid-phase adsorption (Mabuza et al., 2022). To determine the amount of CO<sub>2</sub> that will be absorbed by coal surfaces, Temkin's equation cannot be used.

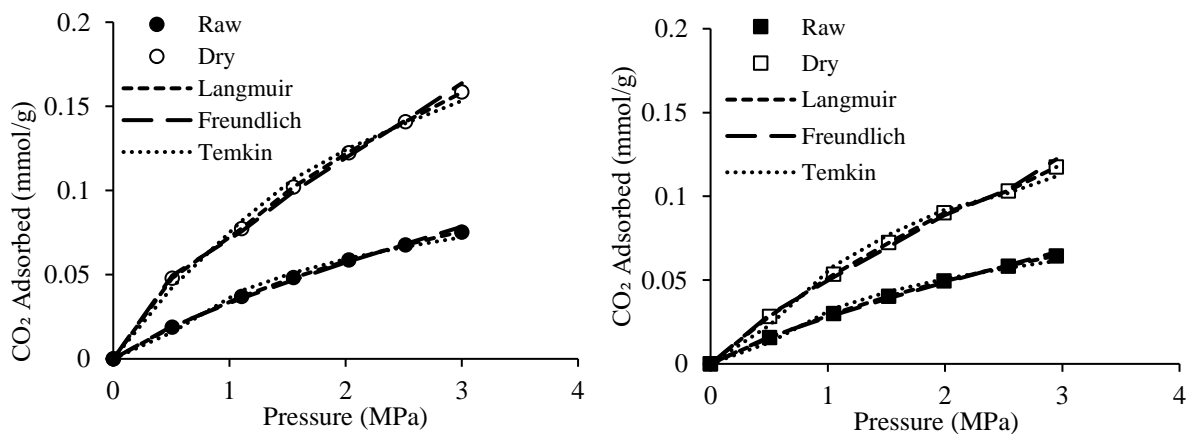


Figure 17 The Langmuir, Freundlich, and Temkin isotherm model fits CO<sub>2</sub> adsorption on B coal seam in raw or dry conditions for (1) powder and (2) block.

#### 4.4.4 Statistical evaluation and model parameters for Langmuir, Freundlich and Temkin

To determine the most appropriate isothermal model, error functions were used instead of the correlation coefficient ( $R^2$ ). SSE and ARE were used for the analysis of the Langmuir, Freundlich, and Temkin isothermal models. There is a difference in the SSE value when the isotherm model is applied to dry conditions compared to when the model is applied to raw conditions (Figure 18). In addition, powder coal has a lower SSE than block coal, which is another significant difference between the two. Overall, the Langmuir isotherm model has the lowest SSE value, while the Temkin isotherm model has the highest SSE value.

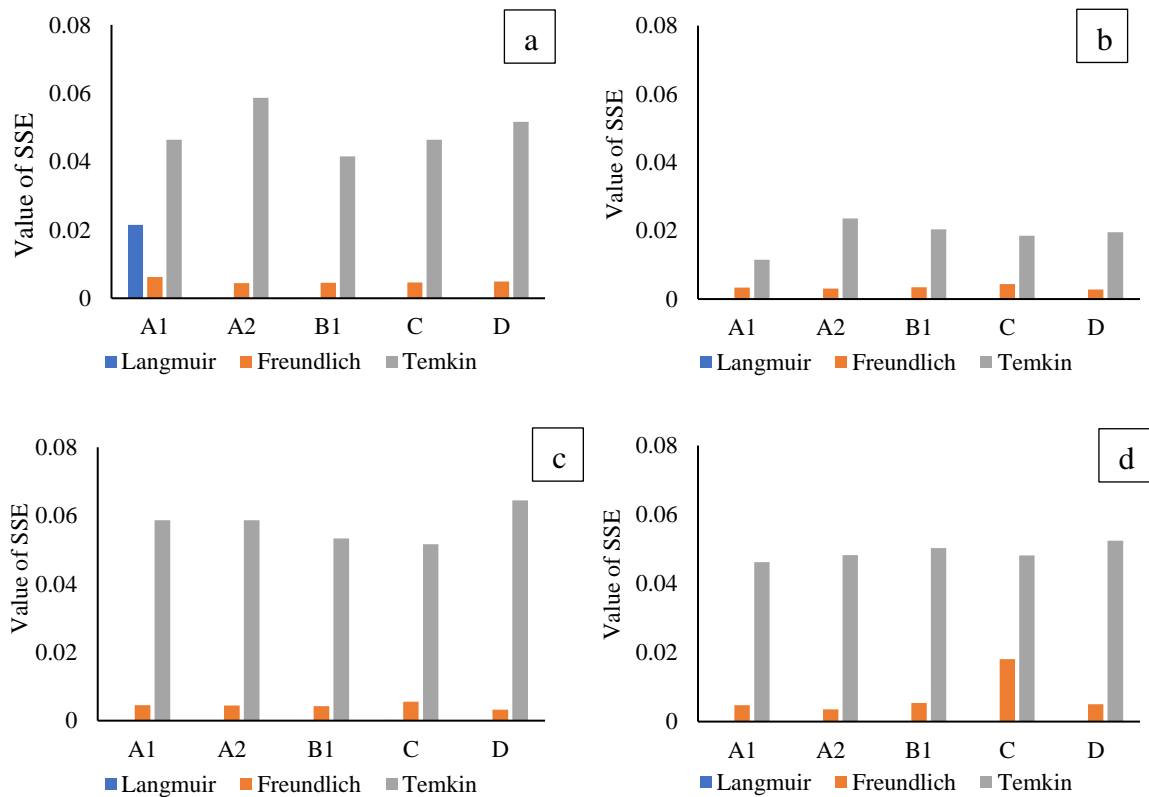


Figure 18 Value of SSE of isotherm models from (a) powder samples under raw condition, (b) powder samples under dry condition, (c) block samples under raw condition, and (d) block samples under dry condition

There is no doubt that in all conditions, the Temkin isotherm model has the largest average relative error (Figure 19). It is likely that an anomaly value indicates that another isotherm model (such as Langmuir or Freundlich) is more appropriate.

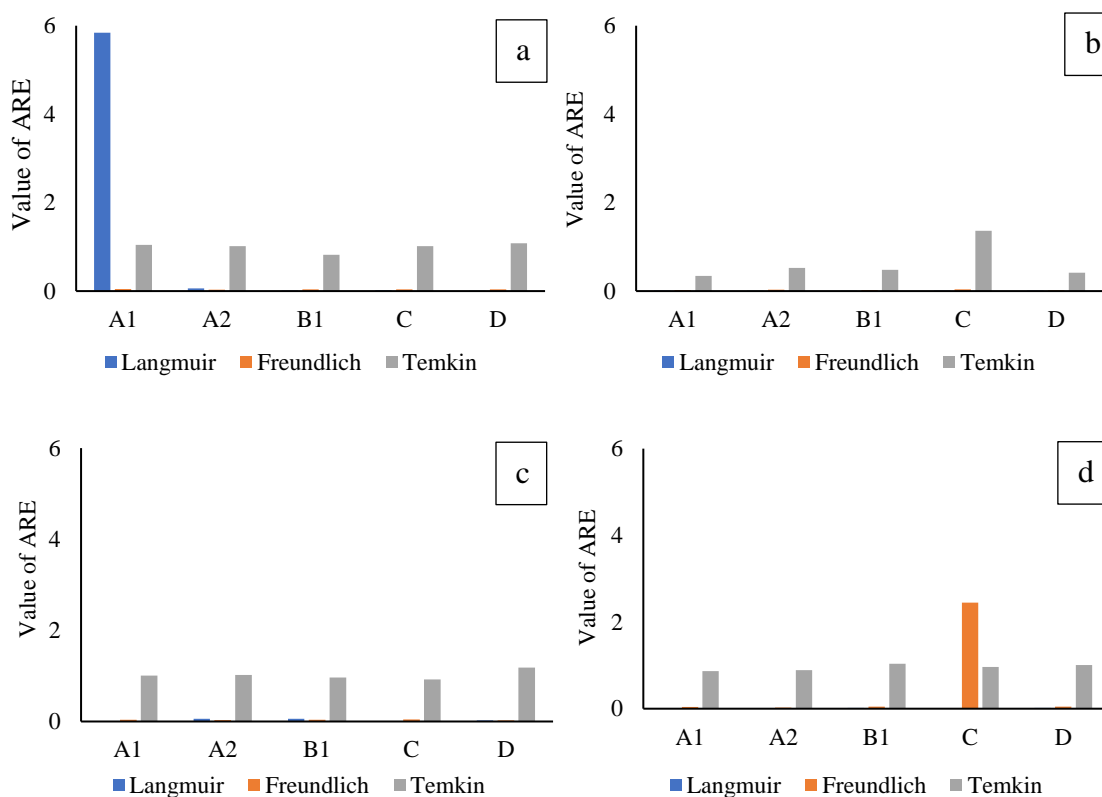


Figure 19 Value of ARE of isotherm models from (a) powder samples under raw condition, (b) powder samples under dry condition, (c) block samples under raw condition, and (d) block samples under dry condition

#### 4.4.5 Henry coefficient of CO<sub>2</sub> on coals

Figure 20 illustrates the results of Henry coefficients ( $K_H$ ) of CO<sub>2</sub> on coal samples. A quadrupole moment on an adsorbent surface results in a stronger electrostatic interaction between the adsorbate molecule and the adsorbent surface, resulting in a greater  $K_H$  value (Song et al., 2017). As a result of this study, the value of  $K_H$  was

determined for all coal conditions as follows: powder dry coal > block dry coal > powder raw coal > block raw coal. The adsorption sites within smaller pores have higher adsorption energies (Xiong et al., 2017). The drying process increases the availability of micropores that can adsorb CO<sub>2</sub> as a result. The coal seams B1 and C have a relatively high adsorption potential due to the fact that their K<sub>H</sub> is larger.

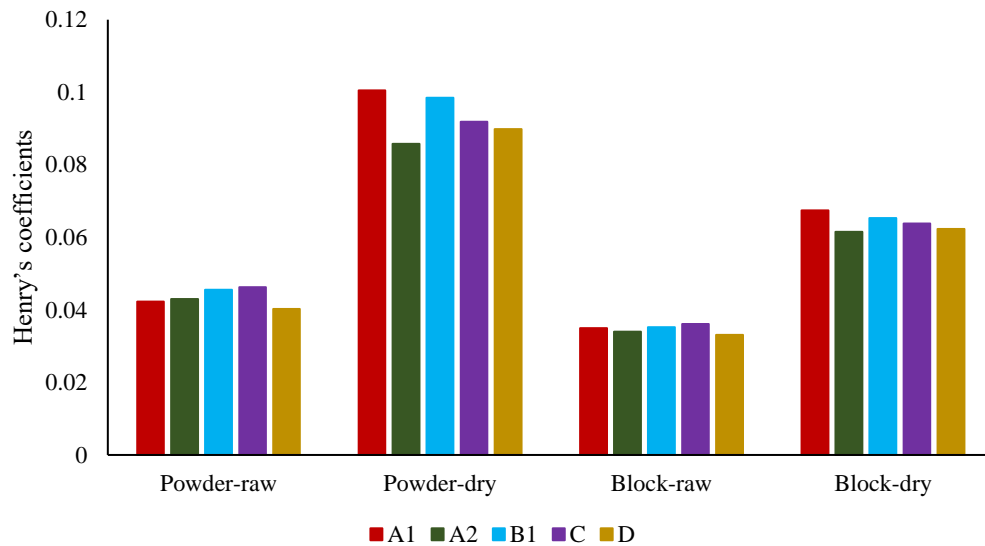


Figure 20 Henry's coefficients of CO<sub>2</sub> on all coal samples

#### 4.4.6 Surface potentials of CO<sub>2</sub> on coals

Figure 21 illustrates the amount  $\Omega$  of CO<sub>2</sub> that was obtained under four different conditions. It is obvious from the graph that  $\Omega$  values reflect negative values. In situations where the pressure approaches zero, the value of  $\Omega$  approaches zero. A continuous increase in pressure has been accompanied by a continuous increase in the absolute values  $\Omega$  of CO<sub>2</sub>. Due to the high pressure, more isothermal work is required to load adsorbate molecules into the pore structure. As a result, the loading of adsorbate increases  $\Omega$ . Figure 21 indicates that there is a difference between dry and raw conditions, in which the dry condition has a higher value of  $\Omega$ . When it comes to raw coal, powder coal has a higher  $\Omega$  than block coal. In raw coal, seams B1 and C were

higher on the  $\Omega$  than other seams in the area. Thus, seams B1 and C are more able to load CO<sub>2</sub> than other seams.

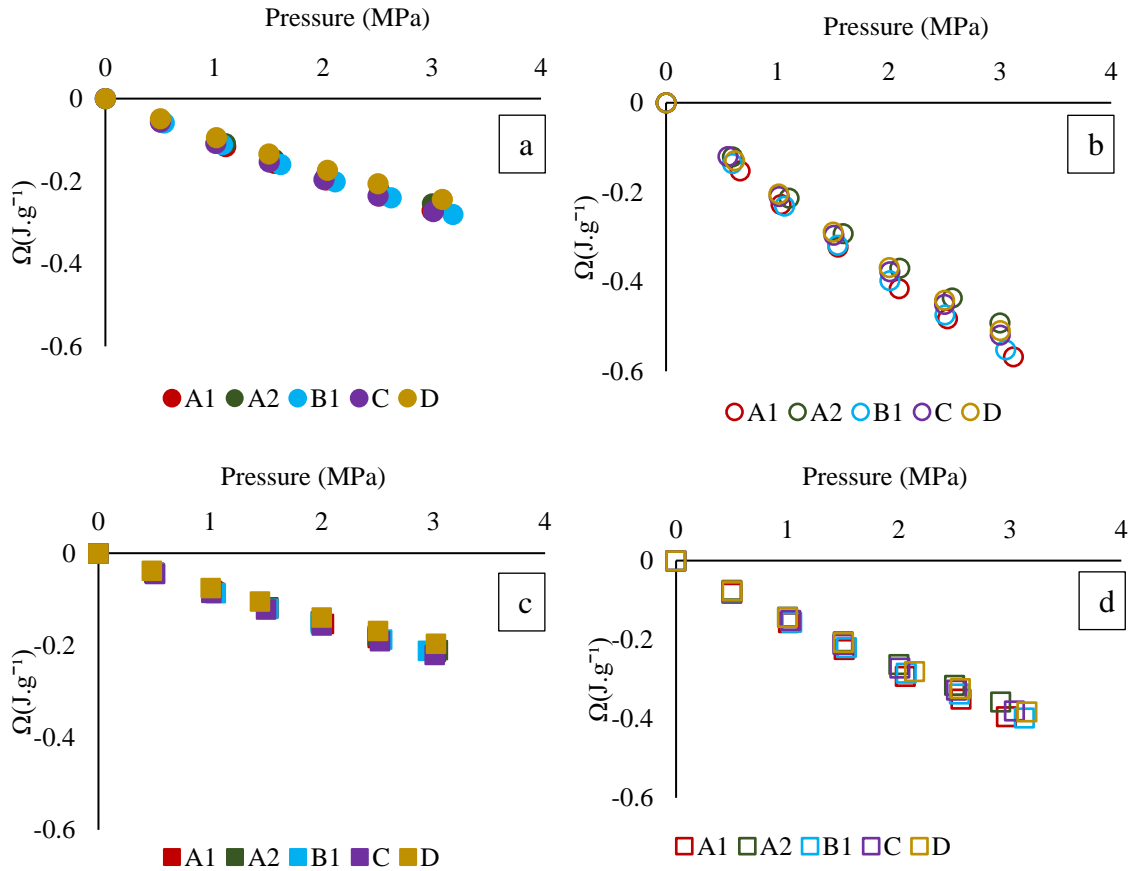


Figure 21. The surface potentials of CO<sub>2</sub> under four different conditions are presented here: (a) powder-raw, (b) powder-raw, (c) block-raw, and (d) block-dry

#### 4.4.7 Gibbs free energy changes of CO<sub>2</sub> on coals

Gibbs free energy is the increase in free energy of an adsorption system when temperature and pressure are constant (L. Zhou et al., 2012).  $\Delta G$  values are all negative, indicating that CO<sub>2</sub> adsorption occurs spontaneously on coal samples (Du et al., 2021b). In general, as the pressure of CO<sub>2</sub> rises, the  $\Delta G$  of CO<sub>2</sub> increases. In order to improve the spontaneity of the adsorption process, high pressure is applied to the sample and promotes adsorption. An illustration of the value of this  $\Delta G$  is shown in Figure 22. As

a result of the experiment, it can be concluded that drying increases spontaneity. As a result of the high moisture levels present in coal, there is a weakening of the physical bond between the individual coal molecules and the molecules of CO<sub>2</sub>. In dry conditions, the uptake of gas increases spontaneously with a pressure increase, but in moist conditions  $\Delta G$  changes from dissolved to adsorbed, weakening spontaneity (Li et al., 2015). In raw condition, powder coal has higher  $\Delta G$  of CO<sub>2</sub> than block coal. In addition, powdering facilitates spontaneous adsorption more than coal blocks, which makes CO<sub>2</sub> adsorption easier. The results demonstrate that  $\Delta G$  in different coal conditions shows a similar trend. Although the coal sample originated from a different coal seam, its characteristics are similar. Some coal seams have a higher potential for CO<sub>2</sub> adsorption than others. As raw coal powder, seam A1 has a higher  $\Delta G$ , but statistical evaluation shows that seam A1 has a large error.

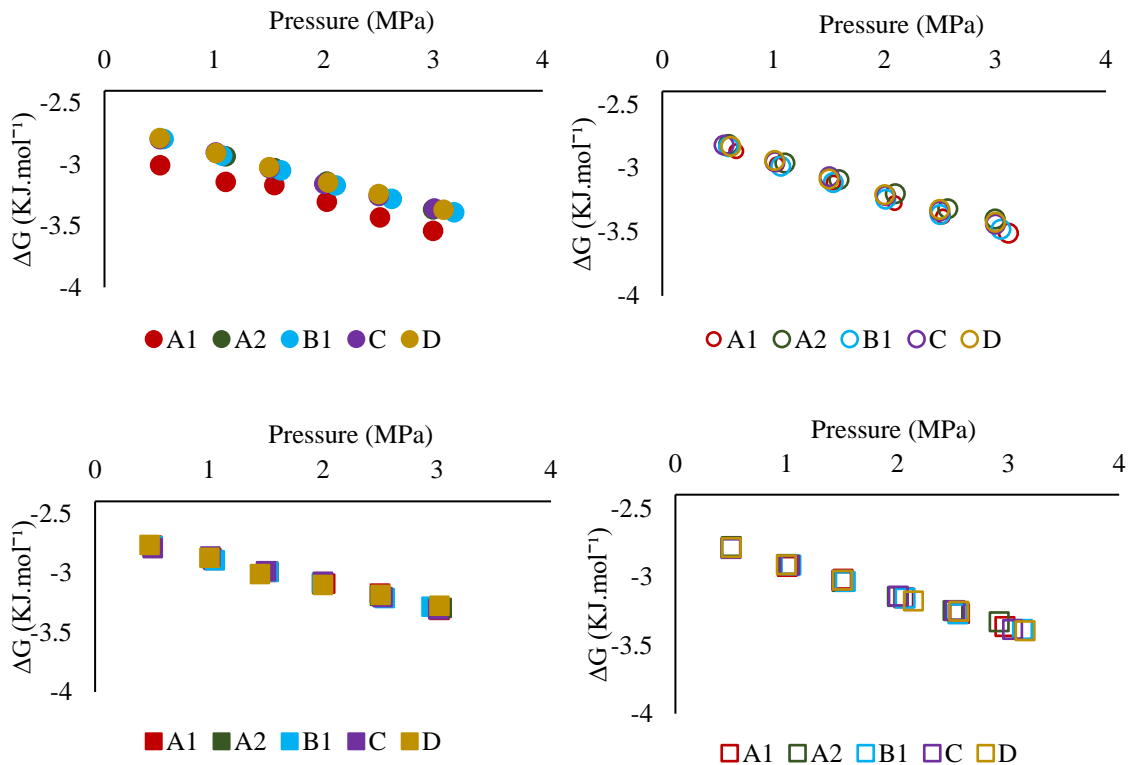


Figure 22 The Gibbs free energy of CO<sub>2</sub> under four different conditions are presented here: (a) powder-raw, (b) powder-raw, (c) block-raw, and (d) block-dry

## 4.5 Conclusions

An analysis of CO<sub>2</sub> adsorption has been conducted on low rank coal from five coal seams in West Banko, South Sumatra. Seam B1 and seam C resulted in higher CO<sub>2</sub> adsorption than other coal seams, due to lower moisture content and higher fixed carbon. As compared to CO<sub>2</sub> adsorption at 3 MPa, the drying effect on blocks increased CO<sub>2</sub> adsorption by 1.6 to 1.8 times, while the drying effect on powder increased CO<sub>2</sub> adsorption by 1.9 to 2.1 times. The Langmuir, Freundlich, and Temkin isotherm models were fitted to experimental data to gain a better understanding of how CO<sub>2</sub> adsorbs on coal. Statistical evaluations such as SSE and ARE were used to validate the most accurate fitting adsorption model. Considering that the experiment was conducted at low pressure, Langmuir and Freundlich are the most accurate adsorption models, as they show CO<sub>2</sub> adsorption on both monolayers and multilayers.

Based on the results of the experiment, KH values were determined for powder dry coal > block dry coal > powder raw coal > block raw coal. Dry coal has a higher KH value than raw coal because the drying process increases the availability of micropores that are capable of adsorbing CO<sub>2</sub>. The drying process increases not only micropore availability, but also surface potential and Gibbs free energy. Under all conditions, CO<sub>2</sub> adsorption on coal is feasible and spontaneous. CO<sub>2</sub> adsorption into low rank coal was facilitated and made more spontaneous by the drying process. The present chapter indicates that despite the similarity of coal samples under all conditions, moisture is not the only factor affecting CO<sub>2</sub> adsorption. Seam B1, for example, has a higher moisture content than seam C, but has a higher fixed carbon content than seam C, resulting in a similar CO<sub>2</sub> adsorption capacity. Seams B1 and C are more suitable for storing CO<sub>2</sub> due to their coal properties.

## **CHAPTER V**

### **5. The Effect of CO<sub>2</sub> Adsorption**

#### **5.1 Introduction**

Sequestration of CO<sub>2</sub> by coal is a potential process for reducing CO<sub>2</sub> emissions, but the effect of adsorption is crucial (Battistutta et al., 2010). However, despite the common use of adsorption isotherm models, the results will vary depending upon the adsorbents and gas used (Guarín Romero et al., 2018; Hao et al., 2021). Various studies have found a correlation between gas adsorption and coal compositions (Anggara et al., 2016, 2014; Dutta et al., 2011; Laxminarayana and Crosdale, 1999). The lithotypes of coal and maceral were investigated in order to determine whether adsorption affects coal structure during adsorption (Karacan and Mitchell, 2003; Liu et al., 2020). Different lithotypes have different porosity characteristics, resulting in different CO<sub>2</sub> adsorption capacities (Lamberson and Bustin, 1993; Mastalerz et al., 2012).

The low rank coal can be divided into five lithotypes which are bright coal, banded bright coal, banded dull coal, dull coal and fibrous coal (Diessel, 2012). It is generally the fibrous coals that have the smallest micropore volumes and the bright coals that have the largest micropore volumes when it comes to low rank coals (Clarkson and Bustin, 1999, 1996). Gas sorption rates and the number of pores also correlated with maceral content, but these relationships were different for coals from different sources (Kiani et al., 2018).

In addition to providing a fundamental understanding of how gas moves through coal in different coal form and conditions, the relationships developed in this study have substantial implications for coal structure prediction. Pore/fracture morphology, including pore size distribution, pore volume, specific surface area, pore shape, and porosity, are all analyzed in order to understand the mechanisms of gas migration in coal seams. For the safe storage of CO<sub>2</sub>, it is critical to know the characteristics of CO<sub>2</sub> sorption and transport in low rank coals.



## 5.2 Experimental work

A total of eight coal samples from different areas and coal seams were collected and analyzed under a variety of conditions and in a variety of forms. As a result of the adsorption of CO<sub>2</sub> on all samples, organic petrography, low temperature nitrogen, and scanning electron microscopy (SEM) were used to study their effects.

### 5.2.1 Organic petrography

Organic petrography was performed by crushing the samples into small particles. This was followed by mounting them in polyester resin, desiccating them for 12 hours, and polishing one of the flat surfaces of the sample. This polished coal sample was examined under a reflecting light microscope in order to determine the maceral and huminite reflectance of the sample. In the maceral analysis for each sample, 550 points were counted per sample (Figure 23).



Figure 23 Reflected light microscope

In accordance with ASTM D2798-06 guidelines, 50 huminite points were analyzed to determine huminite reflectance. The reflectance of huminite can also be determined by its volatile matter value (Rice, 1993).

$$R_0(\%) = -2.172 \times \log (VM_{daf}) + 5.092$$

### 5.2.2 Low pressure nitrogen adsorption (LTNA) isotherm and pore shape

The morphology of macropores and mesopores was determined using low-pressure N<sub>2</sub> adsorption at 77°K. The Figure 24 illustrates five different types of hysteresis loops along with their relationship to pore forms (De Boer, 1958). There are four types of hysteresis: type A corresponds to cylindrical pores; type B corresponds to slit-shaped pores; type C and D correspond to wedge-shaped pores; and type E corresponds to bottleneck pores (Nie et al., 2015).

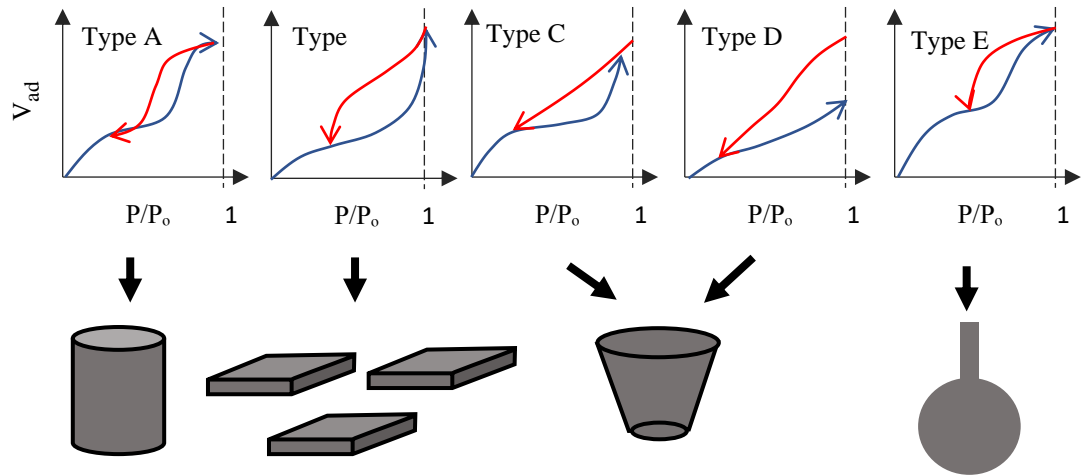


Figure 24 Hysteresis loops and their corresponding pore shapes

There are also different types of coal pores based on their connectivity, including passing pores, interconnected pores, dead-end pores, and closed pores (Figure 25). There is a significant influence on gas adsorption, desorption, and diffusion in coal that is attributed to passing pores, interconnected pores, and dead-end pores.

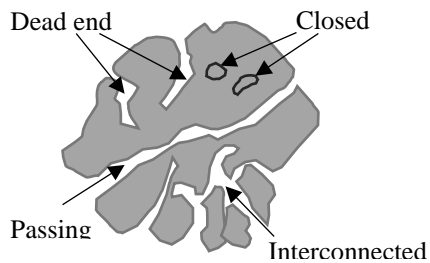


Figure 25. Types of pores

It is proposed that pores be classified as follows by the International Union of Pure and Applied Chemistry (IUPAC) into three main types: macropores ( $\geq 50$  nm in diameter); mesopore or transitional pores (2-50 nm in diameter); nanometers in diameter); mesopores (2-4 nm in diameter); and micropores ( $\leq 2$  nm in diameter) (Zou et al., 2013).

### 5.2.3 Scanning Electron Microscopy (SEM)

The use of SEM has become a common mode of observation of coal pore images and pore fractures in coal reservoirs over recent years (Li et al., 2012; Liang et al., 2020). In order to perform SEM analysis on coal samples, the first step is to place the samples into the system and vacuum them (Figure 26). Then adjust the magnifying, focusing, and acceleration voltages. The system was controlled by a SEM operating system running on Windows XP. SEM is used to evaluate changes in coal structure as a result of drying processes and CO<sub>2</sub> adsorption.

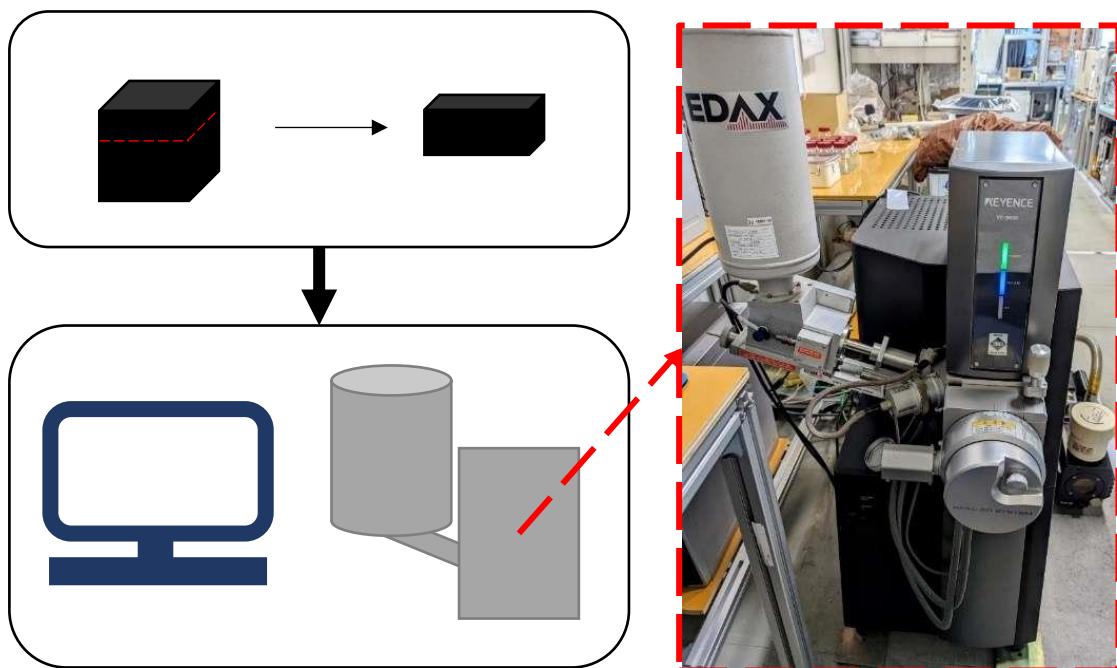


Figure 26 The SEM apparatus

### 5.3 Results and discussion

#### 5.3.1 Coal assay

This Table 7 summarizes the experimental results for lithotypes, petrography, and huminite reflectance ( $R_o\%$ ). Coal samples were mostly banded dull, with only one sample characterized as dull. It was found that huminite content ranged from 52% to 64.8%, liptinite content varying from 18.95% to 31.09%, inertinite ranged from 10.91% to 21.27%, and mineral matter accounted for from 1.09% to 3.27%. Thermal maturity as a percent of  $R_o\%$  ranged from 0.37 to 0.50 (average 0.47), which indicates that the coal is low rank.

Table 7 The experimental data results of lithotypes, petrographic and reflectance ( $R_o\%$ )

	Sample	Lithotype	Total Huminite (%)	Total Liptinite (%)	Total Inertinite (%)	Mineral Matter (%)	$R_o\%$
Different area	WB	Banded dull	64.43	20.69	13.43	1.45	0.49
	EB	Dull	58.92	25.95	12.07	3.06	0.50
	NMTB	Banded dull	52.00	24.73	21.27	2.00	0.50
Different coal seams	A1	Banded dull	63.45	23.45	11.09	2.00	0.49
	A2	Banded dull	56.18	22.36	18.00	3.27	0.37
	B1	Banded dull	64.80	18.95	13.90	2.35	0.50
	C	Banded dull	55.09	31.09	10.91	2.91	0.48
	D	Banded dull	55.82	27.82	15.27	1.09	0.45

According to the results, all coal samples are similar with a few minor differences. Samples from EB were identified as dull coal exhibiting a higher mineral matter content than samples from WB and NMTB, which were identified as banded dull coal. Organic petrography analysis has revealed that the coal sample contains a mineral that may block coal pores and fractures (Figure 27). The presence of minerals can also reduce gas adsorption capacity due to the filling and blocking of pores, cleats, fracture

systems, and a reduction of micropore surface area caused by inherent and extraneous minerals (Kumar et al., 2019; Mangi et al., 2020).

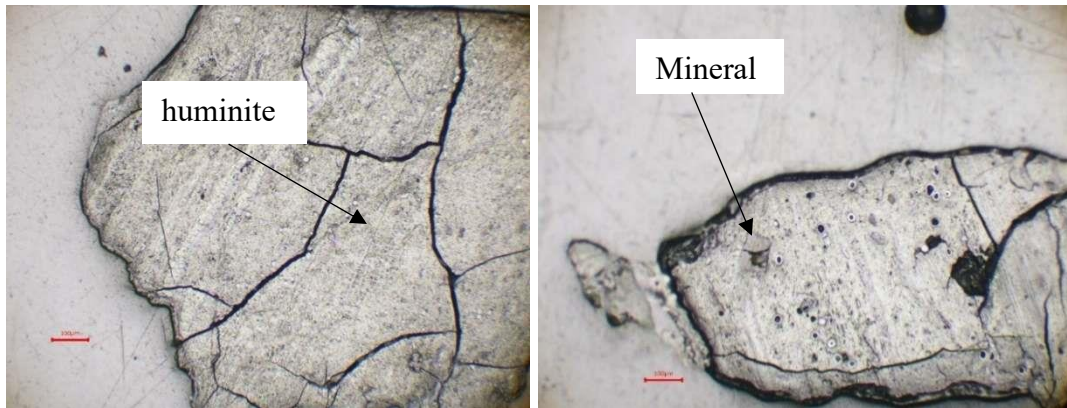


Figure 27 Huminite and mineral on coal sample on image under white light

There is the highest huminite content in the WB region, the highest liptinite content in the EB region, and the highest inertinite content in the NTMB region (Figure 28a). The highest concentration of huminite is found at seam B1, the highest concentration of liptinite is found at seam C, and the highest concentration of inertinite is found at seam A2 (Figure 28b).

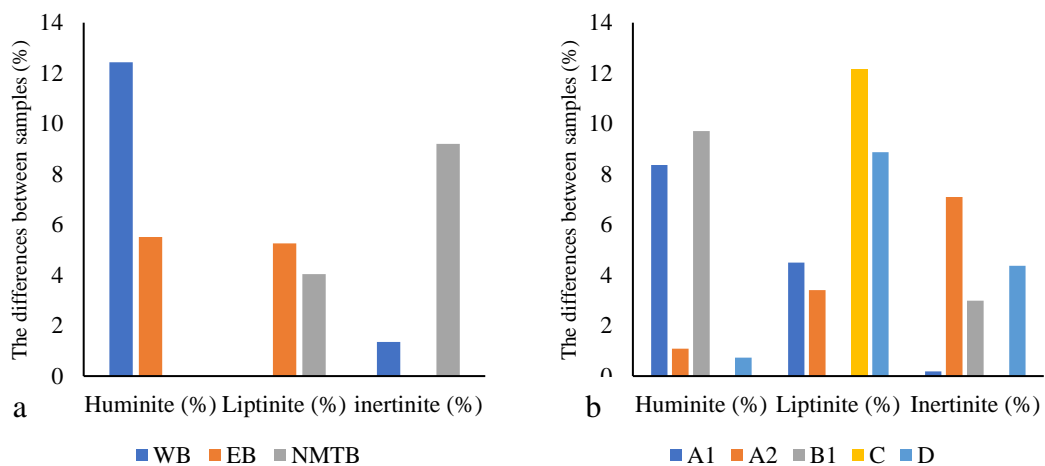


Figure 28 The result of differences coal samples with samples contained the lowest value of huminite, liptinite and inertinite from (a)different area and (b) different coal seams.

During the adsorption of gases on coal, the content of organic matter plays an important role in the adsorption of gases (Mastalerz et al., 2004). In all conditions, there is a positive relationship between CO<sub>2</sub> adsorption and huminite content of coal powder and coal blocks (Figure 29). It has been observed that huminite has a significant impact on the adsorption of CO<sub>2</sub> on coal (Crosdale et al., 1998) probably due to the presence of micropore connections associated with organic matter (Mangi et al., 2022). Powder coal exhibits a stronger relationship than block coal. Additionally, the drying process strengthens the relationship between CO<sub>2</sub> and huminite.

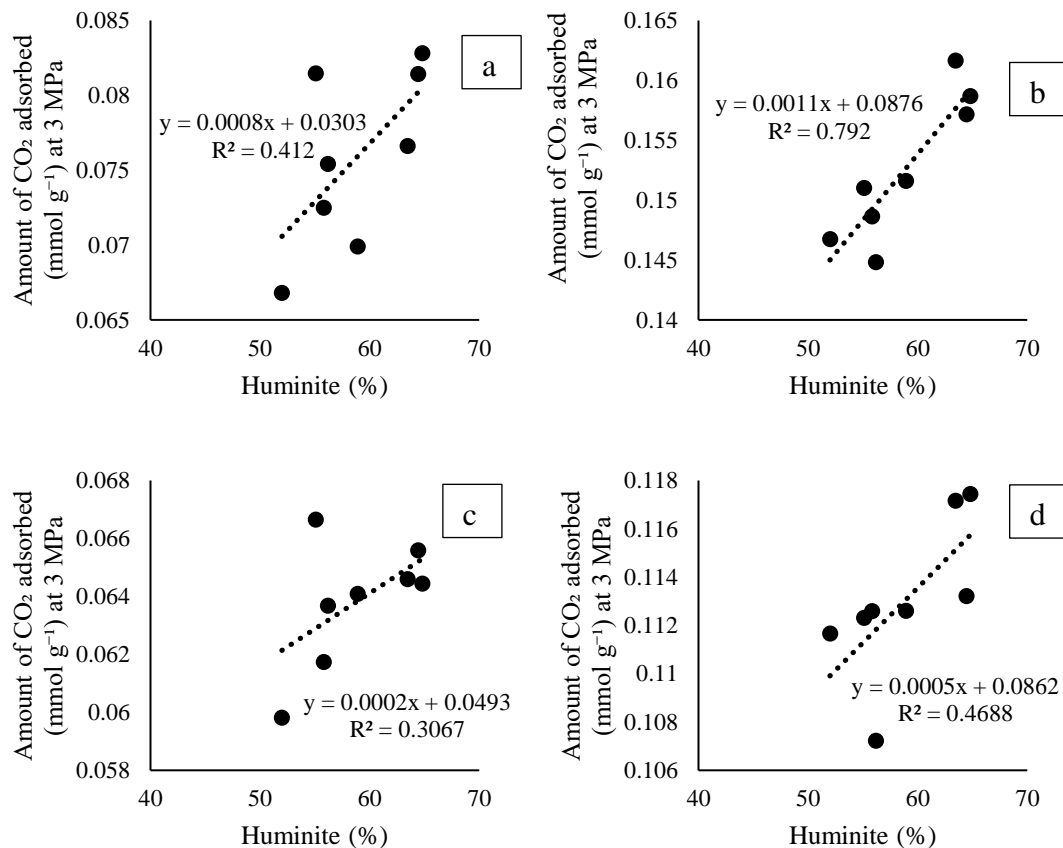


Figure 29 The relationship between CO<sub>2</sub> adsorption and huminite content in (a) powder coal in raw condition, (b) powder coal in dry condition, (c) block coal in raw condition, and (d) block coal in dry condition

Figure 30 illustrates the relationship between CO<sub>2</sub> adsorption and liptinite in this study. The liptinite mineral exhibits some affinity for gas adsorption, although not as much as vitrinite (Karacan and Mitchell, 2003). Compared to the previous study, this study shows different results. Results reveal that liptinite has weak correlations and generally negative values. This study is similar to other studies that demonstrate a negative correlation (Czerw et al., 2021). Only a weak positive correlation exists between liptinite and pore network (Teng et al., 2017), but it exhibits higher mesopores and lower microporosity (Czerw et al., 2021) which are insufficient to support CO<sub>2</sub> adsorption on coal. The drying and powdering processes do not have any significant impact on CO<sub>2</sub> adsorption and liptinite content.

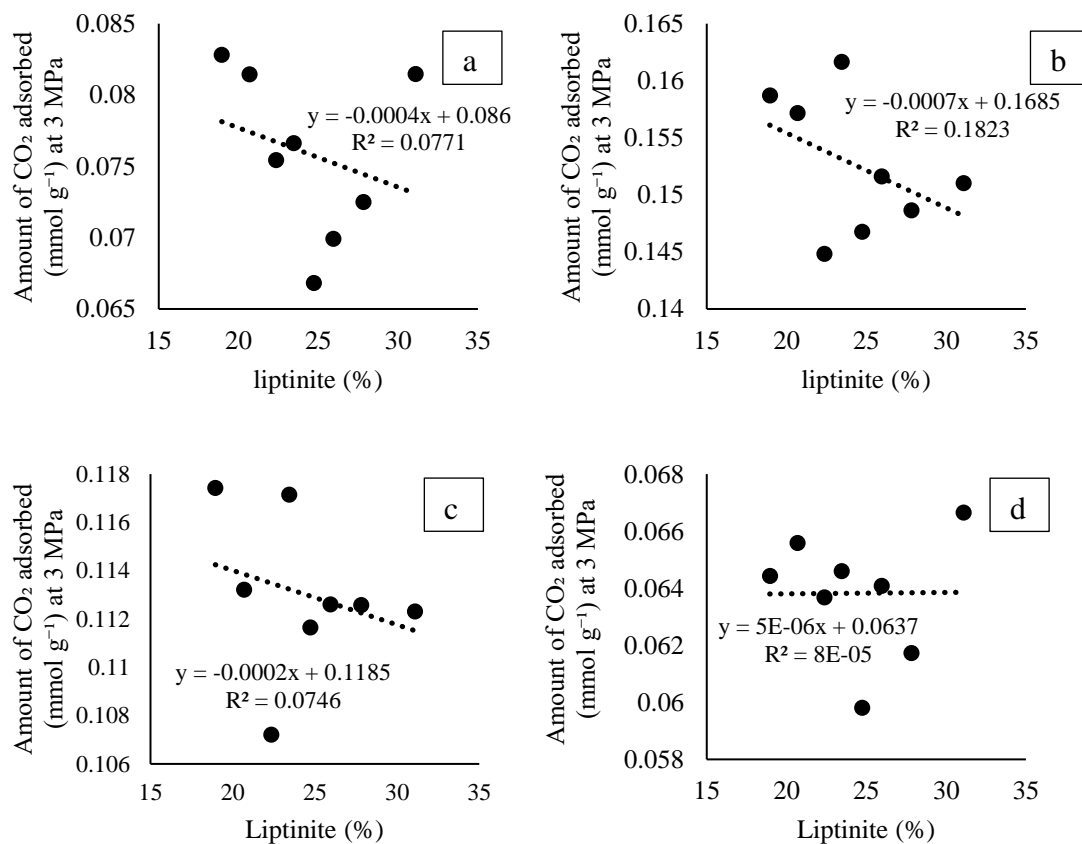


Figure 30 The relationship between CO<sub>2</sub> adsorption and liptinite content in (a) powder coal in raw condition, (b) powder coal in dry condition, (c) block coal in raw condition, and (d) block coal in dry condition

The inertinite, in contrast to huminite and liptinite, has a strong inhibitory effect on the adsorption process (Mangi et al., 2020). The surface properties of inertinite indicate that inertinite is less hydrophobic than huminite/vitrinite, resulting in a difficult time draining water because inertinite is more porous than huminite/vitrinite, and the interaction between inertinite and water is stronger than that between huminite/vitrinite and water (Ping et al., 2021). Figure 31 shows that inertinite has a stronger negative correlation than liptinite. According to this study, drying did not affect the correlation between inertinite and CO<sub>2</sub> adsorption on coal.

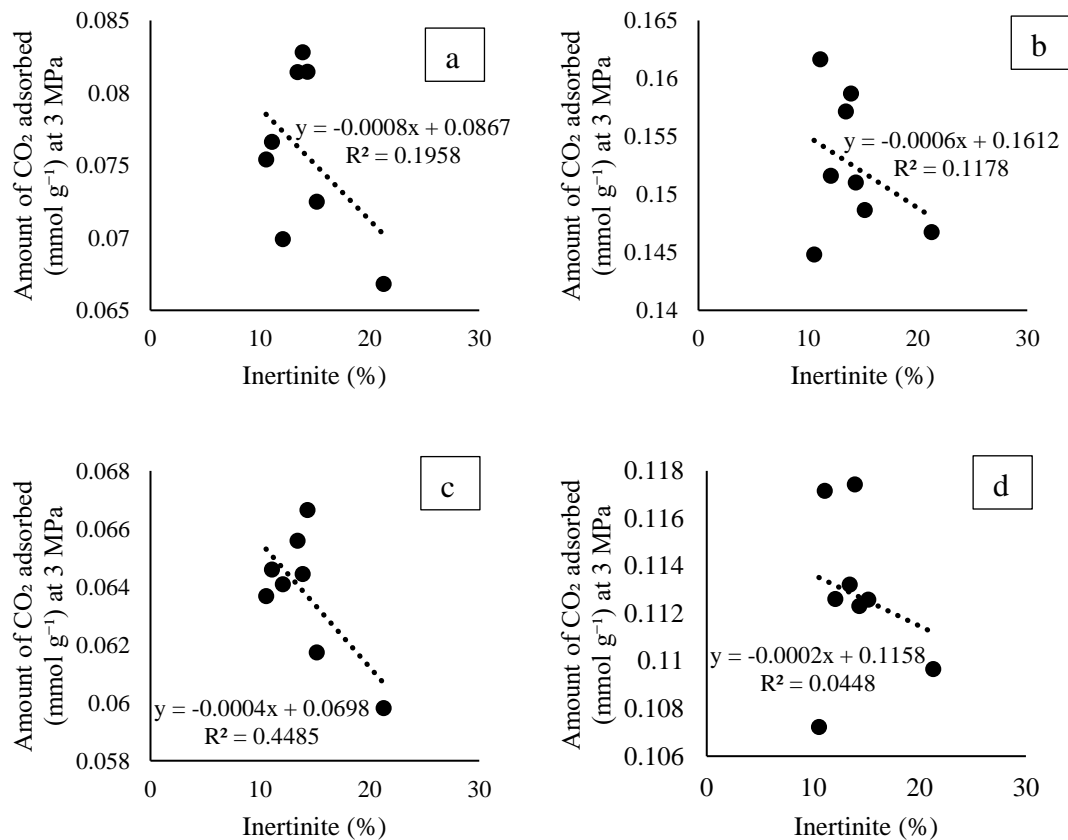


Figure 31 The relationship between CO<sub>2</sub> adsorption and inertinite content in (a) powder coal in raw condition, (b) powder coal in dry condition, (c) block coal in raw condition, and (d) block coal in dry condition



Several studies suggest increased maceral content is correlated with greater affinity for CO<sub>2</sub> uptake, but others do not find a correlation between the competing nature of vitrinite and inertinite components (Premlall et al., 2014). The discussion did not just focus on maceral, but also on lithotype. Research has shown that lithotypes exhibit different reactions due to CO<sub>2</sub> adsorption (Anggara et al., 2014; Cao et al., 2011). There is also a study to prove there is no difference between original lithotypes and lithotypes that have been exposed to high pressure CO<sub>2</sub> as no additional oxygenated bands or free CO<sub>2</sub> appear in the post-CO<sub>2</sub> state (Mastalerz et al., 2010).

### 5.3.2 LTNA analysis

In Figure 32, LTNA isotherms for CO<sub>2</sub> adsorption under various conditions are illustrated. Based on the figure, it can be seen that there is a marked difference between the coal samples studied. Because of the CO<sub>2</sub> adsorption process, these samples are able to adsorb a significant amount of N<sub>2</sub> than raw coal. Observations of the adsorption behavior of raw coal samples before and after injection of CO<sub>2</sub> show a hysteresis loop at higher relative pressures ( $P/P_o > 0.5$ ). This implies that the evaporation from pores is distinct from the condensation within the pores, which suggests that there may also be capillary condensation occurring within the mesopore (Clarkson and Bustin, 1999). As a result of the limitations on detection and measurement, samples in dry conditions after CO<sub>2</sub> injection can only detect the adsorption isotherm.

The hysteresis loop shape indicates that the raw adsorption of a sample in the presence and absence of CO<sub>2</sub> is type B, indicating many cylindrical pores and slit-shaped pores with all sides exposed during adsorption. A large loop is seen in the raw samples after CO<sub>2</sub> adsorption, indicating that there are more pores open and that there is better connectivity between the pores. There has been a study that has shown that the hysteresis loops become wider when the pressure of CO<sub>2</sub> is increased (Wang et al., 2022). CO<sub>2</sub> adsorption may have caused this phenomenon because the adsorption of CO<sub>2</sub> transformed many closed pores into open pores. This resulted in better pore connectivity, enabling gas to flow through coal more easily.

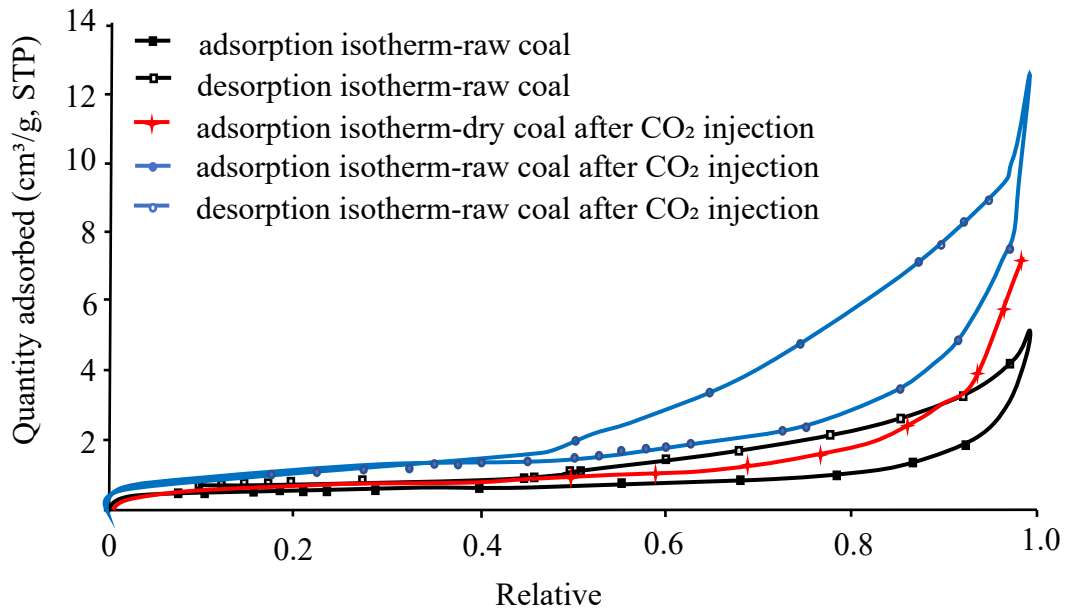


Figure 32 LTNA isotherms of coal samples before and after CO<sub>2</sub> injection in different conditions

For the purpose of computing the SSA and pore volume of the soil, BET and BJH are used in this study. Raw coal has a BET surface area of 1.89 m<sup>2</sup>/g. Raw coal after CO<sub>2</sub> injection has a BET surface area of 3.83 m<sup>2</sup>/g. Dry coal after CO<sub>2</sub> injection has a BET surface area of 2.4527 m<sup>2</sup>/g. The BJH pore volume of raw coal is 0.00813 m<sup>2</sup>/g, the BJH pore volume of raw coal after CO<sub>2</sub> injection is 0.020 m<sup>2</sup>/g, and the BJH pore volume of dry coal after CO<sub>2</sub> injection is 0.0119 m<sup>2</sup>/g. There are peaks in the PSD of micropores in raw coal that range from 0.7 to 1.1 nm, and 1.8 to 1.9 nm (Figure 33). However, CO<sub>2</sub> injection results in the absence of micropores in raw coal. It is possible that the differences are caused by the effect of coal compressibility (Nie et al., 2015). There is a possibility that all the differences between raw coal before and after CO<sub>2</sub> adsorption are the result of swelling caused by the process of CO<sub>2</sub> adsorption. Due to this swelling, micropores become blocked and pores become less accessible. In coal, changes in moisture may be one of the external factors that affect the evolution of pore sizes (Mangi et al., 2020). During the process of drying and removing moisture from coal, the structure of the coal is disrupted and shrinkage occurs (Rong et al., 2020).

The shrinkage of dry coal results in a lower SSA than raw coal. The PSD analysis showed that the loss of moisture resulted in more accessible sites and micropores for CO<sub>2</sub> adsorption, with the peak micropore size being 1.5-1.7 nm.

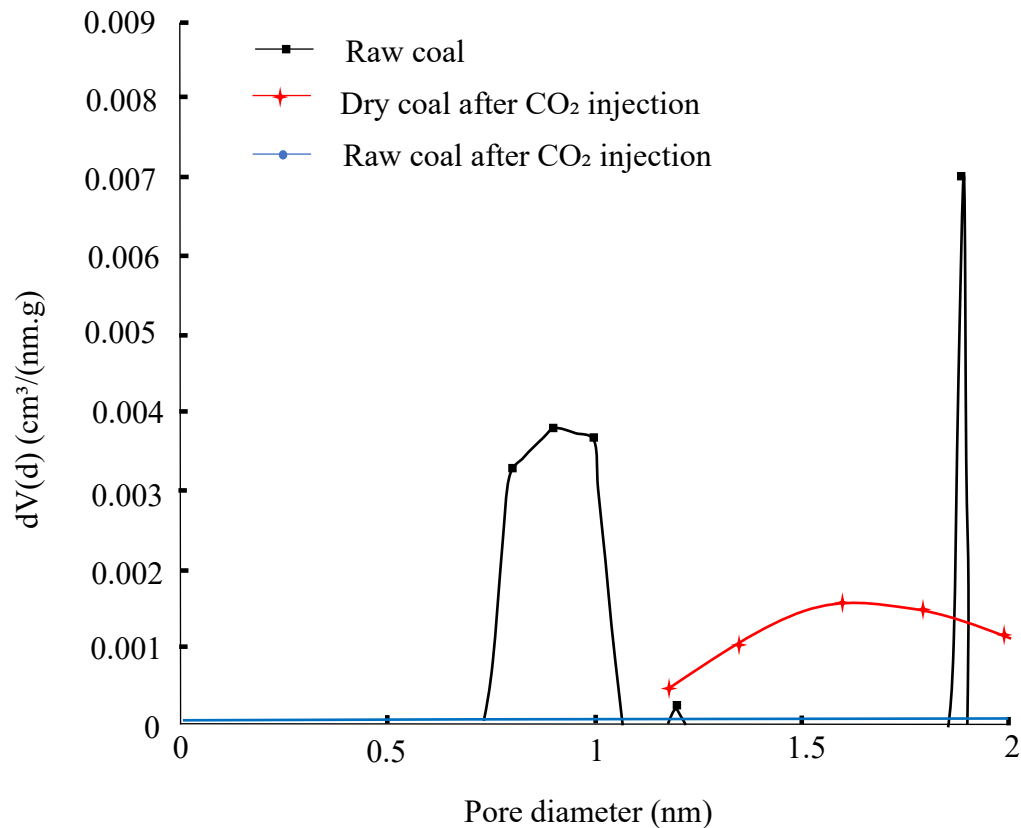


Figure 33 Micropore size distribution of coal samples before and after CO<sub>2</sub> injection under different conditions.

The injection of CO<sub>2</sub> resulted in the formation of micropores as well as mesopores. CO<sub>2</sub> adsorption peaks at 3 nm and 10 nm for dry coal, whereas CO<sub>2</sub> adsorption peaks at 4.5 nm for raw coal (Figure 34). The difference between 5 and 10 nm illustrates the enormous difference between the two. The dehydration effect of this process results in the decrease of coal volume, the increase of small pores ( < 52 nm) and the decrease of large pores (>260 nm) (Rong et al., 2020). Moreover, the swelling effect is not only

observed at micropores, but also at mesopores (Wang et al., 2022). The adsorption of CO<sub>2</sub> on dry coal also leads to swelling (Day et al., 2010), although the swelling effect is less pronounced when compared to coal with moisture content.

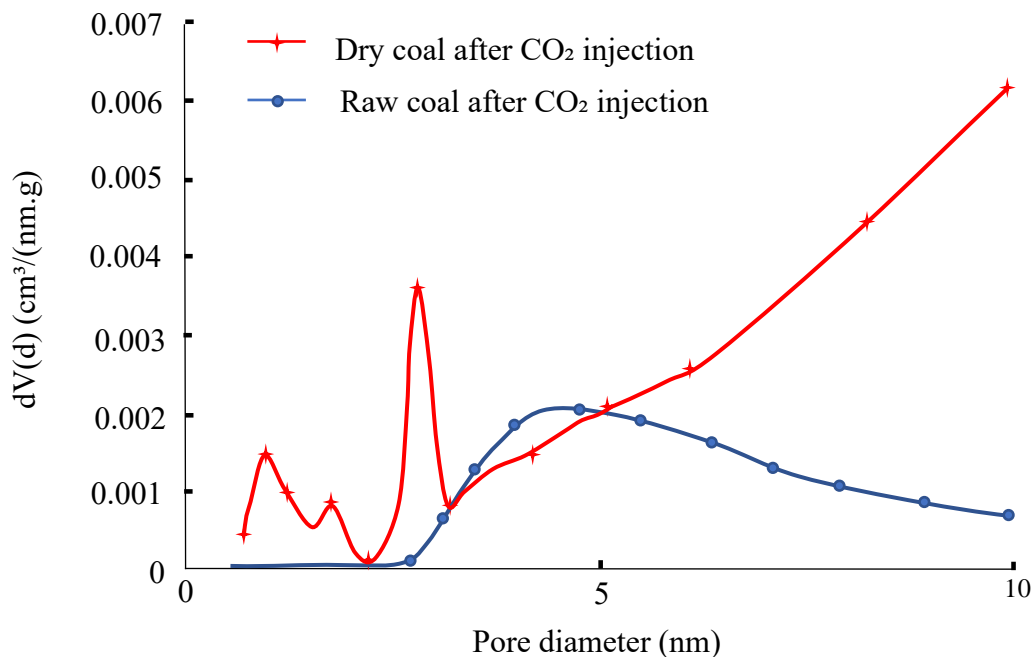


Figure 34 Mesopore size distribution of coal after CO<sub>2</sub> injection under different conditions.

LTNA can be a very useful tool, but it also has a few limitations that are worth mentioning. One of the limitations of LTNA is its inability to measure macropores in coal (Zhou et al., 2019b). Furthermore, the study also showed that higher CO<sub>2</sub> adsorption pressure leads to stronger N<sub>2</sub> adsorption capacity, which can be interpreted as the result of some long pores becoming shorter, and the closed pores eventually transforming into open pores within the coal (Wang et al., 2022). There was a variation in the total pore volume of coal samples as a function of moisture abundance, but the micropore and mesopore volumes remained unchanged. Swelling may be caused by adsorption and the transformation of some pores during the process of adsorption.

### 5.3.3 SEM analysis

There are a number of different magnifications that can be used for SEM analysis. This is the most fundamental parameter for observing qualitative pore structures within the coal matrix. A variety of closed and semi-closed pores are present in coal samples, such as wedge-shaped pores, slit-shaped pores, and channel-like pores with one closed side and a dead end (Figure 35). As a raw condition, there is an obvious presence of cellular detail in plant tissue. The width of the pores varies from micropore to macropore, with a significant contribution from mesopores and macropores.

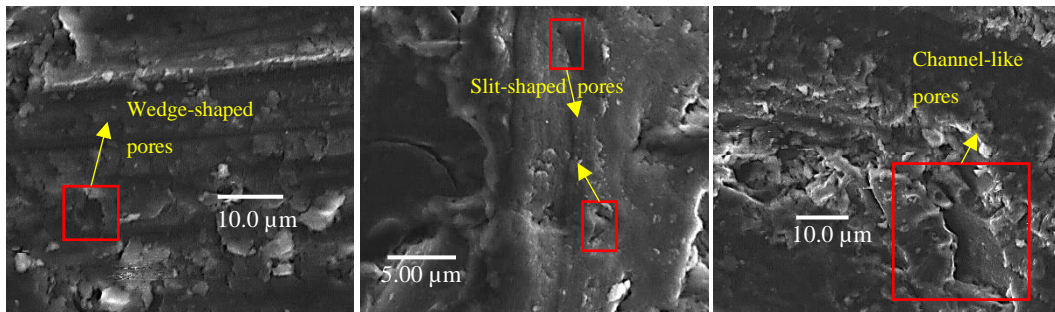


Figure 35 SEM images of different coal samples in raw condition

In raw condition, well preserved cellular structure can be observed. It is generally accepted that these cells have a very regular shape and are oval in shape, as well as being filled with minerals (Figure 36 a). It was observed that raw coal samples after CO<sub>2</sub> injection were dominated by macropore-mesopores, while some pores did not fully fill with minerals (Figure 36 b). There was an acidic environment that developed after CO<sub>2</sub> entered the coal body, which caused the minerals in the coal body to dissolve (Wang et al., 2022). As a result of the drying process, SEM can detect the traces of shrinkage which are caused by the drying process (Figure 36 c). The difference found in dry coal samples after injection of CO<sub>2</sub> can be attributed to the difference in micropore and mesopore sizes. By detecting macropores in a sample, SEM can resolve some of the limitations that cannot be addressed by LTNA analysis. Furthermore, SEM detected coal blocks that had been adapted to natural conditions. In spite of the fact that

SEM has some advantages, it also has some disadvantages. There are limitations to detecting small pores, especially micropores.

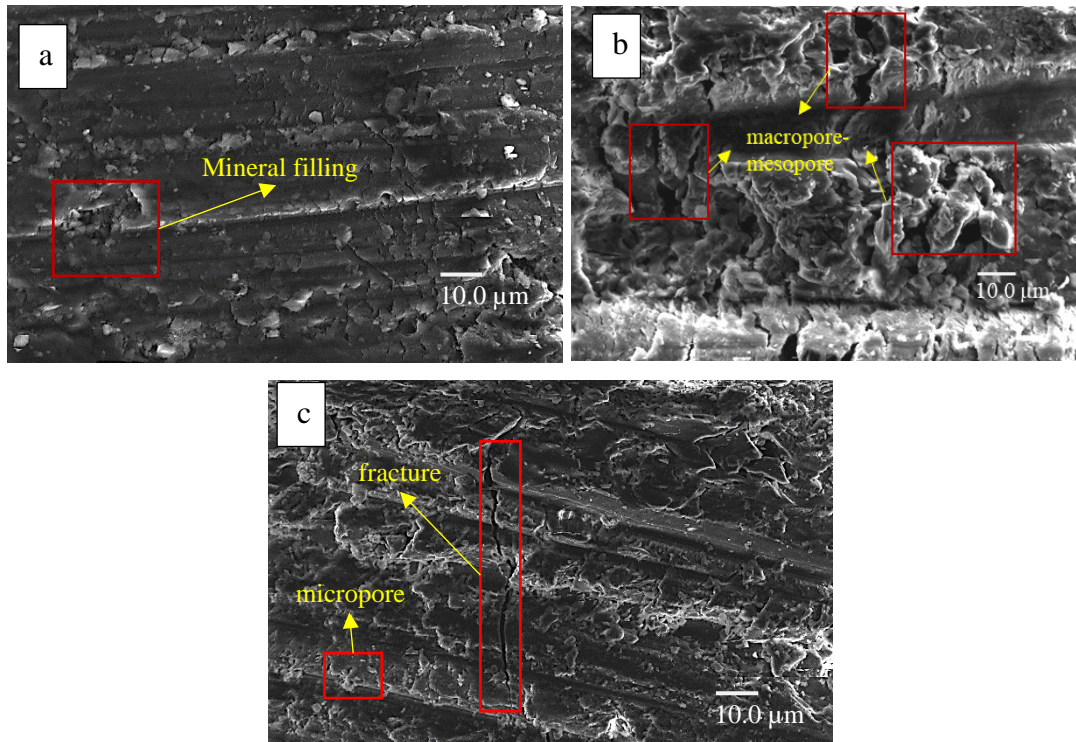


Figure 36 SEM image of different condition, (a) raw condition, (b) raw condition after CO<sub>2</sub> adsorption and (c) dry condition after CO<sub>2</sub> adsorption

#### 5.4 Conclusions

Maceral analysis was used to analyze the relationship between the influence of organic substances on CO<sub>2</sub> adsorption. The combination of LTNA and SEM was used to analyze the change in pore structure characteristic of CO<sub>2</sub> adsorption under different conditions. These findings show remarkable differences in pore structure, which in turn will affect both gas adsorption, storage and transport properties. The following conclusions can be drawn about the pore structure of the samples:

- CO<sub>2</sub> adsorption on coal is strongly correlated with huminite and the drying process, with drying strengthening the relationship between CO<sub>2</sub> and huminite. As Liptinite has a weak relationship with CO<sub>2</sub>, drying and powdering processes

do not have any significant effects on CO<sub>2</sub> adsorption and liptinite content. Inertinite has a negative relationship with CO<sub>2</sub> adsorption. Moreover, drying did not affect the correlation between inertinite and CO<sub>2</sub> adsorption on coal.

- CO<sub>2</sub> adsorption on coal has different effects on coal pores under different conditions. In raw conditions, CO<sub>2</sub> adsorption shows a decrease in micropores due to swelling, but more macropores were opened. Because coal shrinkage during drying increases the accessibility of coal pores, even when CO<sub>2</sub> adsorption tends to swell, the presence of micropores in dry coal after CO<sub>2</sub> adsorption is still detectable.
- By SEM analysis, the pore type, macropore and fracture can be detected. In addition, dissolved minerals on coal pores due to acidic environments from CO<sub>2</sub> adsorption can be analyzed.

This study found that CO<sub>2</sub> injection on dry coal has a lower possibility of swelling than CO<sub>2</sub> injection on raw coal for the safe storage of CO<sub>2</sub> in low-rank coal. Despite the fact that dry coal has a greater potential than raw coal, the drying process results in shrinkage, which is an extremely crucial factor to consider.

## CHAPTER VI

### 6. Conclusions and Outlook

This dissertation deals with the estimation of CO<sub>2</sub> adsorption capacities and the effects of CO<sub>2</sub> adsorption on low-rank coal in various sample preparations. There are two forms of coal that were used to prepare the sample, coal blocks and coal powder. The samples were prepared for each coal form under two conditions of moisture presence, raw coal and dry coal, respectively. For measuring the adsorption capacity of large samples, this study uses a custom-designed volumetric adsorption setup, which is capable of handling large samples. Samples of low-rank coal were taken from several coal seams and areas of Indonesian coal field. These samples were evaluated for their capacity to adsorb moisture at 318.15 K and at pressures up to 3 MPa in steps of 0.5 MPa. To confirm the relationship between adsorption capacity, isotherm models, Henry coefficients, surface potential, and Gibbs free energy change of CO<sub>2</sub> were analyzed based on the adsorption data. Moreover, the effect of CO<sub>2</sub> adsorption on low-rank coal was detected by LTNA and SEM.

First, CO<sub>2</sub> adsorption was measured on low-rank coal from three different areas of the South Sumatra Basin: West Banko (WB), East Banko (EB), and North Muara Tiga Besar (NMTB). The experimental data was analyzed using isotherm adsorption models such as Langmuir, Freundlich, and Temkin. According to the fitted curve and correlation coefficient, CO<sub>2</sub> adsorption was observed on both monolayers and multilayers under different conditions. The adsorption capacity of CO<sub>2</sub> was similar in all four conditions of research, despite a few minor differences. There is a minor difference due to lower moisture in one area than in others, and when moisture is eliminated from coal, the result is similar. Powdered coal has a higher CO<sub>2</sub> adsorption capacity than block coal under raw conditions, which is directly due to its changing pore structure. Furthermore, the drying process made it possible to access more sites



and to increase the capacity for adsorption of CO<sub>2</sub>. The drying process increases the ability of fixed carbon and volatile matter to adsorb CO<sub>2</sub>, even if it does not reflect a realistic situation. The coal samples from WB are more promising in terms of CO<sub>2</sub> storage and ECBM, since they contain a lower level of moisture than those from EB and NMTB.

The WB area has been identified as a promising area for the adsorption of CO<sub>2</sub>. It was necessary to examine the coal seams in detail in order to make an accurate prediction of which coal seams would be most promising. Statistical evaluations such as SSE and ARE were used to validate the most optimal adsorption model. Since the experiment was conducted at low pressure, Langmuir and Freundlich are the most accurate adsorption models, since both monolayers and multilayers show CO<sub>2</sub> adsorption. Due to the drying process, dry coal has a higher K<sub>H</sub> value than raw coal because it has more micropores that can adsorb CO<sub>2</sub>. The drying process increases not only micropore availability, but also surface potential and Gibbs free energy. Under all conditions, CO<sub>2</sub> adsorption on coal is feasible and spontaneous. The drying process facilitated and enhanced CO<sub>2</sub> adsorption into low rank coal. Despite the similarity of coal samples in all conditions, seams B1 and C exhibit a greater potential for CO<sub>2</sub> adsorption due to their coal properties. It has been found that moisture has a significant impact on CO<sub>2</sub> adsorption capacity based on results from different areas and coal seams. However, modification preparations such as drying, and crushing cannot accurately replicate in-situ conditions.

Adsorption of CO<sub>2</sub> under different conditions leads to different effects. The influence of organic substances on CO<sub>2</sub> adsorption was examined using maceral analysis. A strong correlation exists between huminite and CO<sub>2</sub> adsorption on coal especially on dry condition. Liptinite has a weak relationship with CO<sub>2</sub>, so the drying and powdering processes do not significantly affect CO<sub>2</sub> adsorption. Inertinite and CO<sub>2</sub> adsorption on coal have a negative correlation and drying did not affect this correlation. The

combination of LTNA and SEM was used to analyze the change in pore structure characteristics of CO<sub>2</sub> adsorption under different conditions. Micropores were reduced by swelling due to CO<sub>2</sub> adsorption, but macropores were increased. In dry coal after CO<sub>2</sub> adsorption, micropores can still be detected due to coal shrinkage during drying. Minerals dissolved in acidic environments due to CO<sub>2</sub> adsorption can also be analyzed by SEM. For safe CO<sub>2</sub> storage in low-rank coal, CO<sub>2</sub> injection into dry coal has a lower chance of swelling than CO<sub>2</sub> injection into raw coal. However, the drying process results in shrinkage, which plays a crucial role in considering dry coal's potential.

The results of this study can be used to learn how significant CO<sub>2</sub> adsorption occurs at low rank with different coal sample preparation methods for fitting different ECBM scenarios. Additionally, the research can be used to understand the effects of CO<sub>2</sub> adsorption on low-rank coal under low pressure, such as swelling and dissolution of minerals. Therefore, there are some limitations to proving how pressure affects different sample preparations and the amount of methane produced. This limitation allows for the possibility of improving the findings of this study. Also, this research provides an opportunity to compare various methods of coal sample preparation under supercritical CO<sub>2</sub> conditions in order to demonstrate the safety and effectiveness of ECBM.

## References

- Abunowara, M., Bustam, M.A., Sufian, S., Eldemerdash, U., 2016. Characterization of Malaysian coals for carbon dioxide sequestration. *IOP Conf. Ser. Earth Environ. Sci.* 36. <https://doi.org/10.1088/1755-1315/36/1/012001>
- Abunowara, M., Sufian, S., Bustam, M.A., Eldemerdash, U., Suleman, H., Bencini, R., Assiri, M.A., Ullah, S., Al-Sehemi, A.G., 2020. Experimental measurements of carbon dioxide, methane and nitrogen high-pressure adsorption properties onto Malaysian coals under various conditions. *Energy* 210. <https://doi.org/10.1016/j.energy.2020.118575>
- Adams, J.J., 2014. Asphaltene adsorption, a literature review. *Energy and Fuels* 28, 2831–2856. <https://doi.org/10.1021/ef500282p>
- Afikah, R., Sasaki, K., Surjono, S.S., Amijaya, D.H., 2018. The mechanical behaviour of coal relating to CO<sub>2</sub> sequestration of Tanjung Enim, Indonesia. *AIP Conf. Proc.* 2030. <https://doi.org/10.1063/1.5066848>
- Agraniotis, M., Bergins, C., Stein-Cichoszewska, M., Kakaras, E., 2017. High-efficiency pulverized coal power generation using low-rank coals, *Low-rank Coals for Power Generation, Fuel and Chemical Production*. Elsevier Ltd. <https://doi.org/10.1016/B978-0-08-100895-9.00005-X>
- Alexis, D.A., Karpyn, Z.T., Ertekin, T., Crandall, D., 2015. Fracture permeability and relative permeability of coal and their dependence on stress conditions. *J. Unconv. Oil Gas Resour.* 10, 1–10. <https://doi.org/10.1016/j.juogr.2015.02.001>
- AlRassas, A.M., Ren, S., Sun, R., Thanh, H.V., Guan, Z., 2021. CO<sub>2</sub> storage capacity estimation under geological uncertainty using 3-D geological modeling of unconventional reservoir rocks in Shahejie Formation, block Nv32, China. *J. Pet. Explor. Prod.* 11, 2327–2345. <https://doi.org/10.1007/s13202-021-01192-4>
- Amijaya, H., Littke, R., 2005. Microfacies and depositional environment of Tertiary Tanjung Enim low rank coal, South Sumatra Basin, Indonesia. *Int. J. Coal Geol.* 61, 197–221. <https://doi.org/10.1016/j.coal.2004.07.004>

- Anggara, F., 2017. Site selection criteria for Geological CO<sub>2</sub> Sequestration : A Case Study from CO<sub>2</sub>-enhanced CBM recovery ( CO<sub>2</sub> -ECBM ) in Indonesia, in: 6th World Conference on Applied Sciences, Engineering & Technology, 26-27 August 2017, UMPO, Indonesia. pp. 26–27.
- Anggara, F., Sasaki, K., Amijaya, H., Sugai, Y., Setijadji, L.D., 2010. CO<sub>2</sub> Injection in Coal Seams, an Option for geological CO<sub>2</sub> Storage and Enhanced Coal Bed Methane Recovery (ECBM). PROCEEDINGS, Indones. Pet. Assoc. <https://doi.org/10.29118/ipa.1669.10.e.111>
- Anggara, F., Sasaki, K., Rodrigues, S., Sugai, Y., 2014. The effect of megascopic texture on swelling of a low rank coal in supercritical carbon dioxide. *Int. J. Coal Geol.* 125, 45–56. <https://doi.org/10.1016/j.coal.2014.02.004>
- Anggara, F., Sasaki, K., Sugai, Y., 2016. The correlation between coal swelling and permeability during CO<sub>2</sub> sequestration: A case study using Koshiro low rank coals. *Int. J. Coal Geol.* 166, 62–70. <https://doi.org/10.1016/j.coal.2016.08.020>
- Anovitz, L.M., Cole, D.R., 2015. Characterization and analysis of porosity and pore structures. *Rev. Mineral. Geochemistry* 80, 61–164. <https://doi.org/10.2138/rmg.2015.80.04>
- Ayawei, N., Ebelegi, A.N., Wankasi, D., 2017. Modelling and Interpretation of Adsorption Isotherms. *J. Chem.* 2017. <https://doi.org/10.1155/2017/3039817>
- Battistutta, E., van Hemert, P., Lutynski, M., Bruining, H., Wolf, K.H., 2010. Swelling and sorption experiments on methane, nitrogen and carbon dioxide on dry Selar Cornish coal. *Int. J. Coal Geol.* 84, 39–48. <https://doi.org/10.1016/j.coal.2010.08.002>
- Beamish, B.B., Crosdale, P.J., 1998. Instantaneous outbursts in underground coal mines: an overview and association with coal type. *Int. J. Coal Geol.* 35, 27–55. [https://doi.org/10.1016/S0166-5162\(97\)00036-0](https://doi.org/10.1016/S0166-5162(97)00036-0)
- Belkin, H.E., Tewalt, S.J., Hower, J.C., Stucker, J.D., O’Keefe, J.M.K., 2009. Geochemistry and petrology of selected coal samples from Sumatra, Kalimantan, Sulawesi, and Papua, Indonesia. *Int. J. Coal Geol.* 77, 260–268.

<https://doi.org/10.1016/j.coal.2008.08.001>

- Bhowmik, S., Dutta, P., 2013. Adsorption rate characteristics of methane and CO<sub>2</sub> in coal samples from raniganj and jharia coalfields of india. *Int. J. Coal Geol.* 113, 50–59. <https://doi.org/10.1016/j.coal.2013.02.005>
- Busch, A., Gensterblum, Y., 2011. CBM and CO<sub>2</sub>-ECBM related sorption processes in coal: A review. *Int. J. Coal Geol.* 87, 49–71. <https://doi.org/10.1016/j.coal.2011.04.011>
- Busch, A., Gensterblum, Y., Krooss, B.M., 2007. High-pressure sorption of nitrogen, carbon dioxide, and their mixtures on Argonne Premium Coals. *Energy and Fuels* 21, 1640–1645. <https://doi.org/10.1021/ef060475x>
- Busch, Andreas, Gensterblum, Y., Krooss, B.M., 2003. Methane and CO<sub>2</sub> sorption and desorption measurements on dry Argonne premium coals: Pure components and mixtures. *Int. J. Coal Geol.* 55, 205–224. [https://doi.org/10.1016/S0166-5162\(03\)00113-7](https://doi.org/10.1016/S0166-5162(03)00113-7)
- Busch, A., Gensterblum, Y., Krooss, B.M., Littke, R., 2004. Methane and carbon dioxide adsorption-diffusion experiments on coal: Upscaling and modeling. *Int. J. Coal Geol.* 60, 151–168. <https://doi.org/10.1016/j.coal.2004.05.002>
- Busch, A., Krooss, B.M., Gensterblum, Y., Van Bergen, F., Pagnier, H.J.M., 2003. High-pressure adsorption of methane, carbon dioxide and their mixtures on coals with a special focus on the preferential sorption behaviour. *J. Geochemical Explor.* 78–79, 671–674. [https://doi.org/10.1016/S0375-6742\(03\)00122-5](https://doi.org/10.1016/S0375-6742(03)00122-5)
- Bustin, R.M., Clarkson, C.R., 1998. Geological controls on coalbed methane reservoir capacity and gas content. *Int. J. Coal Geol.* 38, 3–26. [https://doi.org/10.1016/S0166-5162\(98\)00030-5](https://doi.org/10.1016/S0166-5162(98)00030-5)
- Cai, Y., Liu, D., Pan, Z., Yao, Y., Li, J., Qiu, Y., 2013. Pore structure and its impact on CH<sub>4</sub> adsorption capacity and flow capability of bituminous and subbituminous coals from Northeast China. *Fuel* 103, 258–268. <https://doi.org/10.1016/j.fuel.2012.06.055>
- Cao, X., Mastalerz, M., Chappell, M.A., Miller, L.F., Li, Y., Mao, J., 2011. Chemical

- structures of coal lithotypes before and after CO<sub>2</sub> adsorption as investigated by advanced solid-state <sup>13</sup>C nuclear magnetic resonance spectroscopy. *Int. J. Coal Geol.* 88, 67–74. <https://doi.org/10.1016/j.coal.2011.08.003>
- Charrière, D., Pokryszka, Z., Behra, P., 2010. Effect of pressure and temperature on diffusion of CO<sub>2</sub> and CH<sub>4</sub> into coal from the Lorraine basin (France). *Int. J. Coal Geol.* 81, 373–380. <https://doi.org/10.1016/j.coal.2009.03.007>
- Chen, M. yi, Cheng, Y. ping, Li, H. ran, Wang, L., Jin, K., Dong, J., 2018. Impact of inherent moisture on the methane adsorption characteristics of coals with various degrees of metamorphism. *J. Nat. Gas Sci. Eng.* 55, 312–320. <https://doi.org/10.1016/j.jngse.2018.05.018>
- Chen, X., 2015. Modeling of experimental adsorption isotherm data. *Inf.* 6, 14–22. <https://doi.org/10.3390/info6010014>
- Clarkson, C.R., Bustin, R.M., 1999. Effect of pore structure and gas pressure upon the transport properties of coal: a laboratory and modeling study. 1. Isotherms and pore volume distributions. *Fuel* 78, 1333–1344. [https://doi.org/10.1016/S0016-2361\(99\)00055-1](https://doi.org/10.1016/S0016-2361(99)00055-1)
- Clarkson, C.R., Bustin, R.M., 1996. Variation in micropore capacity and size distribution with composition in bituminous coal of the Western Canadian Sedimentary Basin: Implications for coalbed methane potential. *Fuel* 75, 1483–1498. [https://doi.org/10.1016/0016-2361\(96\)00142-1](https://doi.org/10.1016/0016-2361(96)00142-1)
- Clarkson, C.R., Bustin, R.M., Levy, J.H., 1997. Application of the mono/multilayer and adsorption potential theories to coal methane adsorption isotherms at elevated temperature and pressure. *Carbon N. Y.* 35, 1689–1705. [https://doi.org/10.1016/S0008-6223\(97\)00124-3](https://doi.org/10.1016/S0008-6223(97)00124-3)
- Crosdale, P.J., Beamish, B.B., Valix, M., 1998. Coalbed methane sorption related to coal composition. *Int. J. Coal Geol.* 35, 147–158. [https://doi.org/10.1016/S0166-5162\(97\)00015-3](https://doi.org/10.1016/S0166-5162(97)00015-3)
- Cui, X., Bustin, R.M., Dipple, G., 2004. Selective transport of CO<sub>2</sub>, CH<sub>4</sub>, and N<sub>2</sub> in coals: Insights from modeling of experimental gas adsorption data. *Fuel* 83, 293–

303. <https://doi.org/10.1016/j.fuel.2003.09.001>
- Czerw, K., Baran, P., Szczurowski, J., Zarębska, K., 2021. Sorption and Desorption of CO<sub>2</sub> and CH<sub>4</sub> in Vitrinite- and Inertinite-Rich Polish Low-Rank Coal. *Nat. Resour. Res.* 30, 543–556. <https://doi.org/10.1007/s11053-020-09715-2>
- Day, S., Fry, R., Sakurovs, R., Weir, S., 2010. Swelling of coals by supercritical gases and its relationship to sorption. *Energy and Fuels* 24, 2777–2783. <https://doi.org/10.1021/ef901588h>
- Day, S., Sakurovs, R., Weir, S., 2008. Supercritical gas sorption on moist coals. *Int. J. Coal Geol.* 74, 203–214. <https://doi.org/10.1016/j.coal.2008.01.003>
- Day, S.J., Duffy, G.J., Saghafi, A., Sakurovs, R., 2005. FACTORS CONTROLLING CO<sub>2</sub> ABSORPTION IN AUSTRALIAN COALS. *FACTORS Control. CO<sub>2</sub> Absorpt. Aust. COALS* 2, 2519–2523.
- De Boer, J.H., 1958. The structure and properties of porous materials.
- De Silva, P.N.K., Ranjith, P.G., Choi, S.K., 2012. A study of methodologies for CO<sub>2</sub> storage capacity estimation of coal. *Fuel* 91, 1–15. <https://doi.org/10.1016/j.fuel.2011.07.010>
- Deng, H., Yi, H., Tang, X., Yu, Q., Ning, P., Yang, L., 2012. Adsorption equilibrium for sulfur dioxide, nitric oxide, carbon dioxide, nitrogen on 13X and 5A zeolites. *Chem. Eng. J.* 188, 77–85. <https://doi.org/10.1016/j.cej.2012.02.026>
- Diessel, C.F.K., 2012. Coal-bearing depositional systems. Springer Science & Business Media.
- Dong, N.S., 2011. Utilisation of Low Rank Coals, IEA Clean Coal Centre.
- Du, X., Cheng, Y., Liu, Z., Yin, H., Wu, T., Huo, L., Shu, C., 2021a. CO<sub>2</sub> and CH<sub>4</sub> adsorption on different rank coals: A thermodynamics study of surface potential, Gibbs free energy change and entropy loss. *Fuel* 283, 118886. <https://doi.org/10.1016/j.fuel.2020.118886>
- Du, X., Cheng, Y., Liu, Z., Yin, H., Wu, T., Huo, L., Shu, C., 2021b. CO<sub>2</sub> and CH<sub>4</sub> adsorption on different rank coals: A thermodynamics study of surface potential, Gibbs free energy change and entropy loss. *Fuel* 283, 118886.

- <https://doi.org/10.1016/j.fuel.2020.118886>
- Dutta, P., Bhowmik, S., Das, S., 2011. Methane and carbon dioxide sorption on a set of coals from India. *Int. J. Coal Geol.* 85, 289–299. <https://doi.org/10.1016/j.coal.2010.12.004>
- Fang, H., Sang, S., Liu, S., 2019. The coupling mechanism of the thermal-hydraulic-mechanical fields in CH<sub>4</sub>-bearing coal and its application in the CO<sub>2</sub>-enhanced coalbed methane recovery. *J. Pet. Sci. Eng.* 181, 106177. <https://doi.org/10.1016/j.petrol.2019.06.041>
- Foo, K.Y., Hameed, B.H., 2010. Insights into the modeling of adsorption isotherm systems. *Chem. Eng. J.* 156, 2–10. <https://doi.org/10.1016/j.cej.2009.09.013>
- Gao, D., Hong, L., Wang, J., Zheng, D., 2019. Adsorption simulation of methane on coals with different metamorphic grades. *AIP Adv.* 9. <https://doi.org/10.1063/1.5115457>
- Gensterblum, Y., Merkel, A., Busch, A., Krooss, B.M., 2013. High-pressure CH<sub>4</sub> and CO<sub>2</sub> sorption isotherms as a function of coal maturity and the influence of moisture. *Int. J. Coal Geol.* 118, 45–57. <https://doi.org/10.1016/j.coal.2013.07.024>
- Godec, M., Koperna, G., Gale, J., 2014. CO<sub>2</sub>-ECBM: A review of its status and global potential. *Energy Procedia* 63, 5858–5869. <https://doi.org/10.1016/j.egypro.2014.11.619>
- Goodman, A.L., Busch, A., Duffy, G.J., Fitzgerald, J.E., Gasem, K.A.M., Gensterblum, Y., Krooss, B.M., Levy, J., Ozdemir, E., Pan, Z., Robinson, R.L., Schroeder, K., Sudibandriyo, M., White, C.M., 2004. An inter-laboratory comparison of CO<sub>2</sub> isotherms measured on argonne premium coal samples. *Energy and Fuels* 18, 1175–1182. <https://doi.org/10.1021/ef034104h>
- Guarín Romero, J., Moreno-Piraján, J., Giraldo Gutierrez, L., 2018. Kinetic and Equilibrium Study of the Adsorption of CO<sub>2</sub> in Ultramicropores of Resorcinol-Formaldehyde Aerogels Obtained in Acidic and Basic Medium. *C* 4, 52. <https://doi.org/10.3390/c4040052>



- Guo, H., Cheng, Y., Wang, L., Lu, S., Jin, K., 2015. Experimental study on the effect of moisture on low-rank coal adsorption characteristics. *J. Nat. Gas Sci. Eng.* 24, 245–251. <https://doi.org/10.1016/j.jngse.2015.03.037>
- Hao, D., Zhang, L., Li, M., Tu, S., Zhang, C., Bai, Q., Wang, C., 2018. Experimental study of the moisture content influence on CH<sub>4</sub> adsorption and deformation characteristics of cylindrical bituminous coal core. *Adsorpt. Sci. Technol.* 36, 1512–1537. <https://doi.org/10.1177/0263617418788444>
- Hao, M., Qiao, Z., Zhang, H., Wang, Y., Li, Y., 2021. Thermodynamic Analysis of CH<sub>4</sub>/CO<sub>2</sub>/N<sub>2</sub> Adsorption on Anthracite Coal: Investigated by Molecular Simulation. *Energy and Fuels* 35, 4246–4257. <https://doi.org/10.1021/acs.energyfuels.0c04337>
- Harpalani, S., Schraufnagel, A., 1990. Measurement of parameters impacting methane recovery from coal seams. *Int. J. Min. Geol. Eng.* 8, 369–384. <https://doi.org/10.1007/BF00920648>
- Hol, S., Peach, C.J., Spiers, C.J., 2011. Applied stress reduces the CO<sub>2</sub> sorption capacity of coal. *Int. J. Coal Geol.* 85, 128–142. <https://doi.org/10.1016/j.coal.2010.10.010>
- Kalam, S., Abu-Khamsin, S.A., Kamal, M.S., Patil, S., 2021. Surfactant Adsorption Isotherms: A Review. *ACS Omega* 6, 32342–32348. <https://doi.org/10.1021/acsomega.1c04661>
- Kapoor, A., Yang, R.T., 1989. Correlation of equilibrium adsorption data of condensable vapours on porous adsorbents. *Gas Sep. Purif.* 3, 187–192. [https://doi.org/10.1016/0950-4214\(89\)80004-0](https://doi.org/10.1016/0950-4214(89)80004-0)
- Karacan, C.Ö., Mitchell, G.D., 2003. Behavior and effect of different coal microlithotypes during gas transport for carbon dioxide sequestration into coal seams. *Int. J. Coal Geol.* 53, 201–217. [https://doi.org/10.1016/S0166-5162\(03\)00030-2](https://doi.org/10.1016/S0166-5162(03)00030-2)
- Karayigit, A.İ., Mastalerz, M., Oskay, R.G., Buzkan, İ., 2018. Bituminous coal seams from underground mines in the Zonguldak Basin (NW Turkey): Insights from

- mineralogy, coal petrography, Rock-Eval pyrolysis, and meso- and microporosity. *Int. J. Coal Geol.* 199, 91–112. <https://doi.org/10.1016/j.coal.2018.09.020>
- Keshavarz, A., Sakurovs, R., Grigore, M., Sayyafzadeh, M., 2017. Effect of maceral composition and coal rank on gas diffusion in Australian coals. *Int. J. Coal Geol.* 173, 65–75. <https://doi.org/10.1016/j.coal.2017.02.005>
- Khanal, A., Shahriar, M.F., 2022. Physics-Based Proxy Modeling of CO<sub>2</sub> Sequestration in Deep Saline Aquifers. *Energies* 15, 4350. <https://doi.org/10.3390/en15124350>
- Kiani, A., Sakurovs, R., Grigore, M., Sokolova, A., 2018. Gas sorption capacity, gas sorption rates and nanoporosity in coals. *Int. J. Coal Geol.* 200, 77–86. <https://doi.org/10.1016/j.coal.2018.10.012>
- Kim, D., Seo, Y., Kim, J., Han, J., Lee, Y., 2019. Experimental and simulation studies on adsorption and diffusion characteristics of coalbed methane. *Energies* 12. <https://doi.org/10.3390/en12183445>
- Kim, H.J., Shi, Y., He, J., Lee, H.H., Lee, C.H., 2011. Adsorption characteristics of CO<sub>2</sub> and CH<sub>4</sub> on dry and wet coal from subcritical to supercritical conditions. *Chem. Eng. J.* 171, 45–53. <https://doi.org/10.1016/j.cej.2011.03.035>
- Kolak, J.J., Burruss, R.C., 2004. A Geochemical Investigation into the Effect of Coal Rank on the Potential Environmental Effects of CO<sub>2</sub> Sequestration in Deep Coal Beds U . S . Department of the Interior.
- Kumar, H., Mishra, M.K., Mishra, S., 2019. Sorption capacity of Indian coal and its variation with rank parameters. *J. Pet. Explor. Prod. Technol.* 9, 2175–2184. <https://doi.org/10.1007/s13202-019-0621-1>
- Kumar Singh, V., Anil Kumar, E., 2018. Comparative Studies on CO<sub>2</sub> Adsorption Isotherms by Solid Adsorbents. *Mater. Today Proc.* 5, 23033–23042. <https://doi.org/10.1016/j.matpr.2018.11.032>
- Lamberson, M.N., Bustin, R.M., 1993. Coalbed methane characteristics of Gates Formation coals, northeastern British Columbia: effect of maceral composition. *Am. Assoc. Pet. Geol. Bull.* 77, 2062–2076.
- Langmuir, I., 1918. The adsorption of gases on plane surfaces of glass, mica and

- platinum. *J. Am. Chem. Soc.* 40, 1361–1403.  
<https://doi.org/10.1021/ja02242a004>
- Larsen, J.W., 2004. The effects of dissolved CO<sub>2</sub> on coal structure and properties. *Int. J. Coal Geol.* 57, 63–70. <https://doi.org/10.1016/j.coal.2003.08.001>
- Laxminarayana, C., Crosdale, P.J., 1999. Role of coal type and rank on methane sorption characteristics of Bowen Basin, Australia coals. *Int. J. Coal Geol.* 40, 309–325. [https://doi.org/10.1016/S0166-5162\(99\)00005-1](https://doi.org/10.1016/S0166-5162(99)00005-1)
- Lee, S., Kim, S., Chun, D., Choi, H., Yoo, J., 2017. Upgrading and advanced cleaning technologies for low-rank coals, *Low-rank Coals for Power Generation, Fuel and Chemical Production*. Elsevier Ltd. <https://doi.org/10.1016/B978-0-08-100895-9.00004-8>
- Levine, J.R., 1993. Coalification: the evolution of coal as a source rock and reservoir rock for oil and gas. In: Law, B.E., Rice D.D.(Eds.), *Hydrocarbon in coal*. American Association of Petroleum Geologists Studies in Geology.
- Li, J., Li, X., Li, Yingying, Shi, J., Wu, K., Dong, F., Li, Yanzun, Yang, J., Bai, Y., 2015. Mechanism of liquid-phase adsorption and desorption in coalbed methane systems - A new insight into an old problem. *Soc. Pet. Eng. - SPE Asia Pacific Unconv. Resour. Conf. Exhib.* <https://doi.org/10.2118/177001-ms>
- Li, S., Tang, D., Xu, H., Yang, Z., 2012. The pore-fracture system properties of coalbed methane reservoirs in the Panguan Syncline, Guizhou, China. *Geosci. Front.* 3, 853–862. <https://doi.org/10.1016/j.gsf.2012.02.005>
- Li, X., Yan, X., Kang, Y., 2018. Effect of temperature on the permeability of gas adsorbed coal under triaxial stress conditions. *J. Geophys. Eng.* 15, 386–396. <https://doi.org/10.1088/1742-2140/aa9a98>
- Li, Z., Liu, D., Cai, Y., Wang, Y., Teng, J., 2019. Adsorption pore structure and its fractal characteristics of coals by N<sub>2</sub> adsorption/desorption and FESEM image analyses. *Fuel* 257, 116031. <https://doi.org/10.1016/j.fuel.2019.116031>
- Liang, Y., Tan, Y., Wang, F., Luo, Y., Zhao, Z., 2020. Improving permeability of coal seams by freeze-fracturing method: The characterization of pore structure changes

- under low-field NMR. *Energy Reports* 6, 550–561.  
<https://doi.org/10.1016/j.egy.2020.02.033>
- Liu, L., Jin, C., Li, L., Xu, C., Sun, P., Meng, Z., An, L., 2020. Coalbed methane adsorption capacity related to maceral compositions. *Energy Explor. Exploit.* 38, 79–91. <https://doi.org/10.1177/0144598719870325>
- Liu, Z., Zhang, Z., Choi, S.K., Lu, Y., 2018. Surface properties and pore structure of anthracite, bituminous coal and lignite. *Energies* 11.  
<https://doi.org/10.3390/en11061502>
- Ma, D., Li, Q., He, Q., Wang, C., 2017. Pore Characteristics of Vitrain and Durain in Low Rank Coal Area. *J. Power Energy Eng.* 05, 10–20.  
<https://doi.org/10.4236/jpee.2017.511002>
- Mabuza, M., Premllal, K., Daramola, M.O., 2022. Modelling and thermodynamic properties of pure CO<sub>2</sub> and flue gas sorption data on South African coals using Langmuir, Freundlich, Temkin, and extended Langmuir isotherm models. *Int. J. Coal Sci. Technol.* 9. <https://doi.org/10.1007/s40789-022-00515-y>
- Mahmoud, M., Eliebid, M., Al-Yousef, H.Y., Kamal, M.S., Al-Garadi, K., Elkatatny, S., 2019. Impact of methane adsorption on tight rock permeability measurements using pulse-decay. *Petroleum* 5, 382–387.  
<https://doi.org/10.1016/j.petlm.2019.01.002>
- Mane, V.S., Deo Mall, I., Chandra Srivastava, V., 2007. Kinetic and equilibrium isotherm studies for the adsorptive removal of Brilliant Green dye from aqueous solution by rice husk ash. *J. Environ. Manage.* 84, 390–400.  
<https://doi.org/10.1016/j.jenvman.2006.06.024>
- Mangi, H.N., Chi, R., DeTian, Y., Sindhu, L., Lijin, He, D., Ashraf, U., Fu, H., Zixuan, L., Zhou, W., Anees, A., 2022. The ungrind and grinded effects on the pore geometry and adsorption mechanism of the coal particles. *J. Nat. Gas Sci. Eng.* 100, 104463. <https://doi.org/10.1016/j.jngse.2022.104463>
- Mangi, H.N., Detian, Y., Hameed, N., Ashraf, U., Rajper, R.H., 2020. Pore structure characteristics and fractal dimension analysis of low rank coal in the Lower Indus

- Basin, SE Pakistan. *J. Nat. Gas Sci. Eng.* 77, 103231.  
<https://doi.org/10.1016/j.jngse.2020.103231>
- Mastalerz, M., Drobniak, A., Walker, R., Morse, D., 2010. Coal lithotypes before and after saturation with CO<sub>2</sub>; insights from micro- and mesoporosity, fluidity, and functional group distribution. *Int. J. Coal Geol.* 83, 467–474.  
<https://doi.org/10.1016/j.coal.2010.06.007>
- Mastalerz, M., Gluskoter, H., Rupp, J., 2004. Carbon dioxide and methane sorption in high volatile bituminous coals from Indiana, USA. *Int. J. Coal Geol.* 60, 43–55.  
<https://doi.org/10.1016/j.coal.2004.04.001>
- Mastalerz, M., Goodman, A., Chirdon, D., 2012. Coal lithotypes before, during, and after exposure to CO<sub>2</sub>: Insights from direct fourier transform infrared investigation. *Energy and Fuels* 26, 3586–3591.  
<https://doi.org/10.1021/ef3003813>
- Masum, S.A., Chen, M., Hosking, L.J., Stanczyk, K., Kapusta, K., Thomas, R., 2022. International Journal of Greenhouse Gas Control A numerical modelling study to support design of an in-situ CO<sub>2</sub> injection test facility using horizontal injection well in a shallow-depth coal seam. *Int. J. Greenh. Gas Control* 119.  
<https://doi.org/10.1016/j.ijggc.2022.103725>
- McGlade, C., Ekins, P., 2015. The geographical distribution of fossil fuels unused when limiting global warming to 2°C. *Nature* 517, 187–190.  
<https://doi.org/10.1038/nature14016>
- Meinshausen, M., Meinshausen, N., Hare, W., Raper, S.C.B., Frieler, K., Knutti, R., Frame, D.J., Allen, M.R., 2009. Greenhouse-gas emission targets for limiting global warming to 2°C. *Nature* 458, 1158–1162.  
<https://doi.org/10.1038/nature08017>
- Merkel, A., Gensterblum, Y., Krooss, B.M., Amann, A., 2015. Competitive sorption of CH<sub>4</sub>, CO<sub>2</sub> and H<sub>2</sub>O on natural coals of different rank. *Int. J. Coal Geol.* 150–151, 181–192. <https://doi.org/10.1016/j.coal.2015.09.006>
- Miller, B.G., 2017. Coal as Fuel, Clean Coal Engineering Technology.

<https://doi.org/10.1016/b978-0-12-811365-3.00002-8>

- Montoya, T., Coral, D., Franco, C.A., Nassar, N.N., Cortés, F.B., 2014. A novel solid-liquid equilibrium model for describing the adsorption of associating asphaltene molecules onto solid surfaces based on the “chemical theory.” *Energy and Fuels* 28, 4963–4975. <https://doi.org/10.1021/ef501020d>
- Mukherjee, M., Misra, S., 2018. A review of experimental research on Enhanced Coal Bed Methane (ECBM) recovery via CO<sub>2</sub> sequestration. *Earth-Science Rev.* 179, 392–410. <https://doi.org/10.1016/j.earscirev.2018.02.018>
- Nie, B., Liu, X., Yang, L., Meng, J., Li, X., 2015. Pore structure characterization of different rank coals using gas adsorption and scanning electron microscopy. *Fuel* 158, 908–917. <https://doi.org/10.1016/j.fuel.2015.06.050>
- Olajossy, A., 2017. Some parameters of coal methane system that cause very slow release of methane from virgin coal beds (CBM). *Int. J. Min. Sci. Technol.* 27, 321–326. <https://doi.org/10.1016/j.ijmst.2017.01.006>
- Oudinot, A.Y., Riestenberg, D.E., Koperna, G.J., 2017. Enhanced Gas Recovery and CO<sub>2</sub> Storage in Coal Bed Methane Reservoirs with N<sub>2</sub> Co-Injection. *Energy Procedia* 114, 5356–5376. <https://doi.org/10.1016/j.egypro.2017.03.1662>
- Ozdemir, E., Morsi, B.I., Schroeder, K., 2004. CO<sub>2</sub> adsorption capacity of argonne premium coals. *Fuel* 83, 1085–1094. <https://doi.org/10.1016/j.fuel.2003.11.005>
- Pan, Z., Connell, L.D., 2007. A theoretical model for gas adsorption-induced coal swelling. *Int. J. Coal Geol.* 69, 243–252. <https://doi.org/10.1016/j.coal.2006.04.006>
- Pan, Z., Connell, L.D., Camilleri, M., Connelly, L., 2010. Effects of matrix moisture on gas diffusion and flow in coal. *Fuel* 89, 3207–3217. <https://doi.org/10.1016/j.fuel.2010.05.038>
- Piccin, J.S., Dotto, G.L., Pinto, L.A.A., 2011. Adsorption isotherms and thermochemical data of FDandC RED N° 40 Binding by chitosan. *Brazilian J. Chem. Eng.* 28, 295–304. <https://doi.org/10.1590/S0104-66322011000200014>
- Ping, A., Xia, W., Peng, Y., Xie, G., 2021. Comparative filtration and dewatering

- behavior of vitrinite and inertinite of bituminous coal: Experiment and simulation study. *Int. J. Min. Sci. Technol.* 31, 233–240. <https://doi.org/10.1016/j.ijmst.2020.12.026>
- Pirzada, M.A., Zoorabadi, M., Lamei Ramandi, H., Canbulat, I., Roshan, H., 2018. CO<sub>2</sub> sorption induced damage in coals in unconfined and confined stress states: A micrometer to core scale investigation. *Int. J. Coal Geol.* 198, 167–176. <https://doi.org/10.1016/j.coal.2018.09.009>
- Pone, J.D.N., Halleck, P.M., Mathews, J.P., 2009. Sorption capacity and sorption kinetic measurements of CO<sub>2</sub> and CH<sub>4</sub> in confined and unconfined bituminous coal. *Energy and Fuels* 23, 4688–4695. <https://doi.org/10.1021/ef9003158>
- Premlall, K., Mabuza, M., Wagner, N., 2014. Evaluating CO<sub>2</sub> Sorption capacity of a number of South African (SA) Coal types: Comparative study of the different coal properties at incremental pressures up to Supercritical pressures. *Energy Procedia* 51, 299–307. <https://doi.org/10.1016/j.egypro.2014.07.036>
- Qi, L., Tang, X., Wang, Z., Peng, X., 2017. Pore characterization of different types of coal from coal and gas outburst disaster sites using low temperature nitrogen adsorption approach. *Int. J. Min. Sci. Technol.* 27, 371–377. <https://doi.org/10.1016/j.ijmst.2017.01.005>
- Qin, L., Li, S., Zhai, C., Lin, H., Zhao, P., Yan, M., Ding, Y., Shi, Y., 2020. Joint analysis of pores in low, intermediate, and high rank coals using mercury intrusion, nitrogen adsorption, and nuclear magnetic resonance. *Powder Technol.* 362, 615–627. <https://doi.org/10.1016/j.powtec.2019.12.019>
- Ramasamy, S., Sripada, P.P., Khan, M.M., Tian, S., Trivedi, J., Gupta, R., 2014. Adsorption behavior of CO<sub>2</sub> in coal and coal char. *Energy and Fuels* 28, 5241–5251. <https://doi.org/10.1021/ef500239b>
- Ranathunga, A.S., Perera, M.S.A., Ranjith, P.G., Wei, C.H., 2017. An experimental investigation of applicability of CO<sub>2</sub> enhanced coal bed methane recovery to low rank coal. *Fuel* 189, 391–399. <https://doi.org/10.1016/j.fuel.2016.10.116>
- Rice, D.D., 1993. Composition and Origins of Coalbed Gas, in: *Hydrocarbons from*

- Coal. American Association of Petroleum Geologists, pp. 159–184.  
<https://doi.org/10.1306/St38577C7>
- Rodrigues, C.F., Lemos De Sousa, M.J., 2002. The measurement of coal porosity with different gases. *Int. J. Coal Geol.* 48, 245–251. [https://doi.org/10.1016/S0166-5162\(01\)00061-1](https://doi.org/10.1016/S0166-5162(01)00061-1)
- Romanov, V., Soong, Y., Schroeder, K., 2006. Volumetric effects in coal sorption capacity measurements. *Chem. Eng. Technol.* 29, 368–374.  
<https://doi.org/10.1002/ceat.200500242>
- Romanov, V.N., Hur, T.B., Fazio, J.J., Howard, B.H., Irdi, G.A., 2013. Comparison of high-pressure CO<sub>2</sub> sorption isotherms on Central Appalachian and San Juan Basin coals. *Int. J. Coal Geol.* 118, 89–94. <https://doi.org/10.1016/j.coal.2013.05.006>
- Rong, L., Xiao, J., Wang, X., Sun, J., Jia, F., Chu, M., 2020. Low-rank coal drying behaviors under negative pressure: Thermal fragmentation, volume shrinkage and changes in pore structure. *J. Clean. Prod.* 272, 122572.  
<https://doi.org/10.1016/j.jclepro.2020.122572>
- Safaei-Farouji, M., Vo Thanh, H., Sheini Dashtgoli, D., Yasin, Q., Radwan, A.E., Ashraf, U., Lee, K.K., 2022. Application of robust intelligent schemes for accurate modelling interfacial tension of CO<sub>2</sub> brine systems: Implications for structural CO<sub>2</sub> trapping. *Fuel* 319, 123821. <https://doi.org/10.1016/j.fuel.2022.123821>
- Schobert, H., 2017. Introduction to low-rank coals: Types, resources, and current utilization, *Low-rank Coals for Power Generation, Fuel and Chemical Production*. Elsevier Ltd. <https://doi.org/10.1016/B978-0-08-100895-9.00001-2>
- Shen, J., Qin, Y., Zhao, J., 2019. Maceral Contribution to Pore Size Distribution in Anthracite in the South Qinshui Basin. *Energy and Fuels* 33, 7234–7243.  
<https://doi.org/10.1021/acs.energyfuels.9b01514>
- Shimada, S., Li, H., Oshima, Y., Adachi, K., 2005. Displacement behavior of CH<sub>4</sub> adsorbed on coals by injecting pure CO<sub>2</sub>, N<sub>2</sub>, and CO<sub>2</sub>-N<sub>2</sub> mixture. *Environ. Geol.* 49, 44–52. <https://doi.org/10.1007/s00254-005-0057-4>
- Siemons, N., Busch, A., 2007. Measurement and interpretation of supercritical CO<sub>2</sub>



- sorption on various coals. *Int. J. Coal Geol.* 69, 229–242.  
<https://doi.org/10.1016/j.coal.2006.06.004>
- Skoczylas, N., Pajdak, A., Młynarczyk, M., 2019. CO<sub>2</sub> adsorption–desorption kinetics from the plane sheet of hard coal and associated shrinkage of the material. *Energies* 12. <https://doi.org/10.3390/en12204013>
- Song, X., Wang, L., Ma, X., Zeng, Y., 2017. Adsorption equilibrium and thermodynamics of CO<sub>2</sub> and CH<sub>4</sub> on carbon molecular sieves. *Appl. Surf. Sci.* 396, 870–878. <https://doi.org/10.1016/j.apsusc.2016.11.050>
- Sosrowidjojo, 2013. Coal Geochemistry of the Unconventional Muaraenim Coalbed Reservoir, South Sumatera Basin: a Case Study From the Rambutan Field. *Indones. Min. J.* 71–81.
- Sripada, P., Khan, M.M., Ramasamy, S., Trivedi, J., Gupta, R., 2018. Influence of coal properties on the CO<sub>2</sub> adsorption capacity of coal gasification residues. *Energy Sci. Eng.* 6, 321–335. <https://doi.org/10.1002/ese3.201>
- Sudibandriyo, M., Pan, Z., Fitzgerald, J.E., Robinson, R.L., Gasem, K.A.M., 2003. Adsorption of methane, nitrogen, carbon dioxide, and their binary mixtures on dry activated carbon at 318.2 K and pressures up to 13.6 MPa. *Langmuir* 19, 5323–5331. <https://doi.org/10.1021/la020976k>
- Sun, X., Yao, Y., Liu, D., Elsworth, D., Pan, Z., 2016. Interactions and exchange of CO<sub>2</sub> and H<sub>2</sub>O in coals: An investigation by low-field NMR relaxation. *Sci. Rep.* 6, 1–11. <https://doi.org/10.1038/srep19919>
- Švábová, M., Weishauptová, Z., Příbyl, O., 2012. The effect of moisture on the sorption process of CO<sub>2</sub> on coal. *Fuel* 92, 187–196.  
<https://doi.org/10.1016/j.fuel.2011.08.030>
- Tang, X., Wang, Z., Ripepi, N., Kang, B., Yue, G., 2015. Adsorption affinity of different types of coal: Mean isosteric heat of adsorption. *Energy and Fuels* 29, 3609–3615. <https://doi.org/10.1021/acs.energyfuels.5b00432>
- Teng, J., Mastalerz, M., Hampton, L.B., 2017. Maceral controls on porosity characteristics of lithotypes of Pennsylvanian high volatile bituminous coal:

- Example from the Illinois Basin. *Int. J. Coal Geol.* 172, 80–94.  
<https://doi.org/10.1016/j.coal.2017.02.001>
- Unsworth, J.F., Fowler, C.S., Jones, L.F., 1989. Moisture in coal. 2. Maceral effects on pore structure. *Fuel* 68, 18–26. [https://doi.org/10.1016/0016-2361\(89\)90005-7](https://doi.org/10.1016/0016-2361(89)90005-7)
- Van Bergen, F., Tambach, T., Pagnier, H., 2011. The role of CO<sub>2</sub>-enhanced coalbed methane production in the global CCS strategy. *Energy Procedia* 4, 3112–3116.  
<https://doi.org/10.1016/j.egypro.2011.02.224>
- Vishal, V., Mahanta, B., Pradhan, S.P., Singh, T.N., Ranjith, P.G., 2018. Simulation of CO<sub>2</sub> enhanced coalbed methane recovery in Jharia coalfields, India. *Energy* 159, 1185–1194. <https://doi.org/10.1016/j.energy.2018.06.104>
- Vo Thanh, H., Sugai, Y., Nguele, R., Sasaki, K., 2019. Integrated workflow in 3D geological model construction for evaluation of CO<sub>2</sub> storage capacity of a fractured basement reservoir in Cuu Long Basin, Vietnam. *Int. J. Greenh. Gas Control* 90, 102826. <https://doi.org/10.1016/j.ijggc.2019.102826>
- Wahid, A., Putra, F.A., Hidayat, M.T., Yusuf, M., 2018. Enhanced coal bed methane (ECBM) recovery: Optimization of CBM production using different injected gas composition and rate for south sumatra CBM field, Indonesia. *E3S Web Conf.* 67, 1–6. <https://doi.org/10.1051/e3sconf/20186703015>
- Wan, Y., Pan, Z., Tang, S., Connell, L.D., Down, D.D., Camilleri, M., 2015. An experimental investigation of diffusivity and porosity anisotropy of a Chinese gas shale. *J. Nat. Gas Sci. Eng.* 23, 70–79. <https://doi.org/10.1016/j.jngse.2015.01.024>
- Wang, Q., Li, W., Zhang, D., Wang, H., Jiang, W., Zhu, L., Tao, J., Huo, P., Zhang, J., 2016. Influence of high-pressure CO<sub>2</sub> exposure on adsorption kinetics of methane and CO<sub>2</sub> on coals. *J. Nat. Gas Sci. Eng.* 34, 811–822.  
<https://doi.org/10.1016/j.jngse.2016.07.042>
- Wang, X., Zhang, D., Geng, J., Jin, Z., Wang, C., Ren, K., 2022. Effects of CO<sub>2</sub> intrusion on pore structure characteristics of mineral-bearing coal: Implication for CO<sub>2</sub> injection pressure. *J. Nat. Gas Sci. Eng.* 108, 104808.  
<https://doi.org/10.1016/j.jngse.2022.104808>

- Wang, X., Zhang, D., Su, E., Jiang, Z., Wang, C., Chu, Y., Ye, C., 2020. Pore structure and diffusion characteristics of intact and tectonic coals: Implications for selection of CO<sub>2</sub> geological sequestration site. *J. Nat. Gas Sci. Eng.* 81, 103388. <https://doi.org/10.1016/j.jngse.2020.103388>
- Wen, H., Hao, J., Ma, L., Zheng, X., 2022. Experimental Study on Replacing Coal Seam CH<sub>4</sub> with CO<sub>2</sub> Gas. *ACS Omega* 7, 1395–1403. <https://doi.org/10.1021/acsomega.1c06050>
- Weniger, P., Franců, J., Hemza, P., Krooss, B.M., 2012. Investigations on the methane and carbon dioxide sorption capacity of coals from the SW Upper Silesian Coal Basin, Czech Republic. *Int. J. Coal Geol.* 93, 23–39. <https://doi.org/10.1016/j.coal.2012.01.009>
- White, C.M., Smith, D.H., Jones, K.L., Goodman, A.L., Jikich, S.A., LaCount, R.B., DuBose, S.B., Ozdemir, E., Morsi, B.I., Schroeder, K.T., 2005. Sequestration of carbon dioxide in coal with enhanced coalbed methane recovery - A review. *Energy and Fuels* 19, 659–724. <https://doi.org/10.1021/ef040047w>
- Wu, D., Liu, G., Sun, R., Chen, S., 2014. Influences of magmatic intrusion on the macromolecular and pore structures of coal: Evidences from Raman spectroscopy and atomic force microscopy. *Fuel* 119, 191–201. <https://doi.org/10.1016/j.fuel.2013.11.012>
- Xiong, J., Liu, X., Liang, L., Zeng, Q., 2017. Adsorption Behavior of Methane on Kaolinite. *Ind. Eng. Chem. Res.* 56, 6229–6238. <https://doi.org/10.1021/acs.iecr.7b00838>
- Yamazaki, T., Aso, K., Chinju, J., 2006. Japanese potential of CO<sub>2</sub> sequestration in coal seams. *Appl. Energy* 83, 911–920. <https://doi.org/10.1016/j.apenergy.2005.11.001>
- Yang, Z., Yin, Z., Xue, W., Meng, Z., Li, Y., Long, J., Wang, J., 2021. Construction of Buertai Coal Macromolecular Model and GCMC Simulation of Methane Adsorption in Micropores. *ACS Omega* 6, 11173–11182. <https://doi.org/10.1021/acsomega.0c04649>

- Yu, J., Tahmasebi, A., Han, Y., Yin, F., Li, X., 2013. A review on water in low rank coals: The existence, interaction with coal structure and effects on coal utilization. *Fuel Process. Technol.* 106, 9–20. <https://doi.org/10.1016/j.fuproc.2012.09.051>
- Yu, Y., Wang, Y., 2020. Characteristics of low-rank coal reservoir and exploration potential in Junggar Basin: new frontier of low-rank CBM exploration in China. *J. Pet. Explor. Prod. Technol.* 10, 2207–2223. <https://doi.org/10.1007/s13202-020-00923-3>
- Zarrouk, S.J., Moore, T.A., 2009. Preliminary reservoir model of enhanced coalbed methane (ECBM) in a subbituminous coal seam, Huntly Coalfield, New Zealand. *Int. J. Coal Geol.* 77, 153–161. <https://doi.org/10.1016/j.coal.2008.08.007>
- Zhang, B., Liang, W., Ranjith, P.G., He, W., Li, Z., Zhang, X., 2018. Effects of coal deformation on different-phase CO<sub>2</sub> permeability in sub-bituminous coal: An experimental investigation. *Energies* 11. <https://doi.org/10.3390/en11112926>
- Zhao, J., Tang, D., Qin, Y., Xu, H., Liu, Y., Wu, H., 2018. Characteristics of Methane (CH<sub>4</sub>) Diffusion in Coal and Its Influencing Factors in the Qinshui and Ordos Basins. *Energy and Fuels* 32, 1196–1205. <https://doi.org/10.1021/acs.energyfuels.7b03032>
- Zhao, Y., Cao, S., Li, Y., Yang, H., Guo, P., Liu, G., Pan, R., 2018. Experimental and numerical investigation on the effect of moisture on coal permeability. *Nat. Hazards* 90, 1201–1221. <https://doi.org/10.1007/s11069-017-3095-9>
- Zheng, G., Pan, Z., Tang, S., Ling, B., Lv, D., Connell, L., 2013. Laboratory and modeling study on gas diffusion with pore structures in different-rank Chinese coals. *Energy Explor. Exploit.* 31, 859–877. <https://doi.org/10.1260/0144-5987.31.6.859>
- Zheng, Y., Li, Q., Yuan, C., Tao, Q., Zhao, Y., Zhang, G., Liu, J., 2019. Influence of temperature on adsorption selectivity: Coal-based activated carbon for CH<sub>4</sub> enrichment from coal mine methane. *Powder Technol.* 347, 42–49. <https://doi.org/10.1016/j.powtec.2019.02.042>
- Zhou, L., Feng, Q., Chen, Z., Liu, J., 2012. Modeling and Upscaling of Binary Gas

- Coal Interactions in CO<sub>2</sub> Enhanced Coalbed Methane Recovery. *Procedia Environ. Sci.* 12, 926–939. <https://doi.org/10.1016/j.proenv.2012.01.368>
- Zhou, X., Yi, H., Tang, X., Deng, H., Liu, H., 2012. Thermodynamics for the adsorption of SO<sub>2</sub>, NO and CO<sub>2</sub> from flue gas on activated carbon fiber. *Chem. Eng. J.* 200–202, 399–404. <https://doi.org/10.1016/j.cej.2012.06.013>
- Zhou, Y., Li, Z., Zhang, R., Wang, G., Yu, H., Sun, G., Chen, L., 2019a. CO<sub>2</sub> injection in coal: Advantages and influences of temperature and pressure. *Fuel* 236, 493–500. <https://doi.org/10.1016/j.fuel.2018.09.016>
- Zhou, Y., Zhang, R., Huang, J., Li, Z., Zhao, Z., Zeng, Z., 2019b. Effects of pore structure and methane adsorption in coal with alkaline treatment. *Fuel* 254, 115600. <https://doi.org/10.1016/j.fuel.2019.06.008>
- Zhu, C., Wan, J., Tokunaga, T.K., Liu, N., Lin, B., Wu, H., 2019. Impact of CO<sub>2</sub> injection on wettability of coal at elevated pressure and temperature. *Int. J. Greenh. Gas Control* 91, 102840. <https://doi.org/10.1016/j.ijggc.2019.102840>
- Zou, M., Wei, C., Zhang, M., Shen, J., Chen, Y., Qi, Y., 2013. Classifying coal pores and estimating reservoir parameters by nuclear magnetic resonance and mercury intrusion porosimetry. *Energy and Fuels* 27, 3699–3708. <https://doi.org/10.1021/ef400421u>